Isolating primary explosive blast effects on neuronal function and structure in traumatic brain injury: changes in rat cortical electrical potentials and dendritic spine density at seven days post-blast exposure

By

John Magnuson

Dissertation submitted to the Faculty of the
Neuroscience Graduate Program
Uniformed Services University of the Health Sciences
In partial fulfillment of the requirements for the degree of
Doctor of Philosophy 2016

UNIFORMED SERVICES UNIVERSITY, SCHOOL OF MEDICINE GRADUATE PROGRAMS
Graduate Education Office (A 1045), 4301 Jones Bridge Road, Bethesda, MD 20814

FINAL EXAMINATION/PRIVATE DEFENSE FOR THE DEGREE OF DOCTOR OF PHILOSOPHY
IN THE NEUROSCIENCE GRADUATE PROGRAM

Name of Student: John Magnuson

Date of Examination: October 27, 2016
Time: 11:00 AM
Place: A2015

DECISION OF EXAMINATION COMMITTEE MEMBERS:

	PASS	FAIL
[redacted]	X	
Denes Agoston, MD, PhD DEPARTMENT OF ANATOMY, PHYSIOLOGY & GENETICS Committee Chairperson		
[redacted]	✓	
Geoffrey Ling, MD, PhD DEPARTMENT OF NEUROLOGY Dissertation Advisor		
[redacted]	X	
Howard Bryant, PhD DEPARTMENT OF ANATOMY, PHYSIOLOGY & GENETICS Dissertation Advisor		
[redacted]	X	
Peter Haaland, PhD DEPARTMENT OF NEUROLOGY Committee Member		
[redacted]	X	
Fabio Leonessa, MD DEPARTMENT OF NEUROLOGY Committee Member		
[redacted]	X	
Mike Roy, MD DEPARTMENT OF MEDICINE Committee Member		

ACKNOWLEDGMENTS

It has been an honor to develop as a scientist while at the same time conducting research in support of U.S. Military personnel in the Neuroscience program here at Uniformed Services University. I wish to thank everyone for their support.

Advisor

Doctor Geoffrey Ling, thank you for taking the time to mentor and guide me. You teach me something every time I speak with you. Your accomplishments and future endeavors are an inspiration and set the example for others to follow. Thank you for giving me the freedom to conduct this research, your advice, funding and support.

Director of Neuroscience

Doctor Sharon Juliano, thank you for your support and affable nature and understanding. It is good to know the neuroscience program is in your hands.

Neurotrauma Laboratory

I would also like to thank the Neurotrauma Laboratory, for providing guidance, support and shelter from the storm. Fabio, Erin, Sandor and Hongna I can't thank you enough for all that you have done for me and this project.

Committee

To the members of my thesis committee, Doctor Ling helped assemble the best committees for advancement and defense. Doctors Agoston and Leonessa, I would like express my true appreciation for all your time and encouragement. Doctor Pete Haaland, thank you for all the work you did on this project in getting the data analyzed, your wealth and breadth of knowledge was invaluable. Thank you Dr Howard Bryant, for all

your time and sharing your knowledge of electrophysiology. You have a gift for taking complex concepts and making them easily understandable; In a world of instructors you are a true teacher. Thank you Dr Mike Roy for your time and helping get this project completed. Thank you Dr Martin Doughty for keeping the advancement committee on task and staying true to the science. Thank you Dr Brian Cox for always providing a smile and good advice.

Doctor Michael Bodo, thank you for teaching me the surgical technique, how to record ECoGs and fVERs and their analysis. Providing the recording equipment, analysis of ECoGs and lunch after crunching the data on your free weekends.

Research Funding:

This work would not have been possible without financial support from Texas A&M University.

I also would like to thank the graduate program and graduate education office for their tireless work that keep USU graduate program running smoothly.

Finally, I would like to thank my family for their unending love, support and encouragement.

DEDICATION

For the Airborne Ranger in the sky, and those left on the ground.

COPYRIGHT STATEMENT

The author hereby certifies that the use of any copyrighted material in the dissertation manuscript entitled: [Isolated-primary injury threshold of explosive blast induced mild traumatic brain injury: Changes in rat cortical electrical potentials and dendritic spine density at seven days post-blast exposure] is appropriately acknowledged and, beyond brief excerpts, is with the permission of the copyright owner.

[Signature] 

[John Magnuson]

[February 2, 2017]

ABSTRACT

Isolating primary explosive blast effects on neuronal function and structure in traumatic brain injury: changes in rat cortical electrical potentials and dendritic spine density at seven days post-blast exposure

John Magnuson, Doctor of Philosophy, 2016

Thesis directed by: Geoffrey S. F. Ling, M.D., Ph.D., FAAN, Professor, Department of Neurology

Explosive blast induced traumatic brain injury (bTBI) is considered the hallmark injury of the Overseas Contingency Operations in Afghanistan and Iraq. During the years 2000 to August of 2016, there have been 352,619 medically diagnosed cases of TBI in military personnel; with an increased incidence of TBI occurring due to explosive blast. In addition, over 82.3% of the military TBIs were classified as mild TBI.

This dissertation describes work identifying the threshold of explosive blast exposure (108-138 kPa) at which cellular injury occurs but is undetectable by current clinical electrophysiology and imaging protocols. The relevance of this work to bTBI is that it will enable development of objective criteria that can be used to support a diagnosis of mild bTBI. Presently, U.S. service members are clinically diagnosed based on exposure to a blast and symptomology.

The main hypothesis therefore was that a mild explosive blast of 108-138 kPa will cause subclinical functional changes as well as consistent neuropathological structural brain changes. The specific goal of this work was to identify the bTBI threshold in rats, as the rat is the most common subject species used in preclinical study of TBI.

To validate this hypothesis, this work studied the effect of a single explosive blast (108-138 kPa) on function (cortical electrical potentials) and neuronal structure (dendritic spine density) in unprotected Sprague-Dawley rats. Explosive blast was generated with a composition-4 (C4) charge, as this is a commonly used military explosive. An explosive driven shock wave generator was used to produce pressure waves and isolate the primary injury mechanism of blast exposure. Forty-eight test subjects were divided into two groups: 24-implanted and 24-nonimplanted. Each group was further divided into two post-blast survival conditions: 12 one-day and 12 seven-day. The implanted group's subjects were surgically implanted with epidural screw electrodes allowing for recording of electrocorticograms and flash-visual evoked responses (fVER) one-day prior to blast, as well as one and seven days post-blast exposure. The non-implanted group test subjects were exposed to a single blast, then euthanized at the one-day or seven-day time point in order to determine changes in cortical layer II/III, pyramidal neuron, dendritic spine density.

Comparison of post-blast conditions to pre-blast conditions indicated no electrocorticogram changes. In contrast, fVER indicated a decrease in amplitude between the P1-N1 and N1-P2 amplitudes. Latency changes were subtle and resolved by 7 days post-blast. Dendritic spine density decreased at one-day (39%) and seven-days post-blast (18%).

The first conclusion that can be made from this study is that exposure to 108-138 kPa explosive blast does not result in significant functional impairment as measured by current clinical electrocorticography or fVER protocols. Alternatively, comparison of pre-blast and post-blast fVER recordings can be used to identify subtle blast induced functional changes. The second conclusion is that this blast intensity can cause structural changes at the level of the synapse without any neuronal death or gross pathologic finding. In addition, dendritic spine density showed improvement over time when comparing the post-blast time points indicating structural changes may be transient.

TABLE OF CONTENTS

LIST OF TABLES

LIST OF FIGURES

LIST OF ABBREVIATIONS

°C: degree Celsius
3D: three-dimension
ANOVA: analysis of variance
AO: apical oblique
BBB: blood brain barrier
BDNF: brain derived neurotrophic factor
BOP: gas driven shock tubes
bTBI: explosive blast induced traumatic brain injury
BWG: blast wave generator
C-4: composition 4
CA: cyano acrylate (dental resin)
CC: correlation coefficient
CCI: controlled cortical impact
CDK5: cyclin-dependent kinase 5
CHI: closed head injury
cm: centimeter
CNS: central nervous system
CO2: carbon dioxide
COX: cyclooxygenase
COX-2: cyclooxygenase isozyme 2
CSF: cerebral spinal fluid
CT: computed axial tomography
CXC: cross-correlation
cTBI: closed head traumatic brain injury
CV: cresyl echt violet
d: day
ECoG: electrocorticogram
ECoGx: Pearson's correlation coefficient for hemispheric ECoG
EEG: electroencephalogram
EEGx: Pearson's correlation coefficient for hemispheric EEG
EP: evoked potential
ER: evoked response
FFT: fast Fourier transformation
FPI: fluid percussion injury
fVEP: flash visual evoked potential
fVER: flash visual evoked response
g: gram
GABA: γ-aminobutyric acid
GC: Golgi-Cox
GCS: Glasgow Coma Scale
GFAP: glial fibrillary acidic protein
GPa: Giga-Pascal
IHC: immunohistochemistry
kPa: kilo Pascal

LAM: laboratory animal medicine
LOD: level of detection
LOQ: level of quantification
LPM: liters per minute
M: molar
mA: milliamp
MANOVA: multivariate analysis of variance
MBP: myelin basic protein
mg: milligram
mL: milliliter
mm: millimeter
mM: millimolar
mmHg: millimeter of mercury
MRI: magnetic resonance imaging
ms: millisecond
MS: multiple sclerosis
mTBI: mild traumatic brain injury
MW: molecular weight
NMDAr: N-methyl D-aspartate receptor
NSE: neuron specific enolase
OCO: Overseas Contingency Operations
OCT: ocular combat trauma
OEF: Operation Enduring Freedom
OHI: open head injury
OIF: Operation Iraqi Freedom
OND: Operation New Dawn
Pa: Pascal
PB: pre-blast
PBS: phosphate buffered saline
PF: paraformaldehyde
PGE_2: prostaglandin E_2
pH: negative log of hydrogen ion concentration
PI: isoelectric point
PMMA: Poly(methyl 2-methylpropenoate) or Poly(methyl methacrylate)
PP: peak pressure
PPD: positive phase duration
ppm: parts per million
pTBI: penetrating traumatic brain injury
PTSD: post-traumatic stress disorder
qEEG: quantitative electroencephalogram
RMANOVA: repeated measures analysis of variance
RPM: revolutions per minute
S/N: signal to noise ratio
SDS: sodium dodecyl sulfate
SD: standard deviation
SDS-PAGE: sodium dodecyl sulfate-polyacrylamide gel electrophoresis

SEM: standard error of the mean
SQ: subcutaneous
TBI: traumatic brain injury
Tc: time constant
USUHS: Uniformed Services University of the Health Sciences
v/v: volume to volume
V: volt
VEP: visual evoked potential
VER: visual evoked response
w/v: weight per volume
X: times
y/o: year old
yrs: years
µg: microgram
µL: microliter
µV: microvolt

CHAPTER 1: Introduction

Explosive blast induced traumatic brain injury (bTBI) is considered the hallmark injury of Overseas Contingency Operations (OCO): Operation Enduring Freedom (OEF), Operation Iraqi Freedom (OIF) and current Operation Resolute Support (ORS) (85). Amongst military personnel, between the period of 2000 to August 2016, there have been 352,619 medically diagnosed cases of TBI; with an increased incidence of TBI occurring due to explosive blast (29). In addition, over 82.3% of the military TBIs were classified as mild TBI (29).

Blast injuries to the eyes may be overlooked due to maxillofacial trauma or more serious systemic injuries (96). From August 2004 to October 2006 the Defense and Veterans Brain Injury Center (DVBIC) found that 66% of TBIs diagnosed at Walter Reed Army Medical Center (WRAMC) also suffered combat ocular trauma (COT). The incidence of COT appears to increase with the severity of TBI resulting in COT being more common in severe and penetrating TBI (96). Complicating the diagnostic process is the occurrence of the less evident closed-ocular (non-penetrating) injury (96). Prevalence of sensory organ injury during blast has been shown by retrospective-analysis of veterans diagnosed with TBI, indicating the strongest predictor of visual impairment is auditory impairment and vice versa (62). Patients with TBI have shown variable changes in event-related electrical potentials compared to controls (31; 84; 95). Long-term depression (LTD) of cortical potentials have been associated with decreased dendritic spine density in the rat model (70). These data indicate that evaluation of changes in visual evoked response may be a beneficial diagnostic method for bTBI.

In the present study, we compared pre-blast to post-blast-exposure recordings of electrocorticograms and flash-visual evoked responses in order to identify changes in electrical potential latency, amplitude, signal coherence and phase-synchronicity. Pyramidal neurons of the cortical layers have been noted as a source of the fore mentioned cortical electrical potentials (1); Therefore, in order to identify the structural/cellular changes corresponding to physiologic changes, quantification of cortical layer II/III pyramidal neuron dendritic spine density was performed.

An important challenge to understanding the pathobiology of mild bTBI is determining the initial point of injury within the brain which can be identified clinically with non-invasive methods. This dissertation project was designed to meet this challenge. The research presented here adds to the diagnosis of bTBI with two major outcomes. First, it demonstrates that exposure to a single explosive blast can result in decreased dendritic spine density without gross brain pathology. Second, it demonstrates that this decrease in dendritic spine density can occur below the resolution of current clinical visual evoked response protocols.

CHAPTER 2: Background

Traumatic brain injury

The National Institute of Neurological Disorders and Stroke of the NIH defines TBI as a form of acquired brain injury occurring when a sudden trauma causes damage to the brain. This broad definition of TBI has provided a basis for identifying types of TBI based on three criteria: type of head injury, mechanism of injury and severity. Head injury is designated as open or closed relative to skull and dura matter integrity. Closed head injury (CHI), describes brain injury where the dura mater remains intact. The most common mechanisms of CHI include falls, motor vehicle collisions, and unintentional blunt trauma (22). Open head injury (OHI) indicates dura mater rupture due to skull fracture, skull fragment compression or penetration by foreign object (pTBI). Penetrating TBI can be further subdivided into low velocity penetration (stab wounds) or high velocity ballistic penetration (gunshot wounds), the latter of which are prone to tissue cavitation and possibly ricochet injury (38). Each OHI is a severe and complex injury requiring immediate and advanced medical support to contend with hemorrhage, swelling and ultimately infection (81). Closed head injury may be more subtle in its presentation than OHI.

Severity of CHI is classified as mild, moderate or severe. A criterion standard diagnostic technique for CHI has not been fully realized; therefore, clinical diagnosis is symptomology based: presence and duration of amnesia, changes in mentation and/or consciousness, Glasgow coma scale rating and changes on imaging e.g., CT and MRI, see Table 1 (91).

Table 1 Department of Veterans Affairs diagnostic criteria for TBI severity.

Criteria	**Mild**	**Moderate**	**Severe**
Structural imaging	Normal	Normal/abnormal	Normal/abnormal
Loss of consciousness	0-30 min	> 30 min to < 24 h	> 24 h
Alteration of consciousness	< 24 h	> 24 h*	> 24 h*
Post-traumatic amnesia	< 1 d	> 1 d to < 7 d	> 7 d
Glasgow coma scale	13 - 15	9 - 12	< 9

* Severity is based on other criteria

Explosive blast induced traumatic brain injury

The conflicts in Afghanistan and Iraq have resulted in an increased incidence of TBI in military personnel (29). Explosive blasts due to road side bombs and improvised explosive devices (IEDs) have been identified as the primary cause for increased explosive-blast induced TBI (bTBI) in warfighters (29; 65). An explosive blast can result in CHI or OHI. Variability in patient presentation is a unique aspect of bTBI. Military physicians have identified vastly different injuries in soldiers injured at the same blast area. Such variability in clinical presentations distinguishes bTBI from a more conventional, pure concussive TBI. There are four mechanisms of injury which contribute to bTBI (26): primary, secondary, tertiary and quaternary. Primary mechanism results from pressure generated from the explosive shock-front. Secondary, is caused by shrapnel, ejecta and/or surrounding debris penetrating the brain. Tertiary, is due to the brain colliding with the skull or skull colliding with the brain; as in coup-contrecoup injuries. Finally, the quaternary mechanism of injury is due to any factors not included in the previous three mechanisms, such as heat, chemical or radiation injury (14). Protecting warfighters from blast injury has focused research on limiting the mechanisms of injury such as: generating body armor to prevent impact by shrapnel/ejecta, preventing inertial

injury with better armored vehicles as well as flame resistant clothing and equipment to protect from the fireball and hot gases.

Dynamic environment of blast induced traumatic brain injury

To better understand the dynamic injury caused by explosive blasts a basic understanding of chemical explosives and how the blast wave interacts with a body is required. An explosion is an event that results from a sudden release of energy. This may occur in any variety of ways such as pressurized steam release, ignition of grain storage bins and chemical explosives. Explosives are materials that are capable of producing explosions by their own chemical energy (23). Energy stored in molecular bonds is released in an exothermic reaction producing a detonation wave of high temperature and pressure driving the reaction forward. Pressure at the leading edge of the detonation wave can be 20-30 GPa and the trailing gas can reach 7000ºC (23). Detonation velocity faster than the speed of sound (343 m/s) is a characteristic of high-velocity explosives such as composition-4 (8000 m/s) (23).

Non-linear physics governs blast wave generation and propagation (23). The energy of the explosive detonation is dissipated by a blast wave, propulsion of surrounding material, heat, acoustic noise and electromagnetic radiation (21; 23). This energy conversion and transfer to the surrounding medium results in formation of a rapidly expanding gaseous sphere of high-pressure and high-temperature known as the blast wave (69). Blast waves are comprised of two parts: the detonation wave (shock wave) and blast wind (12; 16). The detonation wave is a region of high pressure, temperature and density which moves perpendicular and away from the surface of explosive at supersonic velocities and reduces in pressure as the cube-root of the distance

to the explosive. The slower moving blast wind is a result of the mass movement of air displaced as the shock front moves away from the detonation.

Blast waves have characteristic shapes and pressure-time relationships. A free-field explosive blasts produces a uniform blast wave which propagates perpendicular and away from the area of detonation. Characteristics of the blast wave include an instantaneous rise to peak pressure with exponential decay below ambient pressure followed by a period of negative gauge pressure and ending with a return to the ambient pressure. A free-field blast can be approximated with the Friedlander equation. The Friedlander equation is a mathematical approximation of pressure-time relationship of a free-field blast, see Figure 1. It must be stated that the Friedlander equation does not precisely model the negative phase of the free-field blast (72); In Figure 1 there is a red arrow and dotted line to represent the more accurate negative phase. Deviation of real blast from the equation is identified by a sharp pressure increase at the nadir of the negative phase. This is considered a consequence of atmospheric pressure returning displaced air to the explosive-generated-void. The gradual return to ambient pressure has been explained as reflections or residual burning of explosive/materials (23; 72); see Figure 1, and compare to the real explosion recordings in Figure 20.

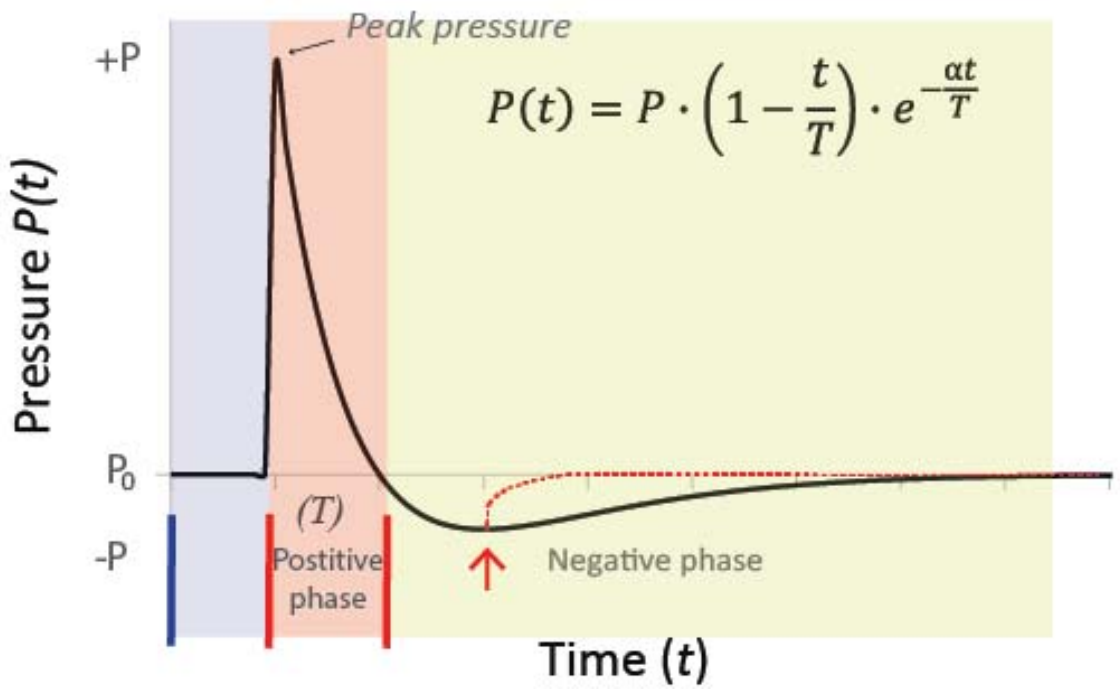

Figure 1 Pressure versus time plot of Friedlander equation representing an idealized free-field explosion. The Friedlander equation can be used to solve for pressure as a function of time. Equation variables include the blast Pressure (*P*), positive phase duration (*T*), time constant (α), time during blast wave propagation (*t*). Blue bar represents detonation. Red arrow and dotted line represent where the equation deviates from a real blast and the corrected negative phase respectively. A plot of the Friedlander equation results in an almost instantaneous rise in positive pressure followed by an exponential decay to below atmospheric pressure, finally ending with a return to atmospheric pressure; the negative pressure phase duration is roughly twice the positive pressure phase duration. Negative and positive pressures are in reference to gauge pressure. Plot values P = 18, T = 10, α = 1.

When a blast wave encounters a solid object, such as the ground, structures, vehicles or people, it reflects off that object, deflects around that object, and transfers energy to that object. As with light or sound waves, detonation waves can reflect from surfaces (23). However, unlike light or sound waves, detonation waves change the medium in which they interact and the angle of incidence does not always equal the angle of reflection (23). Depending on the incident angle with a surface, detonation waves can reflect normal for head-on impacts, obliquely for small angles of incidence or spurt along

the surface for grazing angles as in the mach stem (23), see Figure 2. Thus, real-world blast waves are typically much more complex than the Friedlander curve. Likewise, when a shock front impacts an object and propagates through that object, the magnitude, shape and velocity of that blast wave changes. More importantly, as the energy of the blast wave is transferred into the surrounding environment the blast waves create dynamic and destructive interactions.

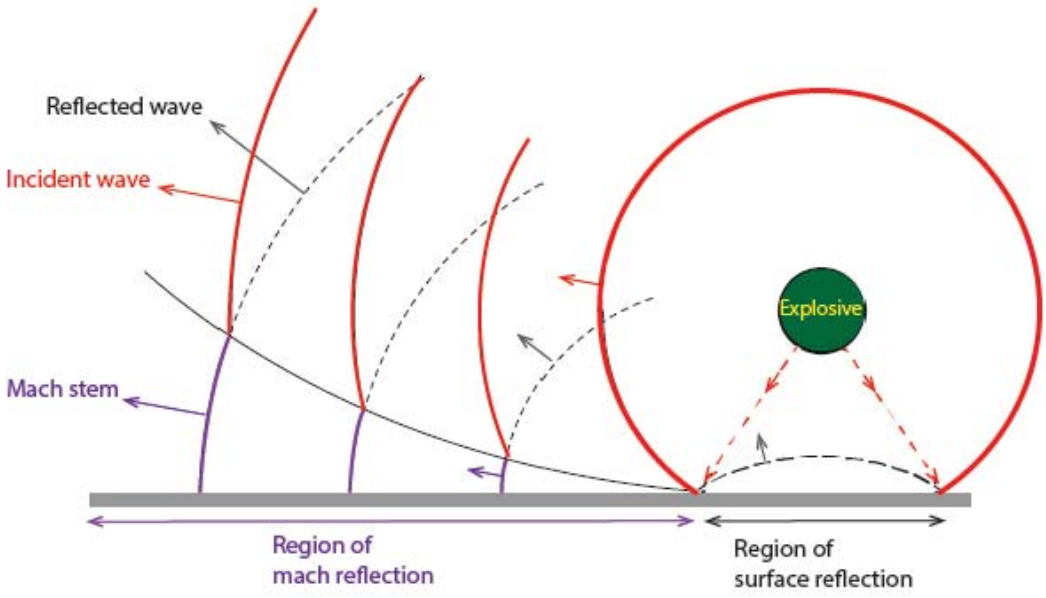

Figure 2 Above ground explosive blast and reflections. The diagram illustrates the formation of the explosive generated (green) detonation wave (red), reflected waves (black) and the resultant mach stem. The waves move perpendicularly away from the surface of the explosive or the incident surface. Normal incident angle results in a reflected pressure which is a non-linear function of the mach number. Image adapted from Iremonger and Bass.

Tissue response to blast waves

Blast waves impinging on a human body can be reflected, transmitted or a combination of both. Early experiments by Clemedson demonstrated that as the shock wave penetrates adjacent tissues the loading pressure rise-time is increased while the

pressure decays as an inverse-function of distance from the impingement (15; 21; 30). The importance of these two points becomes evident due to cellular injury being more related to increased stress-rate rather than total applied stress (30; 33). Intuitively this makes sense, two pressure waves of the same peak pressure but different rise times will result in the pressure wave with a greater rise time having a larger impulse.

A body's internal response to a blast wave can vary due to the wave moving at variable speeds in tissues of differing densities. This can lead to relative motion between the tissue resulting in shearing and tearing at the tissue interface (23). Blast wave transmission occurs faster in dense tissue and slower in less dense tissue. In bTBI research, variable tissue densities and blast transmission are important in selection of a blast model. For example, adult Sprague-Dawley rats, of weight >350 g, show pathologic changes due to blast; however, younger rats < 350 g showed no pathology due to the same intensity blast (60). The importance of using rats > 350 g is due to the density of the its skull approximating the density of a human adults skull, while younger rats have a more pliable skulls (60).

Functional effects of blast induced traumatic brain injury

Mild TBI is the most common severity of bTBI as well as the most prevalent in the military population. Although the lack of a gold standard diagnostic for mild TBI prevents high confidence diagnoses, approximately 82.3% of all military TBI, in the years 2000 to August 2016, were diagnosed as mTBI (29). Questionnaires such as the Neurobehavioral Symptom Inventory (NSI) have been used to better define the symptoms of mild bTBI. The NSI is a 22 individual item analysis divided into somatic, cognitive, affective and sensory deficits filled out by the patient (80). Each test-division

contains items of symptomology which have been reported by patients diagnosed with mild bTBI. A significant result of NSI analysis is that vision and auditory changes are common sensory deficits reported by patients diagnosed with mild bTBI (61; 62; 80).

Cognitive deficits, due to blast exposure may include poor concentration of attention, forgetfulness, impaired decision-making and slowed thinking (63; 80). Since these executive functions require a high degree of cortical involvement, deficits to these processes suggest the presence of pathologic changes at the cortical level that have not been realized.

Combat ocular trauma has occurred more frequent in OIF/OEF than prior U.S. conflicts (96). In addition, visual complaints and impairments were commonly reported by Veterans of OIF/OEF that suffered a blast injury. Clinical evaluation of these Veterans identified vision impairments in 38% of those receiving care (44). As with higher order cognition, changes in the visual system suggest the presence of pathological changes at the cortical level, including changes in cortical neuronal connectivity.

Characterizing functional alterations due to blast

Although functional impairment of the visual and auditory systems is often a consequence of TBI (39; 62), neuroimaging studies of soldiers with bTBI criteria often reveal no gross-pathology in spite of evident cognitive/functional impairment (25; 89). Given both the expense and the temporal resolution limitations functional imaging, such as functional Magnetic Resonance Imaging (fMRI), alternative approaches to characterizing functional alterations due to blast must be identified.

Extracellular recording methods, such as electroencephalography and event related potential (ERP) analysis, can be used to evaluate cortical neuronal function and

suggest alternative to fMRI. Electroencephalography is a method of using an electroencephalograph machine to record an electroencephalogram (EEG) of a patient's brain electrical potentials. Since 1920, electroencephalography has been used to study human brain spontaneous electrical activity over a period of time (73). Clinicians have used electroencephalography as a metaphorical window into brain activity, where normal brain oscillatory synchronization can be correlated with cognitive function and behavioral state (3; 13). Physicians use electroencephalography to monitor brain function in critical care units as well as clinically in order to aid in diagnosis of epilepsy, evaluate encephalopathies and, ultimately, to identify brain death (24). Extracellular potentials are generated by a combination of any excitable membrane and transmembrane ionic currents (9). Discrete membrane potentials spread through the brain by volume conduction and contribute to the local recorded potential for a given volume of extracellular space (73). Placing metal electrodes at varied locations on the head allows recording of voltage differences at the electrodes, see Figure 3. The voltage at each electrode is the weighted sum of the electrical potentials at the respective electrode. The electrical potential amplitude scales with the inverse of the distance between the recording electrode and the potential source. The larger the distance of the recording electrode from the source of the electrical potential will result in less recorded information.

Historically, a recording acquired from the skin surface using scalp electrodes is called an EEG while a recording from the cortical surface using epidural electrodes is an electrocorticogram (ECoG) (9). Electrocorticography techniques improve spatial and temporal resolution by decreasing the distance between recording electrodes and neuronal

potentials in comparison to transdermal scalp EEGs (9). The ECoG electrodes are preferred for animal studies due to the ability to secure the electrodes to the skull allowing researchers to perform multiple recording sessions without worry of intersession variability due to electrode movement. With the advances in digital technology and computer processing, the present day ECoG can be acquired faster and with greater resolution (24; 66).Computer-assisted ECoG analysis allows for derivation of measures, data transforms, and identification of the subtle shifts in ECoG waveforms (2). The ECoG can be very sensitive to movement and sensory stimulation. In order to take advantage of these properties the *evoked* response (ER) was developed.

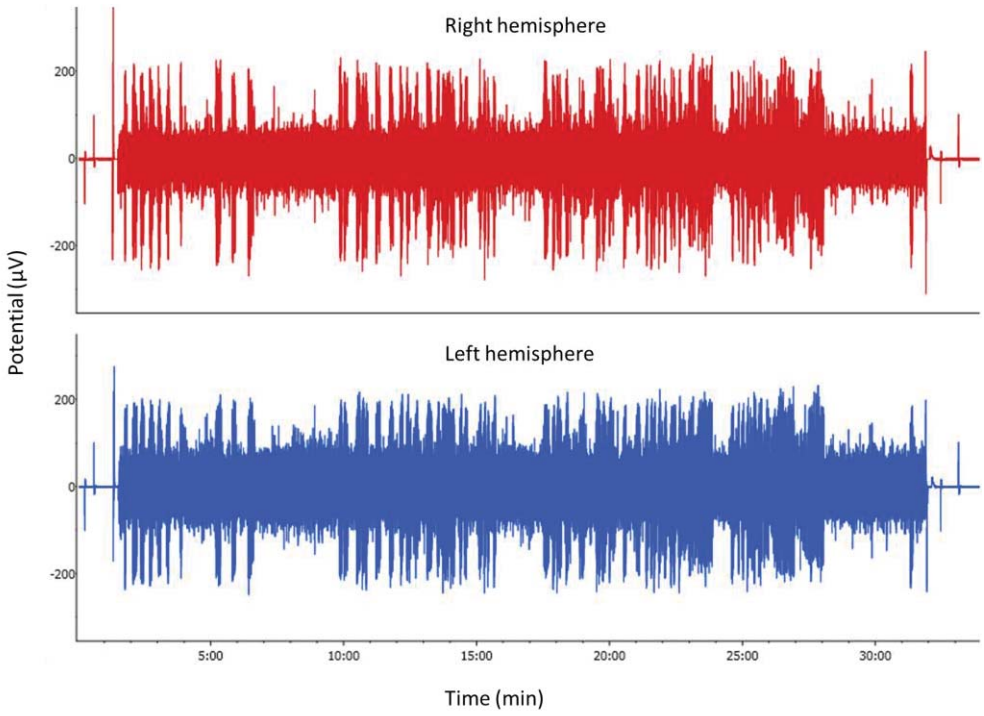

Figure 3 Right and left hemisphere ECoG recording from non-injured rat. The ECoG is a recording of the brain's spontaneous electrical activity (potential) over a period of time. A pair of epidural screw electrodes are placed over each cortical hemisphere of the brain in order to acquire an ECoG from each respective hemisphere. A 100 µV calibration potential is triggered at the start and end of the recording. The two 30-minute ECoG recordings above show the hemispheric electrical activity of an unstressed Sprague-Dawley rat.

Evoked response potentials are extracellular potentials generated following presentation of a stimulus. Visual evoked responses (VERs) have aided in diagnosis of visual pathway pathologies such as retinoblastoma and multiple sclerosis by looking for changes in visual evoked response peak amplitude and latency (36). Visual evoked responses have also been used in pharmacological experiments, such as assessing the neuroprotective effects of compounds, as it provides a method of monitoring neural activity and sensory processing *in vivo* (50).

Flash-visual evoked response (fVERs) use a short duration flash-stimuli resulting in evoked potentials which rise quickly in intensity in order to differentiate the fVERs from baseline potentials. Employing averaging of fVERs that are time-locked to the flash-stimulus enhances the signal-to-noise ratio (S/N), see Figure 24. The S/N is maximized when the response is identical between replicates, response and noise are uncorrelated, and when the noise is random. Ideally, S/N increases with the square root of the number of fVERs averaged (74). Utilizing time and frequency signal analysis to investigate each fVER allows for extraction of information relating to how fVERs and the ECoG co-vary. The fVERs in rats have been described using various electrode configurations such as subdermal needles and screw electrodes (98).

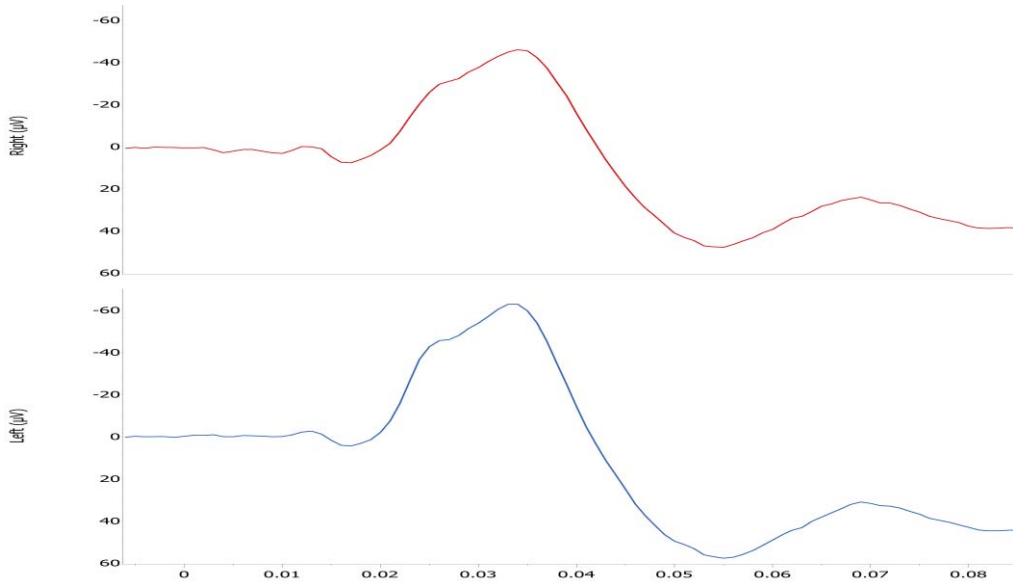

Figure 4 Flash-visual evoked response recording from right and left hemisphere in non-injured rat. Flash-VEP (μV) versus time (s) plots. Right hemisphere recording in the top plot and left hemisphere recording in the lower plot. The initial local minima and maxima of the flash-VEP represent integrity of the optic nerve. Each trace is an average of 180 flash evoked potentials.

Visual evoked response recording became feasible with the development and implementation of summation and computer averaging techniques (20; 74). Clinically, VERs consist of local minima and maxima designated by capital letters, P or N respectively, and labeled with a sequential number. Alternatively, the letter designation may be used along-side the peak average-latency in milliseconds (ms). Due to the smaller size of the rat's brain compared to the human brain, the P1 (P17) and N1 (N32) peaks of the rat correspond to the P60 and N70 peaks, respectively, of the human VER.

The advantages of fVERs to study brain function include temporal resolution, relatively low cost. In addition, the approach is non-invasive when used within the clinical setting. The speed at which neuronal conduction occurs allows for consistent fVER latency measurements with excellent temporal resolution. Electrophysiology techniques such as the EEG and VER are already in use within clinics and hospitals

which allows quick implementation of new use protocols by medical staff with limited training. Finally, the limited invasiveness of clinical EEGs and VERs machines allow wide deployment in various military environments which may be unreachable with larger and more costly techniques such as PET or fMRI. Analysis of ECoGs and fVERs pre- and post-blast exposure allows for identification of electrical potential amplitude and latency changes; however the physiologic change/injury occurring in mild bTBI needs further investigation.

Blast induced structural alterations

Explosive blast can results in immediate CNS-tissue disruption (primary injury). This initial injury may resolve or may be followed by secondary injury caused by a complex biochemical cascade resulting in further injury. Combination of primary and secondary injuries may result in the persistent cognitive, sensory and motor deficits noted in mild TBI victims (68). An example of this injury mechanism has been noted in the granular neurons of mouse hippocampal dentate gyrus (HDG) after controlled cortical impact (CCI)-induced TBI. Despite the granular neuron survival, the mature granular neurons show dendritic spine degeneration, synapse loss and activity impairment (42). Fluid percussion injury (FPI) and CCI TBIs have resulted in subtle neuronal changes at the level of the synapse (11; 41; 42).

Neuronal dendritic spines

Dendritic spines are femtoliter-sized neuronal protrusions which form the post-synaptic part of the synapse. There are three general forms of dendritic spines: mushroom-, stubby- and filopodia-shaped. Mushroom-shaped are considered mature synapses while filopodia-shaped and stubby-shaped are considered to be in the process of

forming new synapses. The mushroom-shaped spines have a head and neck region, 0.5 um and 0.1 um in diameter, respectively. The spine neck is thought to compartmentalize the spine head biochemically and electrically (42).

Transport and structural support for the dendritic spines are provided by actin filaments. The dendrite itself has a combination of actin and microtubules which provide support and transport functions. There are as many as 30,000-40,000 spines present on each large pyramidal neuron (42). Glutamatergic (excitatory) synapses are primarily found on the mushroom shaped terminals.

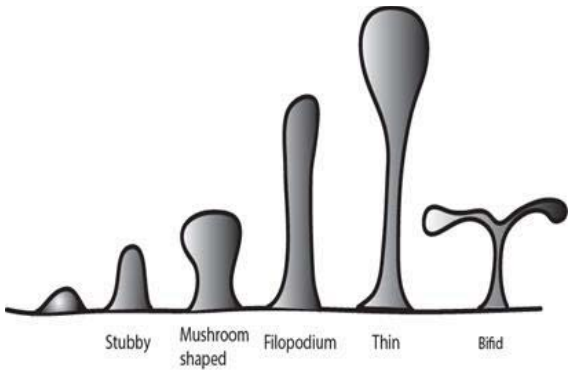

Figure 5 Dendritic spines. There are a variety of dendritic spines depending on brain location and cell type. Commonly, cortical pyramidal neurons possess simple spines: sessile (stubby), pedunculated (mushroom/thin), filopodium and branched. The shapes are believed to be a continuum of growth where mature spines have an enlarged head due to an increase in receptor density. Dendritic spines are usually 0.2-3 μm in length and 0.07-0.5 um in diameter. Spine cytoskeletal architecture is composed of actin filaments allowing for growth and retraction particularly in response to calcium(11). All spine shapes were counted in this investigation.

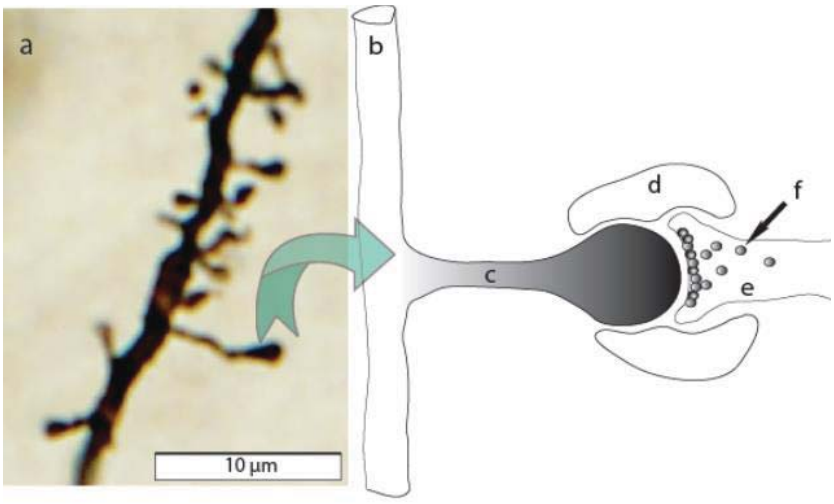

Figure 6 Synapse. Most excitatory synapses in the mammalian brain are formed at dendritic spines. (a) Micrograph of pyramidal-neuron dendrite and dendritic spines. The presynaptic connection is not visible in the micrograph; however, the postsynaptic dendritic spines are clearly visible and various morphologies can be identified. (b) Postsynaptic dendrite which has actin and microtubule cytoskeletal molecules. (c) Dendritic spine / postsynaptic connection. The dendritic spine actin-cytoskeleton is highly plastic in response to calcium flux; thus, allowing the spine to grow and retract with actin polymerization and depolymerization respectively (21). (d) Astrocyte processes. (e) Presynaptic terminal sending afferent signals to release neurotransmitters. (f) Neurotransmitters contained within synaptic vesicles located in the presynaptic terminal.

Reduction of dendritic spine density has been reported in late stage Huntington's disease (37; 45; 86), prion diseases (40), frontotemporal dementia patients (4), Down syndrome patients (79), tauopathies (49) as well as Alzheimer's disease (7). In the mouse model dendrites of the hippocampal dentate gyrus have shown swelling with beading following CCI, which is considered a hallmark of dendritic injury (42).

In order to visualize structural features of the neuron a silver stain, such as Golgi-Cox impregnation, can be performed. The Golgi-Cox method stains approximately 5% of exposed neuronal membranes with mercurous chloride. Elements appear dark in a very clear background (87). The Golgi-Cox method has been usefully applied for qualitative

analysis of neuronal morphology and quantitative evaluations such as dendritic spine counts (53; 54). This method is also useful for bright-field and confocal microscopy (88).

The results of our prior blast studies, utilizing a rat model and explosive-driven blast, show limited pathological markers when using classical histopathological (FD Neurosilver, Fluoro-Jade B) or neurobehavioral parameters of bTBI. At 241 kPa peak overpressure, neurological scores, test of motor coordination, memory, anxiety and hyper arousal are mostly negative, however, acoustic startle response is decreased 1-7 days post-blast. There is one notable aspect of the neuropathological outcome of blast exposure: blast intensity-dependent neuroaxonal degeneration, generally circumscribed to the superficial layers of the superior colliculus. Silver staining shows deteriorations at 24 hours, but is more significant 7 days post-blast. Overall, our previous blast experimental results indicate explosive blast exposure can result in subtle brain injury without gross behavior deficits.

CHAPTER 3: Materials and Methods

EXPERIMENTAL PROCEDURE

This study was conducted with two groups of blast-tested subjects: one group dedicated to collection of functional data via ECoG and fVER, and one group dedicated to collection of structural data via histopathology. Control subjects were also evaluated for each group. As illustrated in Figure 7, the study began with surgery on the rats in the functional evaluation group and their controls to implant electrodes required for ECoG and fVER data collection. After a week, these subjects underwent ECoG and fVER data collection to establish a pre-blast baseline of cortical function. A day after the functional data collection, both of the blast-tested groups (functional and structural) were exposed to an ideal blast wave, simulated via a Blast Wave Generator. A day after the blast, a subset of the functional group and controls underwent the ECoG and fVER data collection, and a subset of the structural group and controls underwent histopathological analysis. Seven days later, the remaining rats in the functional group underwent final ECoG and fVER data collection, and the remaining rats in the structural group underwent histological analysis. The following pages provide additional information about this procedure, including the animals, blast model, functional data collection, histopathological data collection, and data analysis.

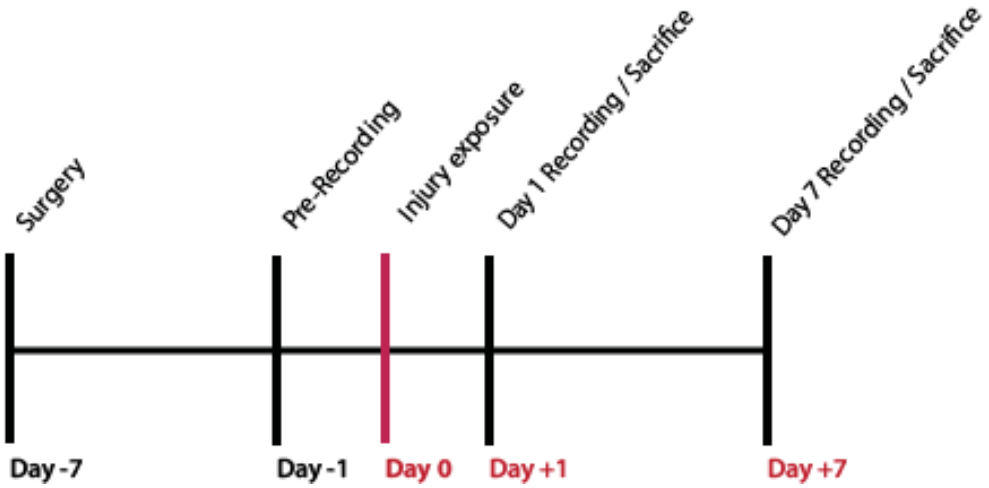

Figure 7 Experimental paradigm for unprotected single blast injury and electrophysiology recording. The diagram depicts the initial surgery and the five-day recovery period prior to the initial ECoG and flash-VER recording session. The blast injury occurs at Day 0 where upon the test subjects are exposed to a single blast then allowed to recover for 24 hours. The initial post-blast recording (ECoG and flash-VER) occurs 24 hours after the blast exposure (Day +1). Depending on group assignment the 1 day survival animals are sacrificed after the recording session while the 7 day survival animals have another recording session at Day 7 post-blast then are sacrificed. Tissue procession occurs after test subject sacrifice.

Test Subjects

Male Sprague-Dawley (Charles River, MD) rats (n = 96; 48 blast exposed and 48 control) were recruited as testing subjects for this study. Test subjects were on average four months of age and weighing 490 ± 65 g at the time of study. After model development, only 64 rats were enrolled, with 49 assigned to a blast group and 15 controls. Forty-five test subjects were removed from the study due to death, injury or technical loss, see Table 14. Final experimental data was generated from 11 rats exposed to blast and 15 non-blast controls that completed full evaluation. Final experimental numbers used for analysis are listed in Table 2.

Of the 11 rats that underwent blast testing, six underwent electrophysiological testing of fVER and ECoG and five underwent histopathological analysis. Of the six

blast-exposed rats with electrophysiology measurement, one underwent fVER and ECoG data acquisition one day after the blast event; the other five underwent fVER and ECoG data acquisition at both one day and seven days post-blast. Six of the control rats also underwent electrophysiological testing at the same time as the blasted rats. Of the five rats that underwent histopathological analysis, one was analyzed one day post-blast, and the remaining four were analyzed at seven days post-blast. Nine of the control rats also underwent histopathological testing at the same time as the blasted rats. Of the nine controls, two underwent histopathological analysis at one day post-blast and seven underwent histopathological analysis at seven days post-blast. Table 2 summarizes the test subjects for the blast experiments and control groups.

Table 2 Summary of rat groups and conditions for blast experiments.

Experiments	*Blast exposed (#)*		*Controls (#)*	
	1 day	*7 day*	*1 day*	*7 day*
Structural Group (Dendritic spine counts)*	1	4	2	7
Functional Group (ECoG and fVER)**	1	5	3	3

**No electrodes implanted; test subjects for dendritic spine quantification post-blast.*
***Implanted with monopolar epidural screw electrodes; test subjects for fVER evaluation post-blast.*

TEST SUBJECT PREPARATION

Rats were housed in pairs prior to surgery and individually after surgery in standard rat cages, in a room maintain at 64-74^{o}C and 50% humidity, free of noxious odors and noise. A reverse light schedule was maintained (light from 1800-0600 h). Purina Lab Chow (St. Louis, MO) and tap water were provided ad libitum. Animal care

was provided by Laboratory Animal Management staff. All surgical procedures and experimental procedures were performed in accordance with and approval of the established Animal Care and Use Committee at Uniformed Services University.

After at least one week of adaption to new living environment and one week prior to pre-blast data collection, functional group test subjects and controls were surgically implanted with ECoG recording electrodes (Appendix 9:), see Figure 8. The arrangement of electrodes was in a fronto-occipital orientation allowing ECoG and fVER recording from the visual cortex, see Table 3.

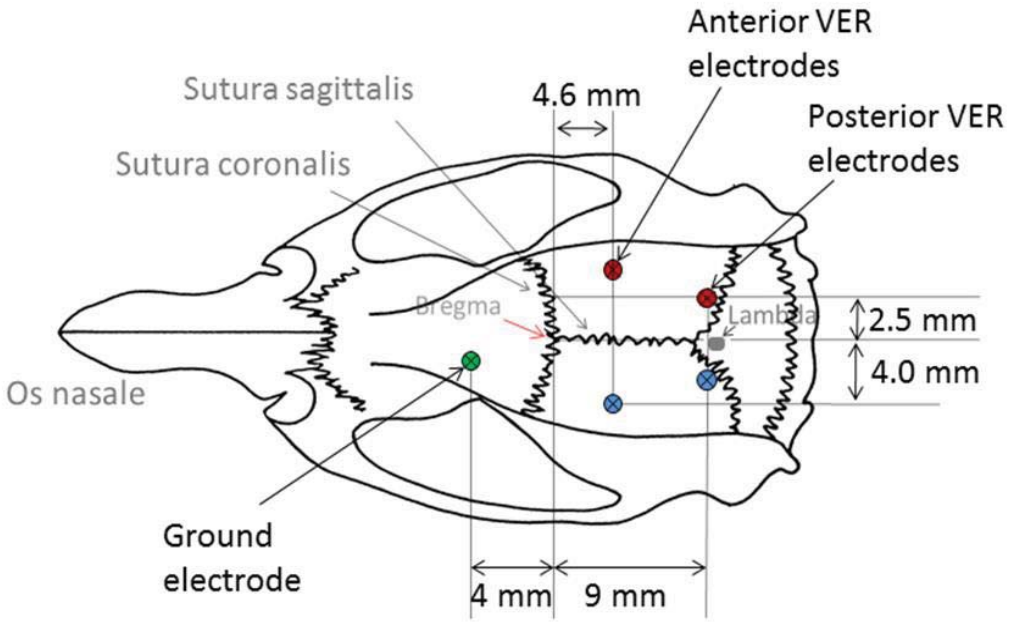

Figure 8 Epidural ECoG screw-electrode coordinates depicted on rat skull. The green circle represents the ground (reference) electrode, red circles are the right hemisphere electrodes while the blue circles are the left hemisphere electrodes. All electrode locations are referenced from bregma and lateral to the sagittal suture. Coordinates are taken from stereotaxic coordinate atlas (78): ground 4L1; anterior -4.6L4; Posterior -9.0L2.5. Figure abstracted from diagram provided by Michael Bodo, M.D., Ph.D.

Test subjects with electrodes were housed in their own individual cages. Test-subjects were checked daily for signs of distress and allowed to recover for 1 week prior to pre-blast recording session. At the conclusion of testing, electrode locations were verified histologically by looking for tissue injury on cresyl violet stained brain slices.

Table 3 Stereotaxic placement of epidural screw electrodes.

				
A. Stereotaxic coordinates	B. Drill holes	C. Place epidural screw electrodes	D. Secure electrodes	E. Secure wires and pedestal

A) Stereotaxic marking of electrode location. B) Holes drilled in skull with 0.4 mm trephine bit. C) Screw electrodes placed; tip of screw flush with inferior aspect of skull. D) Primary layer of cyanoacrylate poured over screws to ensure no movement during pedestal placement or blast exposure. E) Secondary layer of cyanoacrylate placed to secure electrode wires and pedestal; would closed with staples.

BLAST INJURY

To study the primary mechanism of injury the other mechanisms must be eliminated by prevent impact by shrapnel/ejecta, preventing movement of the test subject during blast and protecting from the explosive fireball and gases. A blast wave generator (BWG) addresses these needs by modeling an idealized explosive blast in controlled and reproducible conditions, see Figure 9 (27; 67). A BWG simulates an ideal blast wave, but requires less explosive material than would be required in a free-field simulation. The BWG is a controllable environment where shrapnel/ejecta are limited due to use of

caseless explosives in a debris free environment. Additionally, test subject movement is prevented due to use of a securing frame, and the test subject protected from heat by placing the subject in a protective sleeve located at a distance outside the explosive fireball (6). Comparison of blast waves produced by the BWG and most gas-driven shock tubes indicate that the BWG simulates a better curve fit to the Friedlander equation than the gas-driven shock tubes in parameters such as pressure and duration (43; 67).

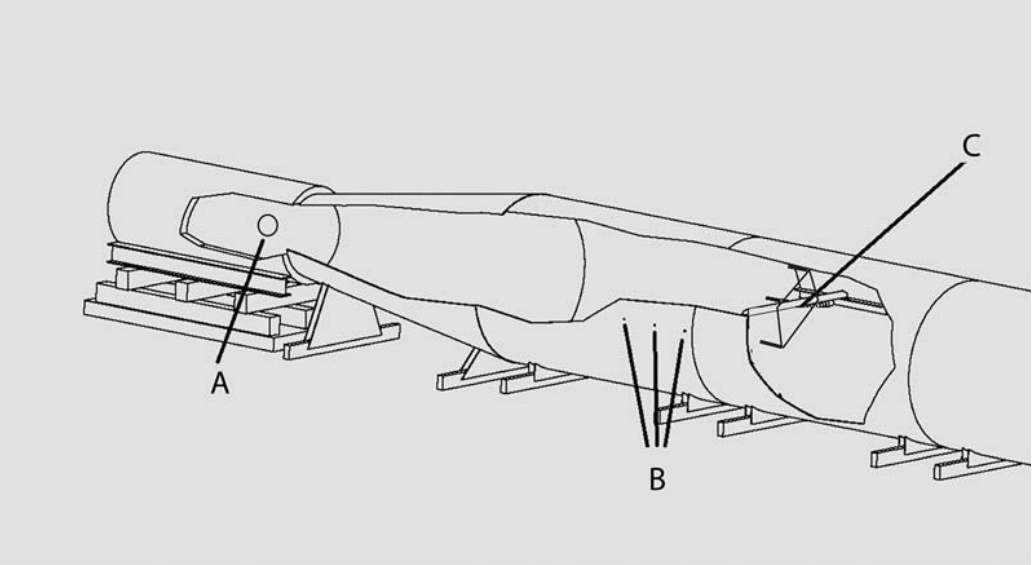

Figure 9 Blast wave generator. The BWG allows for consistent, reproducible explosive blast experimentation, controlling each of the mechanisms of injury, while minimizing the explosive charge. Spherical explosive is suspended in the driver section, location A. Gauges for recording pressure versus time are located in the conduction chamber at B and C. Test subject is secured in a holder at location C.

The BWG used for this study was located at a military test range in southern Maryland. Explosives were prepared and implemented by a contracted licensed blast-specialist. Blast-over pressure was generated by the detonation of a high performance explosive, composition-4 (C-4). The BWG is a cylindrical steel tube 22.96 meters in length, 0.86 meters in diameter at the explosive position and 1.83 meters in diameter at the opposite end, see Figure 10. Calibration blasts were conducted with piezoelectric

pressure-transducers in order to establish the explosive charge size needed to obtain the target peak pressures and ensure correct pressure sensor function. The test subjects were exposed to a single explosive blast (108-138 kPa). This blast range was selected based upon levels found in literature (52) and unpublished lab data which established the limit of lung barotrauma at 126 kPa.

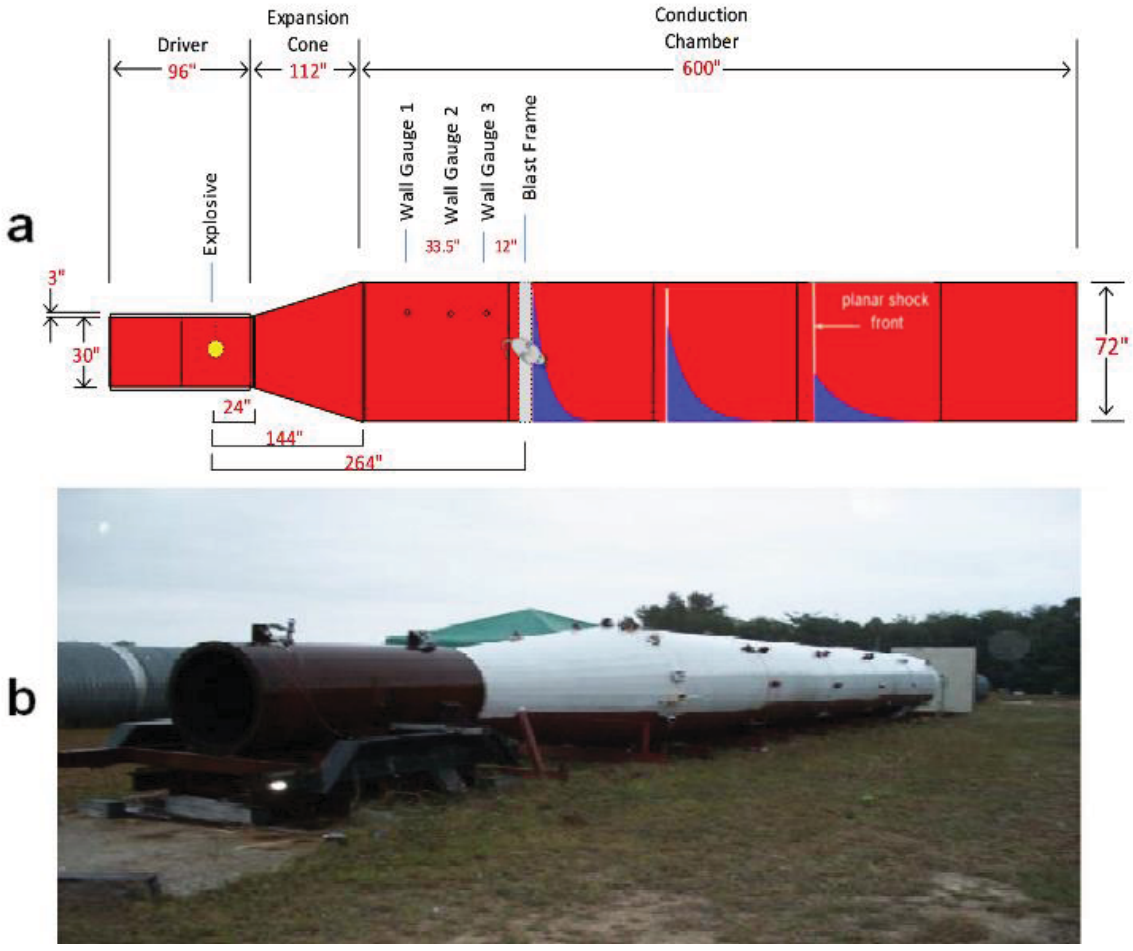

Figure 10 Blast wave generator (BWG). (a) Two-dimensional diagram of the BWG, which is comprised of the explosive containing driver section, expansion cone ending with the conduction chamber where the test subjects are exposed to the blast wave. The test subjects are secured to the blast frame, located in the conduction chamber, approximately 22' away from the explosive charge. Peak pressure decays while duration increases as blast wave progress along conduction chamber. (b) Photograph of the BWG where the driver section is closest to the observer and conduction chamber is in the distant view. Graphics and image abstracted from Richard Bauman, Ph.D.

Rats were anesthetized with ketamine-xylazine anesthetic (60/5 mg/kg). The anesthetized test rats were placed in an elastic-cloth securing sleeve to ensuring uniform positioning of limbs. The secured test subject were placed on a steel grill, ventral side down, then Velcro® strapped to the grate, at the nose shoulder and hips, in order to limit movement during blast. Two rats were placed on each grate and two grates were used, allowing four rats to be exposed to the same explosive blast, see Figure 11. The holder was fixed on a horizontal blast frame within the BWG, with the superior aspect of the rat head facing the explosive at a distance of six meters, see Figure 11 and Figure 13. Positioning of the rat in this manner is intended to optimize uniform blast exposure of the cortex.

The distance between rat and explosive was great enough to avoid exposure to the blast fire-ball, but close enough for effective blast-wave impingement. Printed Circuit Board Piezoelectric (PCB) gauges were placed at the rats' position and in the wall of the BWG at one, two and three-feet from the rat. These transducers recorded the external blast wave pressure as a function of time at a rate of 500 kHz. Pressure gauges recorded incident and reflective pressure at the position of the rat and were equidistant from the explosive. Proper positioning of pressure gauges ensures the accuracy of the recorded pressures acting on the rats and allows graphical analysis of blast curve, see Figure 12. After blast exposure the rats were examined for distress and returned to their cages to recover. Rats were followed either one-day or seven-days depending on group assignment.

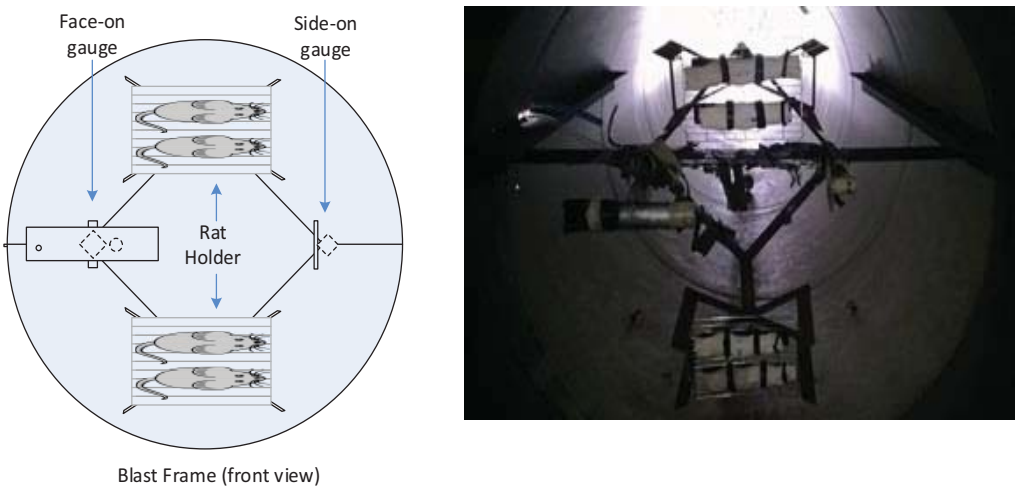

Figure 11 Test subject securing grate and blast frame within the blast wave generator. Looking from location of explosive. Test rats are wrapped in elastic tubular nylon, with back to explosive and nose pointing to the right. Rats secured to metal grids using Velcro® straps at the hip, shoulder and nose. Dampening foam placed over animals eyes. Four animals exposed for each iteration, two on bottom holder and two on top holder.

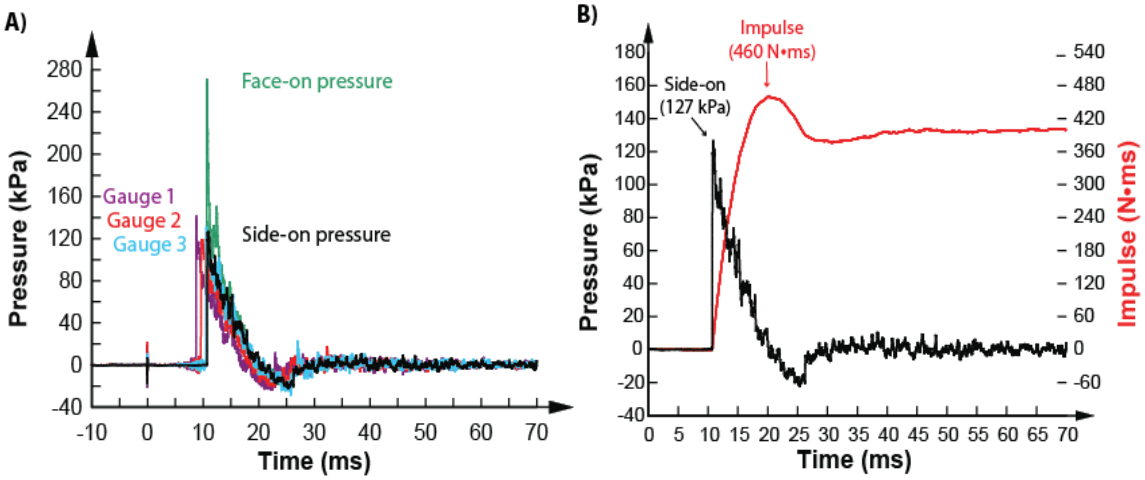

Figure 12 Blast wave pressure-time relation for a single explosive detonation in a blast wave generator. A) Pressure versus time plot for a single blast with all gauge recordings placed on one plot. Purple, red, and blue curves are wall gauge pressures while the green and black plots are the face-on (reflection) and side-on (incident) pressures respectively. Side-on and face-on gauges are located equidistant from the explosive so they have the same time point for the initial rise in pressure. (b) Pressure versus time plot showing the side-on pressure as the black plot and the impulse as the red plot. The impulse is the integral of the pressure versus time curve. The peak value of the red curve is the maximum impulse of the blast.

To ensure the test subjects and mounting apparatus did not interfere with the quasi-steady flow of the blast wave within the BWG we maintained blockage at <5% (72) and positioned the mounting frame behind the test subjects. All experimental blasts occurred in a BWG with a cross-sectional area of 4071 in^2. Blockage of the BWG, due to test subject positioning, was determined using an on-face area of 132-192 in^2. These factors were used to determine the blockage of test-subjects within BWG to be between 3.2-4.7%;

$$BWG\ Blockage\ percentage = \frac{Total\ test\ subject\ on{-}face\ area}{BWG\ cross\ sectional\ area} \times 100$$

FUNCTIONAL DATA ACQUISITION

Functional data as measured using ECoG and fVER was acquired one day prior to blast exposure, one day following blast exposure and seven days following blast exposure. As illustrated in Figure 14, rats were placed in a "mirror box" for the data collection. A PS33 Plus photic stimulator, (Grass, Warwick, RI) with flash intensity of 32 Lux, was used as the flash stimulus and time-locked to the VER.

Analog waveforms were recorded at a rate of 1000 samples/sec for fVERs and 200 samples/sec for ECoGs, with a 16-bit resolution AD card (National Instruments, Austin, TX) using the DataLyser® software developed at Walter Reed Army Institute of Research. The setup is illustrated in Figure 13, and additional details regarding the data acquisition equipment are available in Appendix 10:.

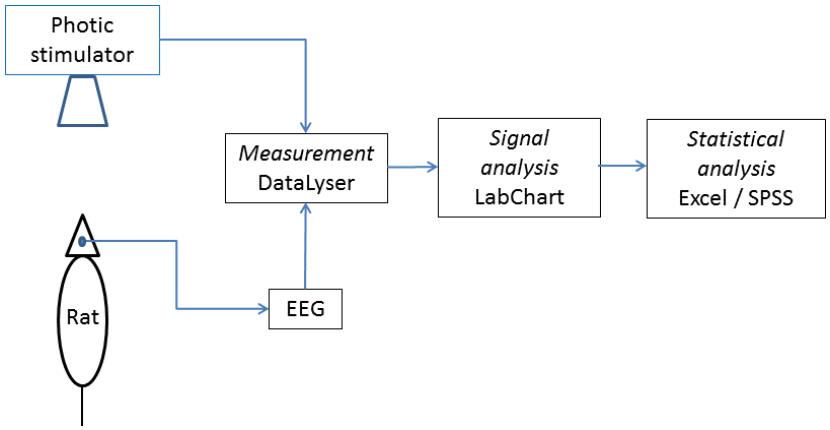

Figure 13 Block diagram of rat electrophysiology recording and data processing. Sampling rate of analog digital conversion was 200 samples/sec for ECoG and 1000 samples/sec for fVER, 60 Hz notch filter was used, and low-to-high band-pass filter was set 0.3-75 Hz. Photic stimulator was only used for fVER recording sessions. Raw data was acquired with Datalyser® software, converted to a text file with MATLab® software followed by frequency analysis with LabChart® software. Statistical analysis and plotting of data was performed with Microsoft Excel®, IBM SPSS® and GraphPad Prism® software. Figure abstracted from diagram provided by Michael Bodo, M.D., Ph.D.

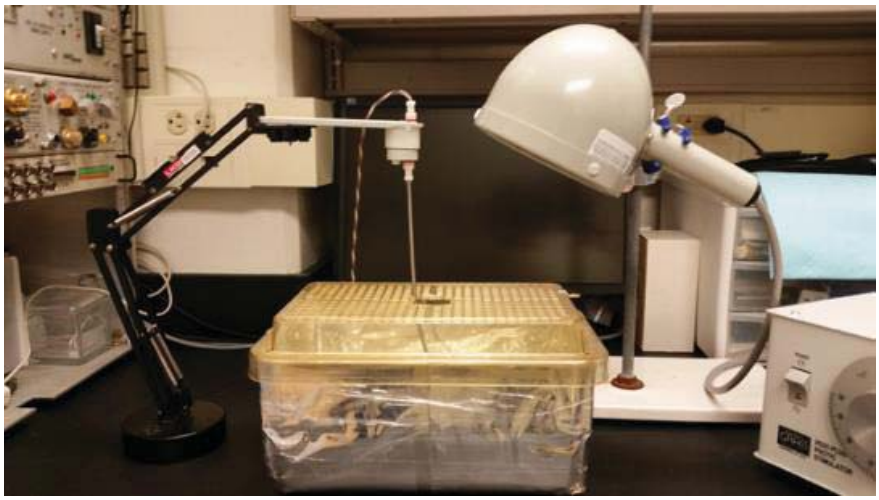

Figure 14 Electrophysiology recording equipment. A mirrored box is used to maximize test-subject exposure to the flash of the photic stimulator. The mirrored box was produced from a standard translucent laboratory mouse housing-box. The box was covered with Mylar (98% reflectivity), allowing reflection of light. A hole is cut in the housing-lid to allow passage of commutator cable during test-subject movements.

Flash-visual evoked response (fVER)

Prior to the fVER recording session, test-subjects were placed in isoflurane induction chamber for no more than three minutes at 4% isoflurane and 1 LPM O_2. Once induction started, identified by slowed movement, the test-subject was attached to the commutator via commutator cable then placed in the recording chamber (mirror box), laying on its left side, with its nose facing the direction of the PS-flash lamp. Once the test-subject was awake and moving, the recording session began with 30 minutes of dark adaption to maximize sensitivity to the PS-flash. Thereafter, data were collected through three sets of 5 minute baselines followed by 60 flashes. Data collection concluded with a final 5-minute baseline. All recordings took place under red light conditions. The flash interval was between 1 and 5 seconds. A total of 180 fVERs were recorded during each test-subjects recording session, see Figure 15.

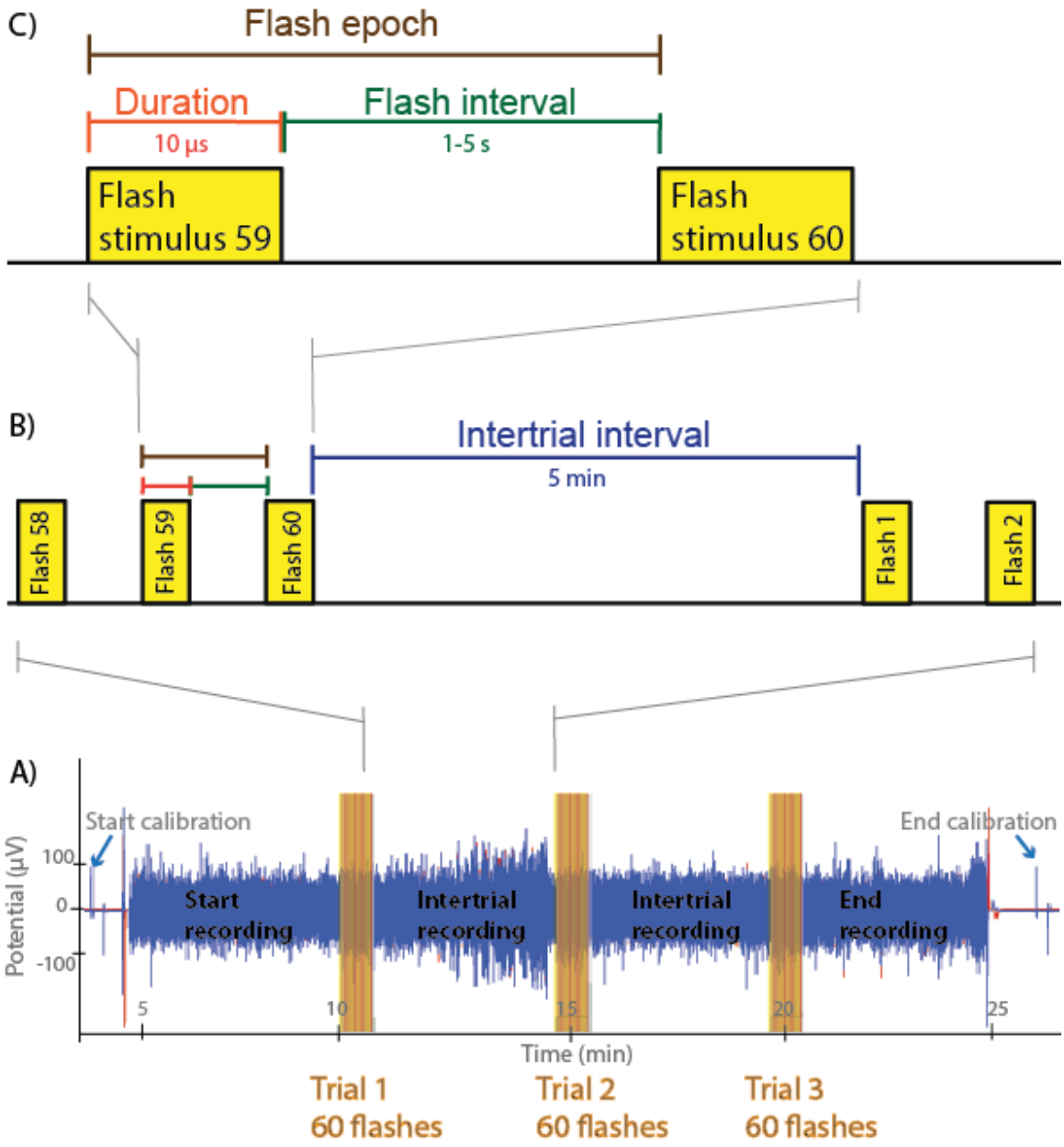

Figure 15 Overview of Flash-Visual Evoked Response Procedure. A) Recording (dark blue) of cortical electrical potential (µV) versus time (min). Yellow bars are the software generated indices of PS-flashes. Calibration of recording was performed by using ±100 µV reference voltages (light blue) at the start and end of the recording. Three trials of 60 PS-flashes were performed with five-minutes separating each trial. B) Illustration showing an enlargement of the last three PS-flashes of trial 1, followed by the five-minute intertrial interval and the first two PS-flashes of trial 2. Each trial contained 60 fVERs followed by a five minute intertrial interval. Electrical potentials are not shown. C) Enlarged illustration of PS-flash 59 and 60 of trial 1. Each PS-flash has a duration of 10 µs. Time between flashes (interflash interval) is on to five seconds.

Pre-blast, post-blast 1-day and post-blast 7-day sessions were analyzed with LabCharts7 software (1000 potentials/sec recording rate, 300 ms recording epoch, 180 epochs averaged per recording session). A typical recording with VER is shown in Figure 16.

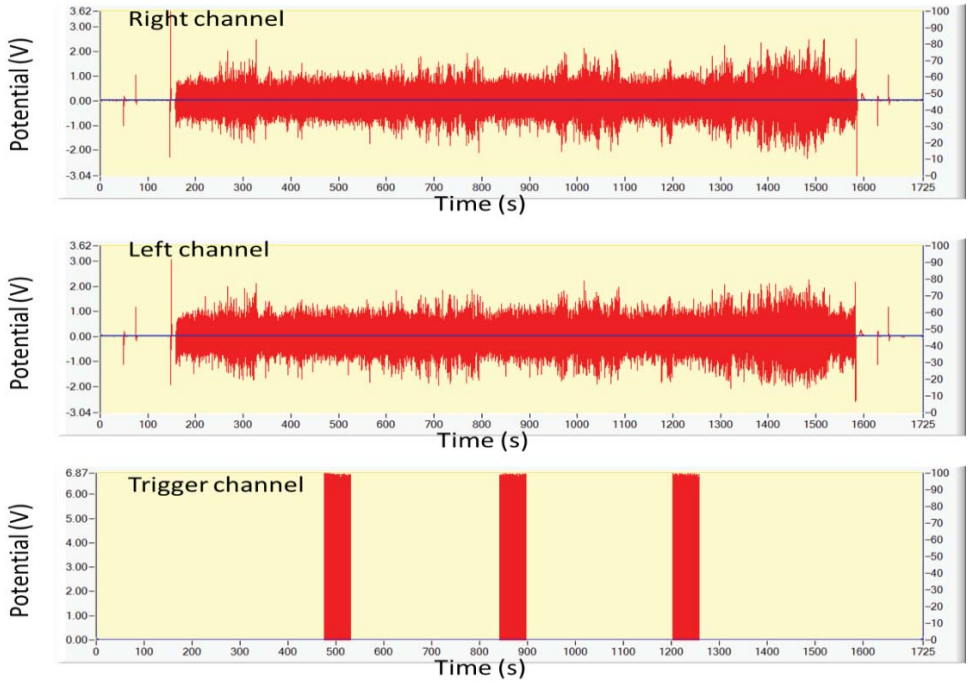

Figure 16 Recording of 180 flash-visual evoked responses from bilateral epidural electrodes. Visual evoke response recordings for the right and left hemisphere, upper and middle plot respectively. Channels were calibrated with 100 µV at the beginning and end of recording session which can be seen in the right and left channel recordings; this allowed conversion of the recording voltage to microvolts. Three iterations of sixty photic stimulator flashes were performed for each session. The lower plot is the trigger channel; each orange vertical bar contains 60 triggered photic-stimulator flashes. Flash interval was between 1-5 s and five minutes occurred between each of the three sessions. All three plots align vertically which allows visualization of both channel responses to each flash iteration.

STRUCTURAL DATA ACQUISITION

To evaluate structural changes caused by explosive blast exposure, Golgi-Cox (GC) staining was performed using the NoraUltra Golgi-Cox Stain Kit (IHCWorld LLC.

Woodstock, MD). Using the procedure abstracted from IHCWorld, at one day or seven days post-blast exposure, rats were euthanized and transcardially perfused with 250 mL of ice-cold 0.9% normal saline followed by 250 mL of ice cold 4% paraformaldehyde (PF), in 1x PBS.

Brains were removed and post-fixed in the 4% PF overnight at 4 °C. Brains were blocked and placed in 22 mL of Golgi-Cox impregnation media for at least 14 days, stored at room temperature and shielded from light. The GC impregnation media was changed after 48 h. After 14 d the brains were cryoprotected in a 30% sucrose-1x PBS solution for 24 h, changed after the first hour. The brain was then flash-frozen in dry ice chilled 2-methylbutane. Brains were mounted and sectioned at -10 °C for 150 μm sections and mounted on gelatin-coated slides (FD NeuroTechnologies, Ellicott City, MD). Bright-field microscope images of pyramidal neurons in cortical layers II/III were captured using 63x objective on an Olympus BX60 microscope (Olympus Optical Co. Japan).

Double-blind dendritic spine counts were performed by two independent investigators. Dendritic spine density was calculated for apical and basilar dendrites. Spine density of the first branch of the primary basilar dendrite was determined by counting the number of spines 30-100 μm from the soma. Apical oblique (AO) dendritic branches, emerging from the primary apical dendrite, were used to determine apical spine density at least 30 μm but less than 100 μm from the soma. A single neuron was used for each measure of AO or basilar spine density; only healthy pyramidal neurons were used in the count. Any neurons with broken segments, swelling or crenation of projections were not counted (97), see Figure 17.

Bright field microscope dendritic spine counts were confirmed using reflective confocal microscopy (11; 42; 87).

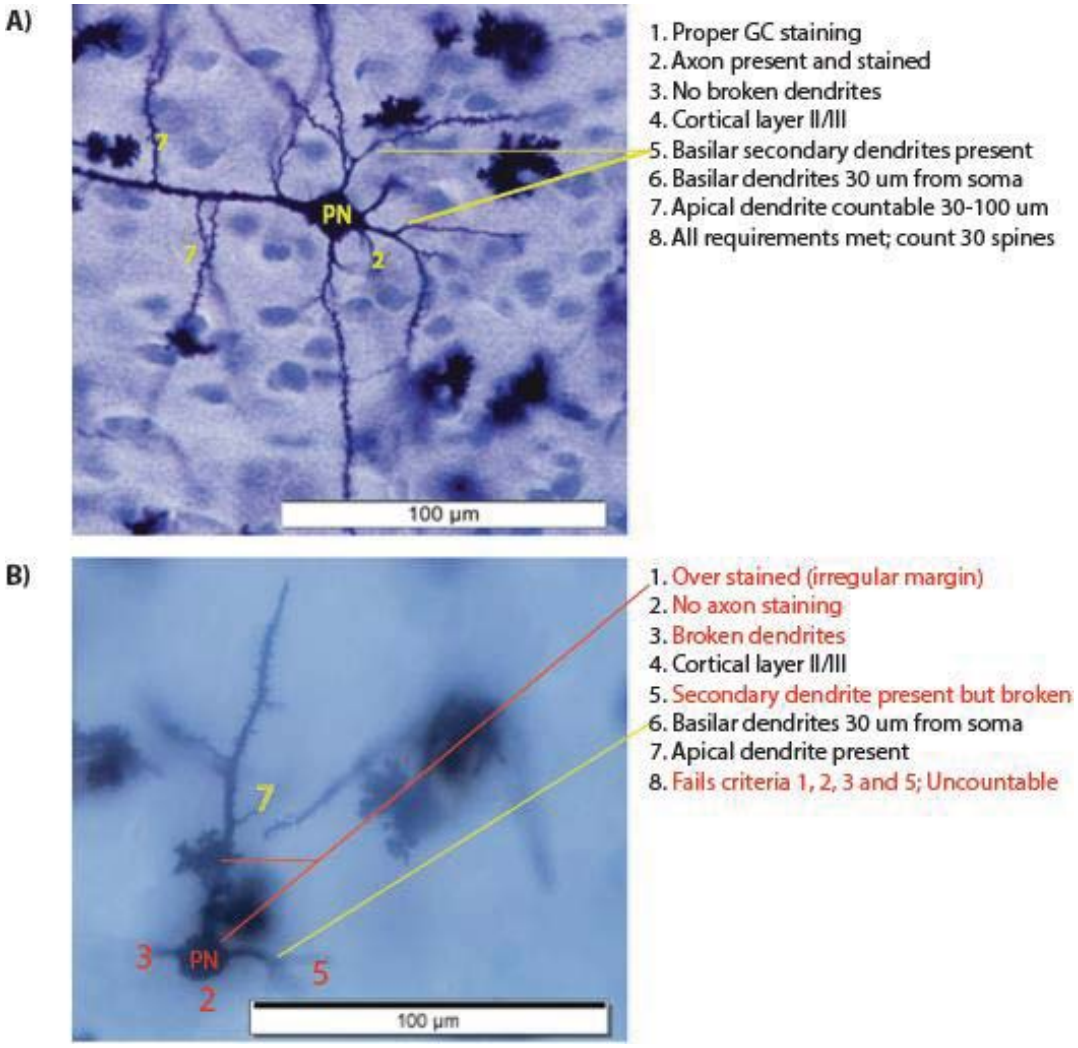

Figure 17 Requirements for counting cortical layer II/III pyramidal neuron (PN) dendritic spines stained with Golgi-Cox primary stain and cresyl-violet counterstain. A) Micrograph shows a neuron meeting the criteria for counting dendritic spines. B) Micrograph shows uncountable neuron that is over impregnated, no axon and has broken dendrites. Requirements for counting pyramidal neurons: 1. Sufficient Golgi-Cox staining, 2. Intact: axon, apical dendrites and basilar dendrites, 3. No broken segments, 4. Located in cortical layer II/III, 5. Secondary dendrite, 6. Basilar dendrites 30 µm from soma, 7. Apical dendrites 30-100 µm from soma, 8. 30 spines per count, 9. ≤ 6 counts per hemisphere of section.

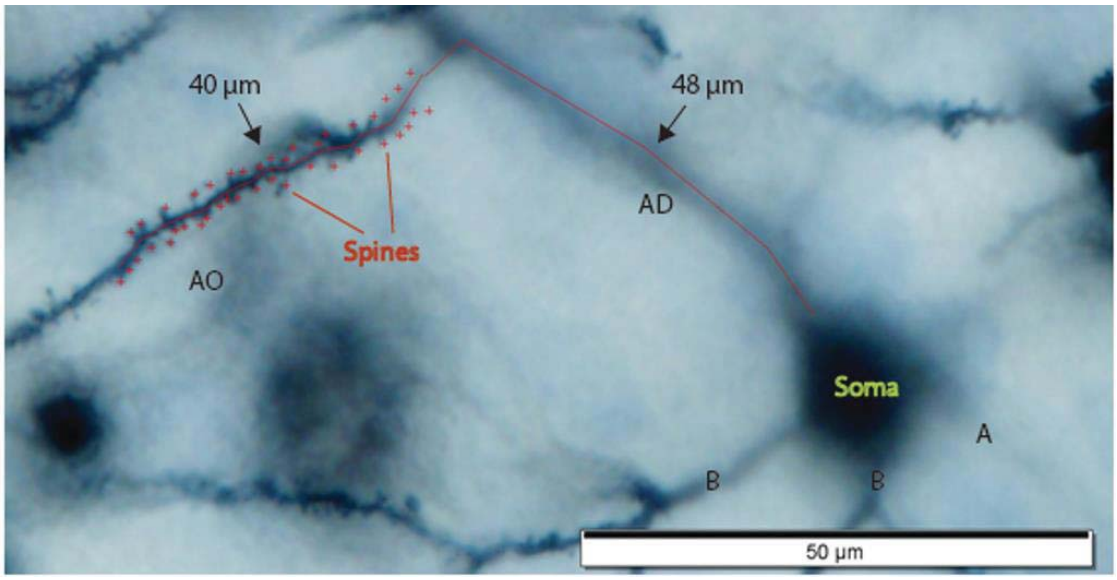

Figure 18 Apical dendrite spine counting. An intact cortical layer II/III pyramidal neuron with apical dendrite (AD). The containing countable region on apical oblique (AO) dendrite 30-100 µm from the soma. Dendritic spines, marked with red crosses, were counted then divided by the length over which the count occurred. Apical spine density shows 0.75 spines/µm. The axon (A) projects deeper into the micrograph and is next to two basilar (B) dendrites.

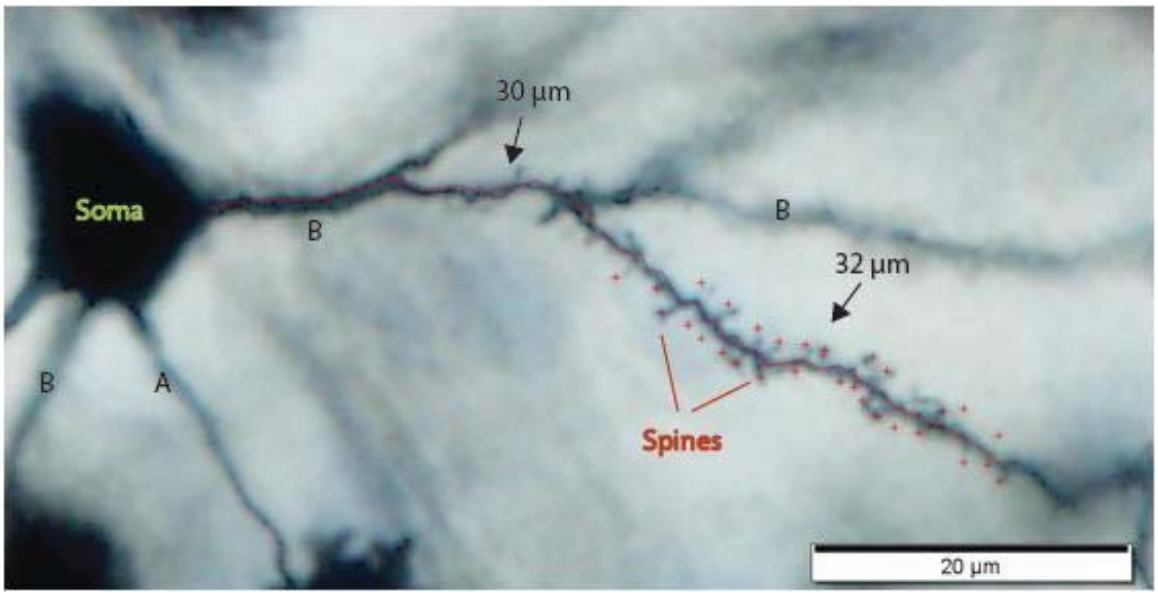

Figure 19 Basilar dendrite spine counting. An intact cortical layer II/III pyramidal neuron with a secondary basilar dendrite 30 µm from the soma. Thirty dendritic spines were counted then the resultant number of spines was divided by the length over which the counts occurred. Micrograph basilar spine density is 0.94 spines/µm. Axon (A), basilar dendrite (B), red crosses mark dendritic spines.

DATA ANALYSIS

VER Peak amplitude and latency

Signal averaging was performed from 0.1 ms before flash stimulus to 250 ms after flash stimulus. Recordings of durations less than 100% of the recording interval (250 ms) were excluded from the average. One hundred and eighty VERs were averaged and the results exported to and plotted using MS Excel®. Local maxima and minima were obtained from the spreadsheet and averaged between groups. Repeated measures analysis of variance (RMANOVA) was used to determine the variance of peak amplitude and latency between and within groups.

VER Cross-correlation

The cross-correlation is used to identify time lag which may be due to electrode placement or hemispheric signal conduction defects. The correlation coefficient assumes zero time lag when comparing left and right hemisphere recordings; therefore, the correlation coefficient is affected if the delay between the trigger pulse and the VER transient are different for left and right hemisphere recordings.

To calculate the cross-correlation, the data analyzed using an in-house generated MATLAB script that automated VER waveform analysis of the cross-correlation of left and right hemisphere waveforms. The leading edge of the trigger waveforms was used to collect the subsequent 250 ms for analysis. A correlation sequence was calculated from the sliding dot product at all positive and negative lag positions. For left and right hemisphere fVERs, $\boldsymbol{X}$ and $\boldsymbol{Y}$, of recording length N, the cross-correlation between $\boldsymbol{X}$ and $\boldsymbol{Y}$ at lag τ is defined as:

$$r(\boldsymbol{X},\boldsymbol{Y},\tau) = \frac{1}{N-\tau}\sum_{N-\tau}^{i=1}\frac{(x_i-\bar{X})-(y_{i+\tau}-\bar{Y})}{\sigma_X\sigma_Y},$$

In which $\overline{X}$ and $\overline{Y}$ are the means, σ_X and σ_Y are the standard deviations of $\boldsymbol{X}$ and $\boldsymbol{Y}$. A probability plot was used to illustrate the results. Increase in the maximum cross-correlation value indicates a greater similarity of the two signals at a given lag position.

ECoG data processing

Electroencephalograms were analyzed using three approaches. First, the Hjorth mobility was calculated with DataLyser® software using a thirty second analysis window. Hjorth mobility represents the proportion of standard deviation of the power spectrum and is determined by the square root of the variance of the first derivative of the signal divided by the signal. The Hjorth mobility was compared (control - before blast, day 1 and 7 after blast) using an analysis of variance. Second, a Fast Fourier transformation was applied and the results were presented from 0-20 Hz. Electrocorticogram Fast-Fourier transforms were used to indicate the frequencies within the theta bandwidth (4-8 Hz) that were the most common. Third, Pearson's correlation coefficient was calculated for comparison of right and left hemisphere ECoG-activity with a brain monitor script. A positive index (positive correlation) implies identical phase, while a negative index (inverse correlation) implies opposite phase.

Morphometry; dendritic spine density

Mean dendritic spine densities were separated into cortical layers and apical or basilar counts. The mean dendritic spine density in blast exposed subjects were

statistically compared to spines from similar areas of non-blast control subjects using Student's *t*-tests.

CHAPTER 4: Results

BLAST LOADS

The blast wave pressure versus time data were collected with five PCB piezoelectric gauges positioned along the BWG, see Figure 10. The side-on gauge (PCB5) data, located at the level of the animal, was used to determine the peak pressure for each of the 14 blast sessions. Figure 20 illustrates all fourteen blast recordings collected over three days. On the second day of blast sessions the blast grid was damaged and replaced with a new grid for the final blast day. The grid replacement positioned the test subjects ~2 inches closer to the explosive. Peak over-pressure ranged from 108 kPa to 138 kPa, across the blast sessions (n = 14). The mean peak over-pressure recorded at the side-on (incident) PCB gauge was 124 ± 8.85 kPa, with an average positive phase duration of 9.97 ± 0.10 ms. The average reflective pressure was recorded at the face-on PCB gauge. Table 4 summarizes characteristics of blast measurements.

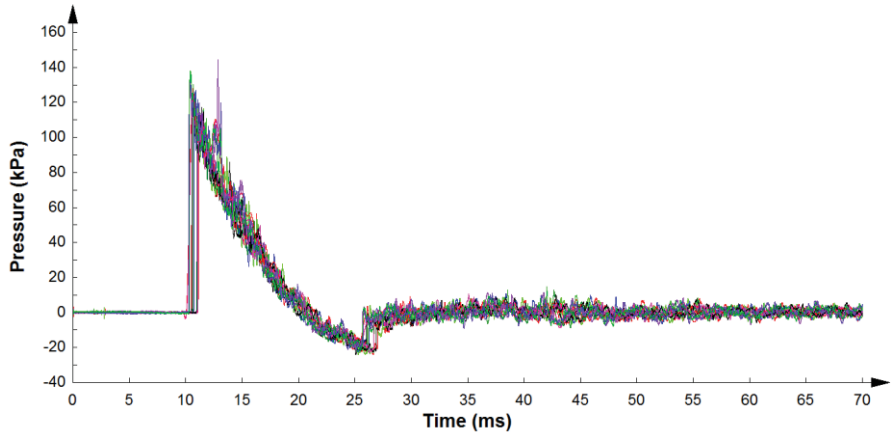

Figure 20 Combined pressure versus time recordings for blast wave generator experiments. All blast recordings (n = 14) occurred over three separate testing days and are recorded from the side-on gauge (PCB5). Rat-holder was replaced for the third blast session (animals ~4 cm closer to blast) which resulted in the rise in pressure occurring earlier and can be noted by the time difference noted in the green and red curves.

Table 4 Summary of blast wave characteristics for 14 detonations, 108-138 kPa

	Mean		*SEM**	*SD***
Peak pressure (kPa)	123.6	±	2.37	8.85
Positive phase duration (ms)	9.97	±	0.10	0.38
Reflective pressure (kPa)	313.0	±	12.5	43.2
Impulse (N·ms)	485.0	±	13.3	49.8
Wavelength (m)	3.99×10^{-2}	±	7.72×10^{-4}	2.89×10^{-3}
Frequency (kHz)	12.0	±	0.173	0.648

*Standard error of the mean (*SEM*)
**Standard deviation (*SD*)

FUNCTIONAL RESULTS

Electrocorticography Results

The ECoG recordings were analyzed to determine whether the correlation of frequencies between the left and right hemispheres was impacted by the blast (Frequency Correlation). They were also analyzed to determine whether the Hjorth mobility was impacted by the blast, and whether the peak frequency calculated in a Fast Fourier Transform was impacted by the blast. The following sections provide a summary of these results.

Frequency Correlation

The ECoG recordings were analyzed to determine the correlation between the left and right hemisphere responses. To do so, a correlation coefficient was calculated for each test subject's recordings, see Figure 21, with a coefficient of one indicating identical left and right hemisphere ECoGs and a coefficient of zero indicating now similarity between the ECoG recordings.

The correlation coefficients from the pre-blast recordings (M=0.598, SD=0.164) were not statistically significantly different from those from the recordings taken one day

post-blast (*M*=0.602, *SD*=0.174), t (20) = 0.094, *p* = .93. In fact, looking across all three timepoints, there were also no statistically significant effects of blast exposure on the correlation coefficients (*F* (1.6, 4.8) = 1.1, *p* =.32); see Figure 21.

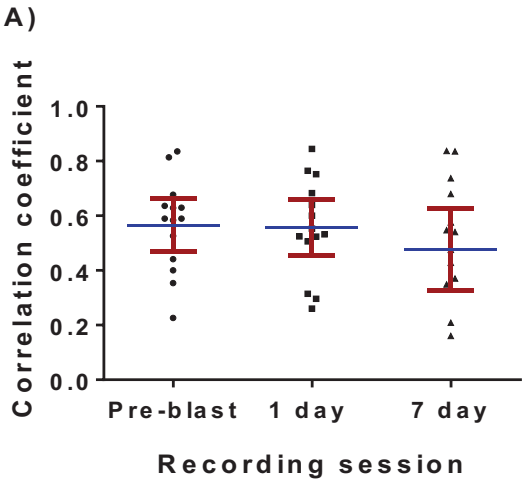

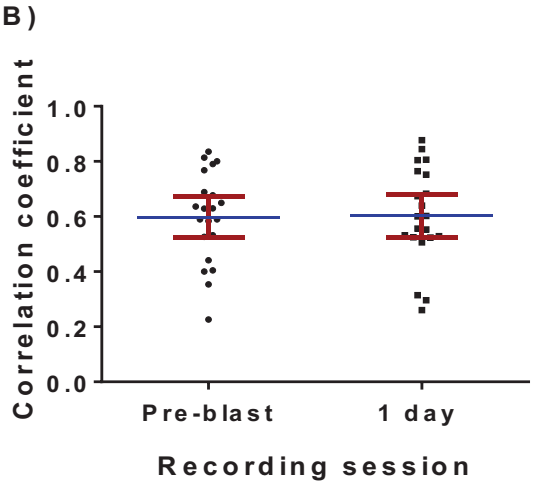

Figure 21 Correlation coefficient of left and right hemisphere ECoG frequencies. Each data point is a test subject's correlation coefficient between left and right hemisphere ECoG for the recording session. Correlation coefficient of 1 or 0 indicate identical or dissimilar ECoG respectively. There is a non-significant decrease in similarity between left-right ECoGs at 7 days post-blast.

Hjorth Mobility

The ECoG time domain analysis was performed by calculating the Hjorth mobility. Hjorth mobility represents the proportion of standard deviation of the power spectrum and is determined by the square root of the variance of the first derivative of the signal, divided by the signal. The Hjorth mobility was calculated across the three

recording sessions in the left and right hemispheres of 21 test subjects one day post-blast and 14 subjects seven days post-blast, see Figure 22.

There was no statistically significant change in Hjorth mobility between the pre-blast condition (M=0.32, SD=0.045) and the one-day post-blast condition (M=0.325, SD=0.035), t (41)=1.44, p=.16. There was also no statistically significant effect of explosive blast exposure on mobility when looking across all three timepoints (F (1.86, 50.13) = 0.97, p=.38).

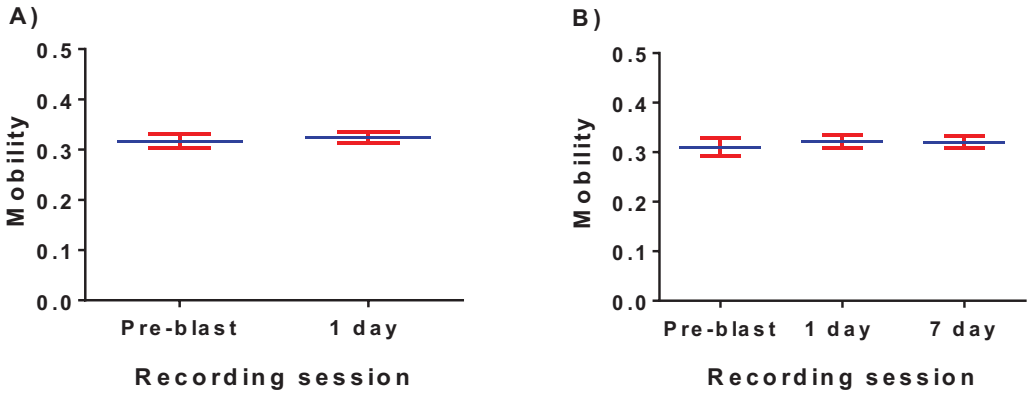

Figure 22 Hjorth mobility of left and right hemisphere ECoG recordings. A) Test subjects (N = 14) pre-blast, post-blast 1d and post-blast 7d recordings. B) Test subjects (N = 21) pre-blast and 1 day post-blast recordings. All recording sessions are displayed on mobility vs recording session plot. Each data point is a group members left or right hemisphere ECoG-mobility; red error bars represent the 95% confidence interval around the around the mean (blue).

Fast-Fourier Analysis

Electrocorticogram frequency domain analysis was performed using Fast-Fourier analysis of the recordings from the left and right hemispheres of the eight one-day survival and sixteen 7 days survival subjects. Electrode failure and signal loss resulted in 11 recordings for the 7 day group and 8 recordings for the 1day group being unusable.

Thus, a total of 21 recordings were analyzed from the three sessions of data collection from the rats that survived seven days, and 40 recordings were analyzed from the two sessions of data collection from the combined one and seven-day survival groups.

The ECoG Fast-Fourier transforms (FFT) indicated that frequencies within the theta bandwidth (4-8 Hz) were the most common, see Figure 23. There was no statistically significant difference between the pre-blast condition (M=6.30, SD=0.66) and the one-day post-blast condition (M=6.35, SD=0.54) peak FFT frequencies, t (0.44) = 39, p=.66. There was also no statistically significant change in peak FFT frequency across the three time points (F (1.75, 35.06) = 2.39, p=.11).

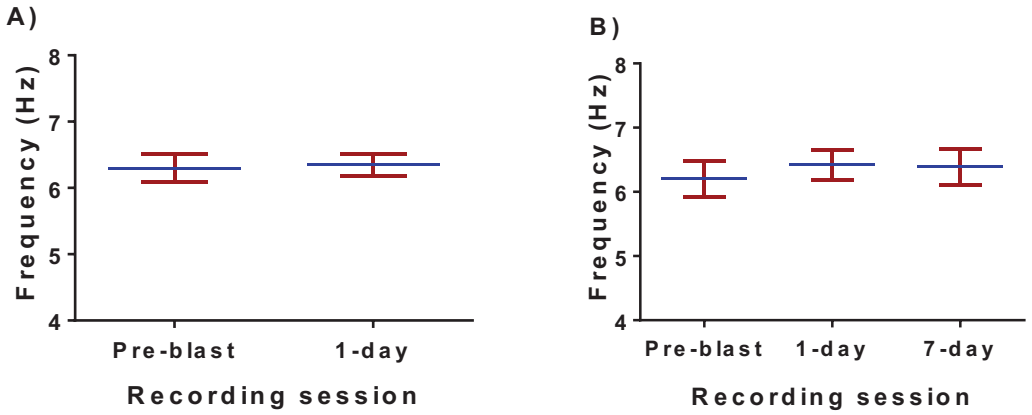

Figure 23 Theta dominant bandwidth of left and right hemisphere ECoG recordings. A) Test subjects (N = 20) with two ECoG recording sessions. B) Test subjects (N = 11) with three ECoG recording sessions; One test subject only had a right hemisphere recording for the three sessions. The theta bandwidth (4-8 Hz) produced the dominant frequencies for all recording sessions however there were no statistically significant changes in frequency. Cortical ECoGs were recorded from the left and right hemisphere of all test subjects. Fast-Fourier transformation of each ECoG was performed and the largest frequency component of the FFT was plotted versus recording session. Each data point is a left or right hemisphere FFT peak frequency. Red error bars represent the 95% confidence interval about the mean (blue).

Flash-Visual Evoked Response

Signal averaging increases the S/N of fVER peak amplitude and latency. In order to illustrate this increase, we plotted an increasing number of fVERs recorded from one hemisphere of a non-injured test subject. Averaging 20 fVERs or 40 fVERs produced very different plots; however, averaging 160 fVERs or 180 fVERs resulted in overlying plots. Plotting an increasing number of the fVERs versus time illustrates how an average of >160 fVERs results in consistent latency and amplitude for peaks P1 and N1, see Figure 24.

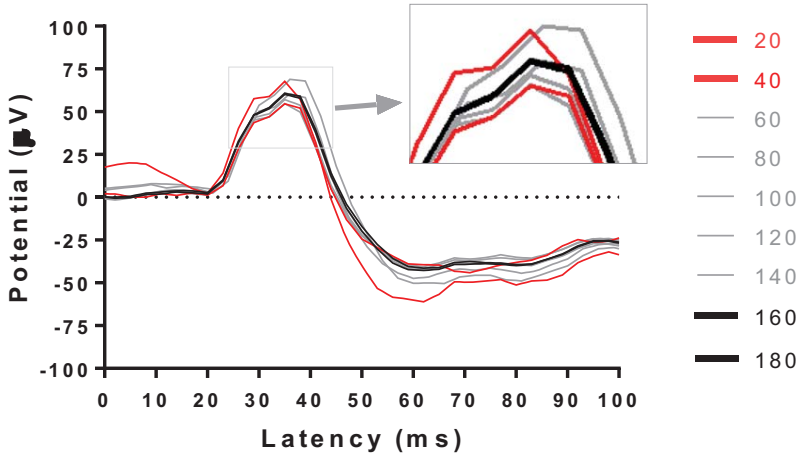

Figure 24 Signal averaging of fVERs increases consistency of peak amplitude and latency. Evoked response recordings have high temporal resolution (i.e., peaks consistently occur at the same time point) but low spatial resolution (i.e., peaks amplitude is highly variable). In order to increase spatial resolution multiple fVERs must be averaged. Plot of fVERs versus time for a hemisphere recording with increased number of fVERs averaged per curve; the number of fVERs averaged per curve are identified to the right of the image. Curves that are closer to each other represent an increase in the signal to noise ratio. The inset diagram of the N1 peak shows how signal averaging can increase S/N and identify consistent latency and amplitude of local maxima and minima. Each curve represents a recording session of increasing fVER averages where red curves are the average of 20 or 40 fVERs (note separation) while the overlapping black curves are averages of 160 and 180 fVERs. The individual grey curves are an increasing average of 60-140 fVERs. This indicates that a minimum of 160 fVERs must be averaged in order to get a representative fVER amplitude.

Local maxima/minima latency and potential

Each test subject's post-blast fVER was compared to its pre-blast fVER in order to determine changes in peak amplitude and latency. Figure 25 shows a plot of one test subject's fVER recordings in which each plot is the average of 180 fVERs. The initial local minima is the P1 occurring at ~17 ms peak while the following local maxima is the N1-peak occurring at ~31 ms. Peak latencies and changes in amplitude were compared between post-blast and pre-blast recordings. The fVER analysis concluded by calculating the maximum cross-correlation (CXC) to determine the similarity between an individual test subject's left and right hemisphere fVER while accounting for any time lag between the signals. The results of each of these analyses are provided in the following pages.

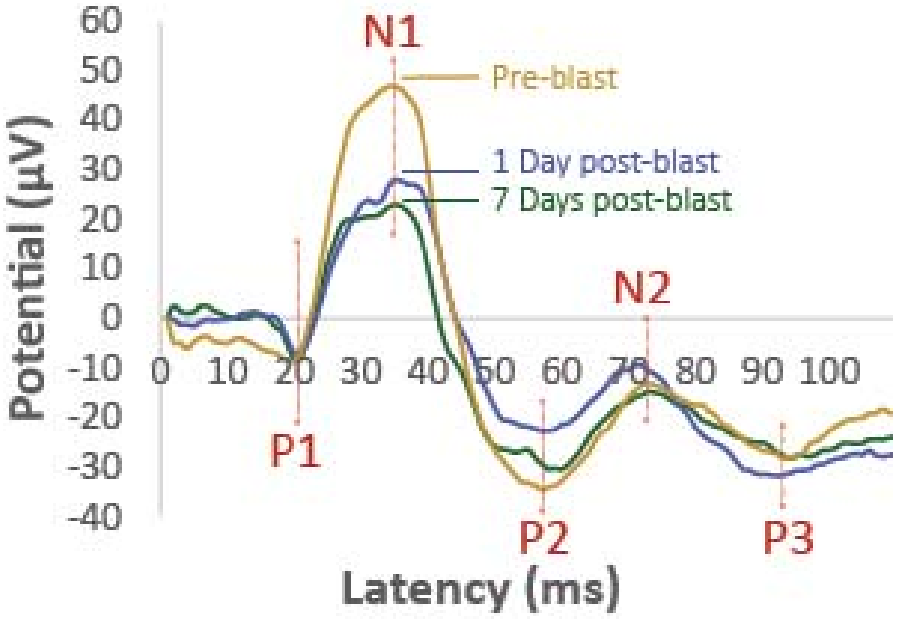

Figure 25 Flash-visual evoked potentials before and after blast exposure. The plot of fVEP electrical potential versus latency of onset. Pre-blast (gold), 1-day post- (blue) and 7-days post-blast (green) recordings. Photic stimulator flash occurred at the zero time point. Electrical potential vs latency plot identifies the initial five local minima and maxima of the fVER. The P1 to N1 components reflect integrity of the optic nerve while P2 onwards reflects processing by higher cortical centers. Flash-VERs have high temporal resolution even though our resolution was ± 2 ms. Latency of minima and maxima are identified by red vertical lines. Each trace is an average of 170-180 fVERs.

Flash-VER peak latency pre-blast and post-blast

All hemispheric recordings were compared to determine changes in peak latency between pre-blast and post-blast exposure conditions, see Figure 26. Five test subjects left and right hemisphere latency data were averaged and plotted, see Figure 26. All data was pair matched allowing each individual test subject's recording to be analyzed for pre-blast vs post-blast latency changes. Paired two-way repeated measures analysis of variance (RMANOVA) with post-hoc Tukey's multiple comparisons test were used to compare cortical hemisphere latency changes. Two-way paired RMANOVA results indicated there were significant changes in latencies for P1, N1, P2 and N2 peaks, see Table 6; however, post hoc Tukey's multiple comparisons test showed no significance for P1 and N1 latencies in either hemisphere. Transient latency changes for right hemisphere P2 and N2 peaks at one day post-blast were significant by post hoc Tukey's multiple comparisons test but were not significant at seven days post-blast. The limit of resolution of the recording equipment being ±2 ms combined with small sample size and subtle transient changes in latency indicate this data must be considered with skepticism, see Table 5 and Table 6 for summary of results.

Table 5 Latency of Local Minima and Maxima for Left and Right Hemisphere fVER recordings

Peaks (ID)	Hemisphere	Pre-blast Latency *Mean* ± *SD* (ms)	1-day Latency *Mean* ± *SD* (ms)	7-day Latency *Mean* ± *SD* (ms)
P1	Left	17 ± 1	18 ± 1	18 ± 1
	Right	17 ± 2	18 ± 2	18 ± 1
N1	Left	31 ± 4	33 ± 2	32 ± 4
	Right	28 ± 2	30 ± 4	29 ± 5
P2	Left	58 ± 3	61 ± 10	61 ± 7
	Right*	53 ± 7	62 ± 11	55 ± 7
N2	Left	67 ± 2	71 ± 6	68 ± 4
	Right*	66 ± 3	76 ± 9	66 ± 1
P3	Left	99 ± 12	96 ± 13	87 ± 11
	Right	94 ± 13	93 ± 9	88 ± 8

*Indicates a significant ($P < 0.05$) change in latency for 2-way RMANOVA and post hoc Tukey's test at 1 day.

Table 6 Two-Way Repeated Measures Analysis of Variance for Testing Latency of Local Minima and Maxima of Left and Right Hemispheric fVER Recordings

Peaks (ID)	Interactions	*F*-test	
P1	Interaction	$F(2, 16) = 0.05$	$P = 0.954$
	Day*	$F(2, 16) = 5$	$P = 0.017$
	Hemisphere	$F(1, 8) = 0.006$	$P = 0.940$
N1	Interaction	$F(2, 16) = 0.01$	$P = 0.987$
	Day*	$F(2, 16) = 5$	$P = 0.017$
	Hemisphere	$F(1, 8) = 2$	$P = 0.192$
P2	Interaction	$F(2, 16) = 1$	$P = 0.350$
	Day*	$F(2, 16) = 4$	$P = 0.037$
	Hemisphere	$F(1, 8) = 0.6$	$P = 0.467$
N2	Interaction	$F(2, 16) = 2$	$P = 0.176$
	Day*	$F(2, 16) = 9$	$P = 0.002$
	Hemisphere	$F(1, 8) = 0.06$	$P = 0.817$
P3	Interaction	$F(2, 16) = 0.2$	$P = 0.810$
	Day	$F(2, 16) = 2$	$P = 0.134$
	Hemisphere	$F(1, 8) = 0.3$	$P = 0.592$

Interaction: refers to the variance of all hemisphere recordings. Day: refers to the variance of the latency between recording sessions. Hemisphere refers to the variance of latency between left and right hemisphere recordings. *Indicates a significant ($P < 0.05$) change in latency for 2-way RMANOVA and post hoc Tukey's test at 1 day. *Indicates significance by 2-way RMANOVA but not significant by post hoc test. All latencies showed no significant changes at the 7 day condition.

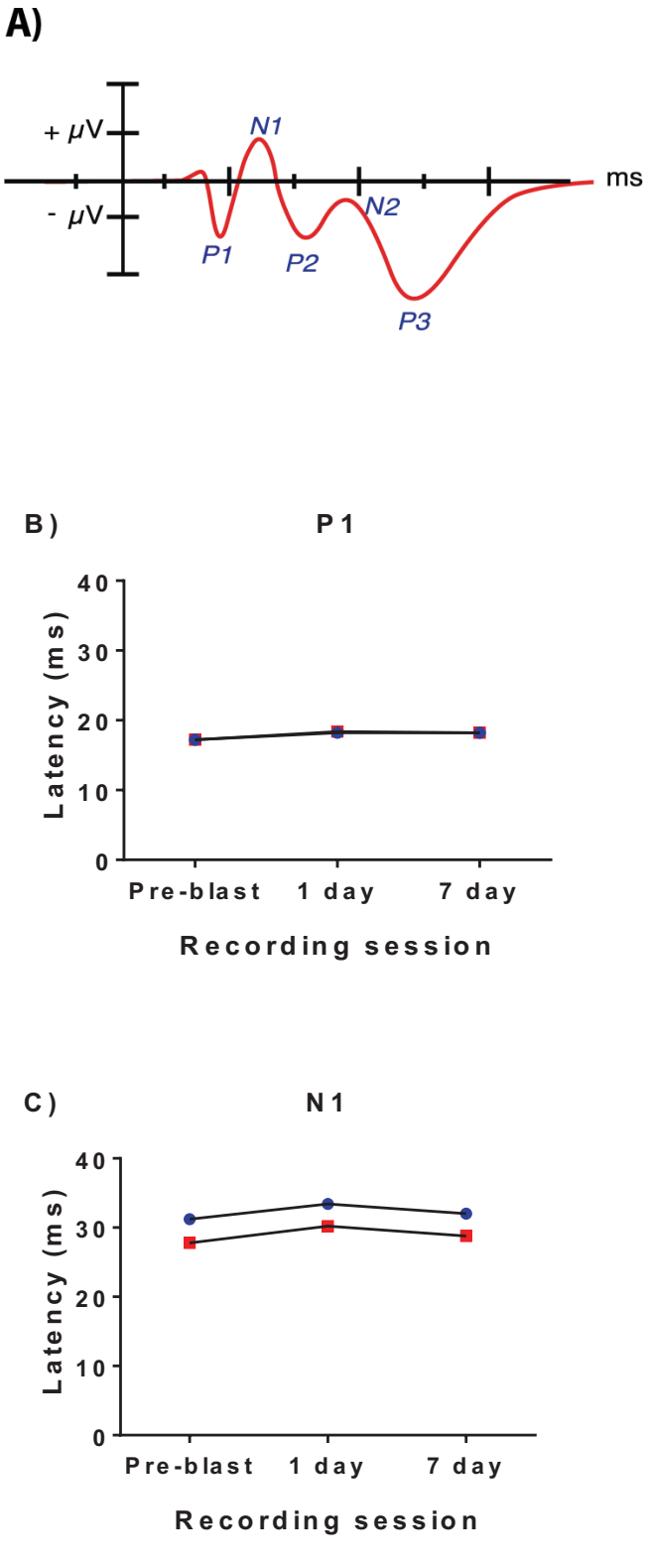

Figure 26 Flash VER peak latency for left and right hemisphere fVER recordings pre-blast, 1 day post-blast and 7 days post-blast exposure. Plot data are peak latency (ms) versus recording session for five test subjects. Each data point is an average of five left or right hemisphere recording of 180 averaged fVEPs. Red (square) plot represent the right hemisphere recordings, blue (circle) plot represents the left hemisphere recording. Red asterisk indicates a significant increase in latency by post-hoc Tukey's test $p < 0.05$. A) Reference depiction of fVER and the peak location. B) and C) P1 and N1 peaks respectively, show nonsignificant latency changes.

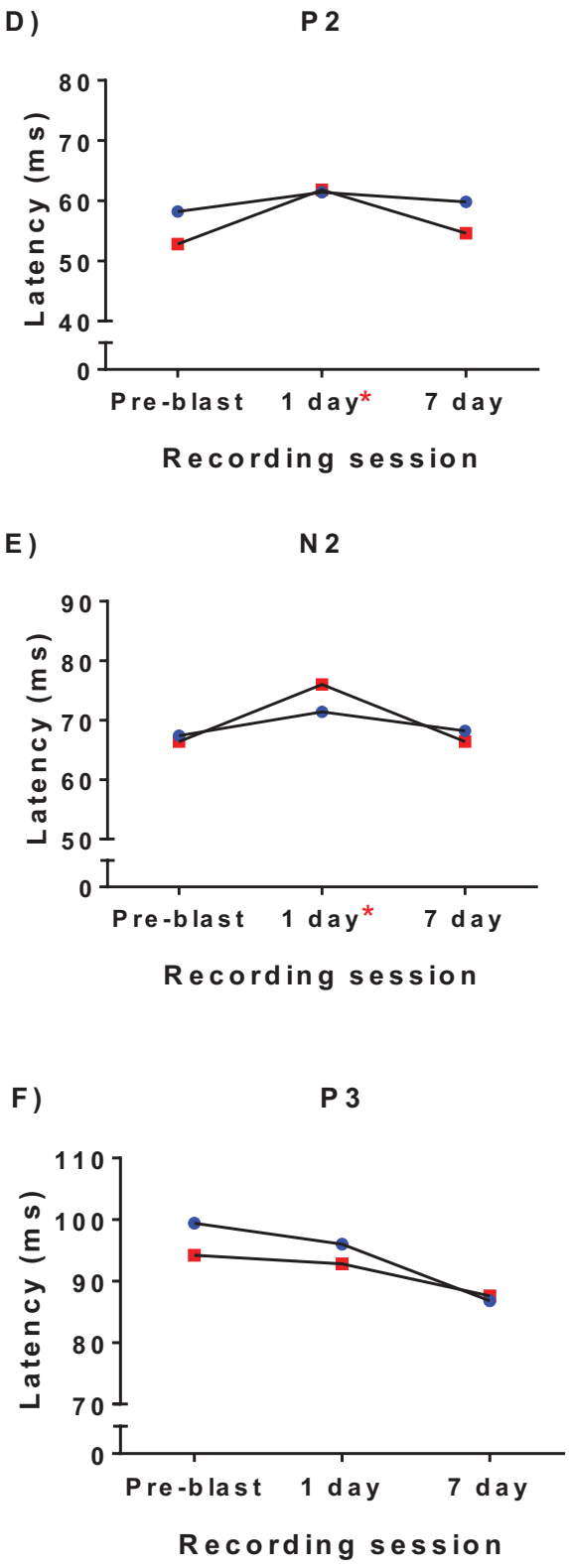

Figure 27 Flash VER peak latency for left and right hemisphere fVER recordings pre-blast, 1 day post-blast and 7 days post-blast exposure. Plot data are peak latency (ms) versus recording session for five test subjects. Each data point is an average of five left or right hemisphere recording of 180 averaged fVEPs. Red (square) plot represent the right hemisphere recordings, blue (circle) plot represents the left hemisphere recording. Red asterisk indicates a significant increase in latency by post-hoc Tukey's test $p < 0.05$. D) P2 latency. Right hemisphere P2 latency for the 1 day post-blast condition ($M = 62$, $SD = 11$) compared to the pre-blast condition ($M = 53$, $SD = 7$) shows a significant increase (F (2,16) = 4, $p = 0.027$); however, there is no significant change in latency between the 7 days and pre-blast conditions. E) Right hemisphere N2 latency is significantly increased at the 1 day condition ($M = 76$, $SD = 9$) compared to the pre-blast condition ($M = 66$, $SD = 3$), (F (2,16) = 9, $p = 0.004$); however, the 7 days latency is not significantly different from the pre-blast latency. F) P3 latency shows no significant changes.

Flash-VER peak amplitude changes pre-blast and post-blast exposure

A pre-stimulus baseline was established by averaging 200 ms of recording prior to the PS-flash. The difference between the first local minima (P1) and the baseline amplitude (BL) was determined for each hemisphere for each of the three recording sessions for each subject. Next, the difference in amplitude was determined between P1 and N1 (P1N1) and the other peaks listed in Table 7. Figures 30 and 31 show the changes in peak amplitudes for each set of peaks.

A two-way repeated measures analysis of variance was used to test the difference between peak amplitudes in left and right hemisphere fVER recordings before and after explosive blast exposure, to determine if there was an effect due to either hemisphere and, finally, to determine if the recording conditions had the same interaction/effect at each hemisphere. Significant decreases in amplitude were noted between the P1N1 peaks (F (2, 12) = 11, P = 0.0018), and the N1P2 peaks (F (2, 12) = 12, P = 0.0014). However, there was not a significant difference between left and right hemisphere recordings (Table 8) or a significant variance of test-subject data within each individual recording session, see Figure 29 and Figure 28.

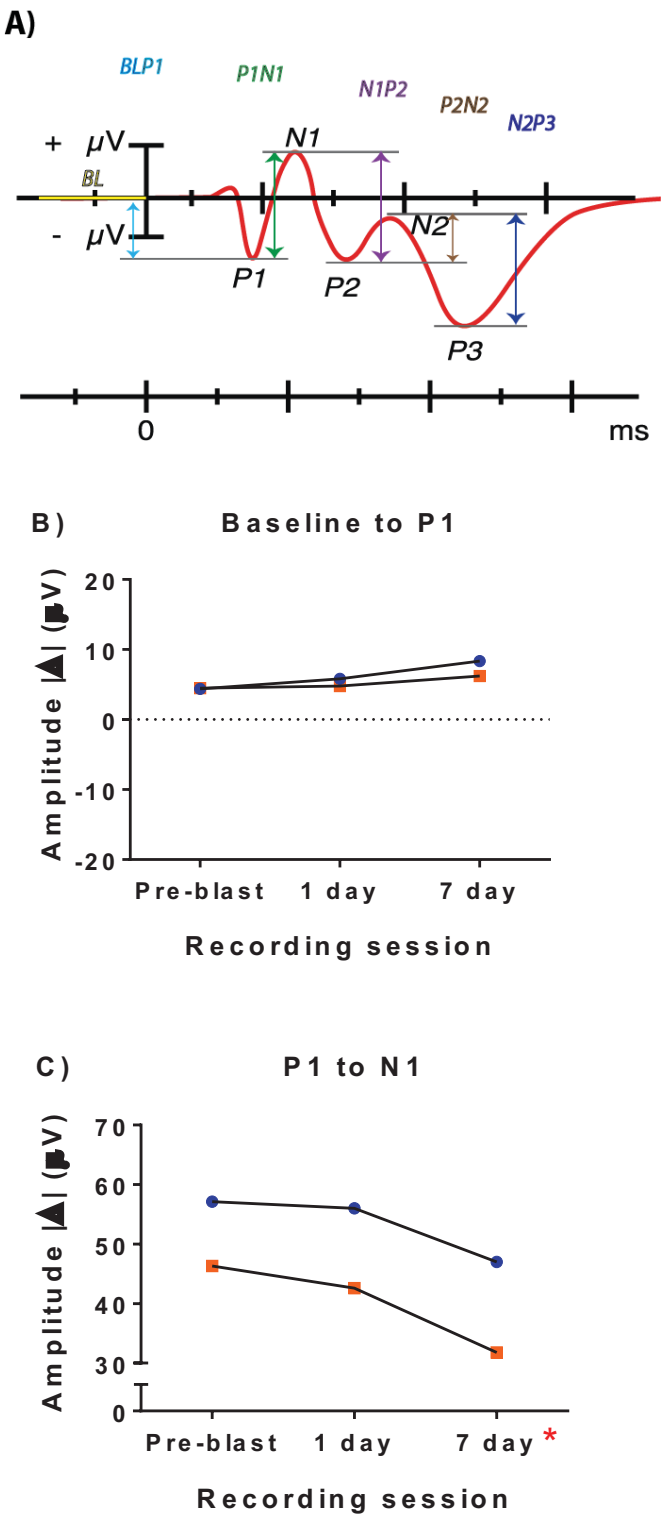

Figure 28 Flash-VER peak amplitude differences for left and right hemisphere recordings pre-blast, 1 day post-blast and 7 days post-blast exposure. Each plot data are the absolute value of the amplitude difference (|Δ|) between two peaks potentials (μV) versus recording session for n = 5 test subjects. Data points are the averaged left (blue) or right (red) hemisphere. A) Illustration of an fVER depicting local minima and maxima; latency scale (ms) below. Baseline (BL) occurs before the zero point and is in yellow. Following minima and maxima are labeled P and N respectively. Difference between minima and maxima are labeled by the two values e.g., P1N1 marked with a green arrow. Label colors match respective arrows color spanning amplitude change between peaks. The zero time point would be the initiation of the flash stimulus. A) Baseline potential was determined by averaging 200 ms of pre-stimulus recording. There was no significant change in P1-amplitude relative to baseline however there is trend of increasing amplitude post-blast. B) P1 to N1 showed a significant decrease in amplitude in both hemispheres at 7-days post-blast exposure (F (2, 12) = 11, P = 0.0018). C) N1 to P2 showed a significant decrease in amplitude in both hemispheres at 7 days post-blast exposure (F (2, 12) = 12, P = 0.0014). See Table 7 and Table 8 below for *Mean, SD* and F-test results.

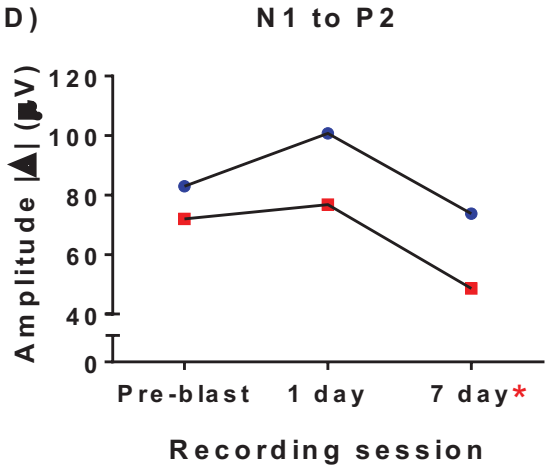

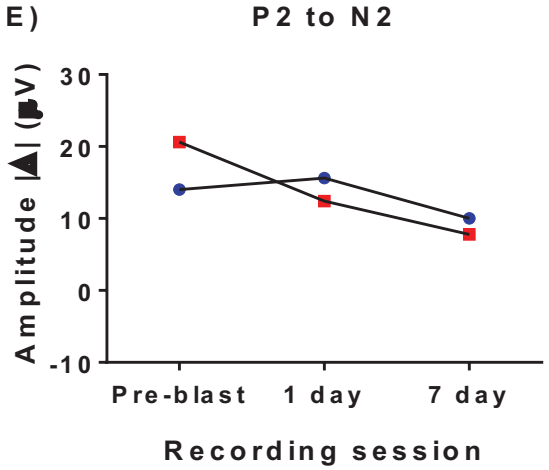

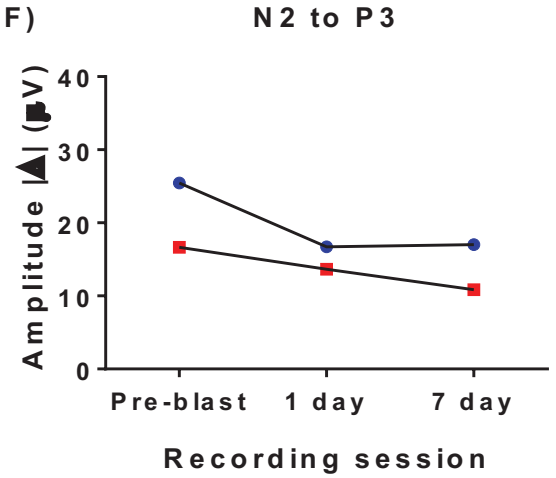

Figure 29 Flash-VER peak amplitude differences for left and right hemisphere recordings pre-blast, 1 day post-blast and 7 days post-blast exposure, continued... Each plot data are the amplitude difference between two peaks (μV) versus recording session for $n = 5$ test subjects. Data points are the averaged left (blue) or right (red) hemisphere amplitude-differences between respective peaks for averaged test-subject data. Red asterisk indicates a significant change in amplitude $p < 0.05$. See Figure 28 A) for a description of the peaks and difference interval. There was a significant change in the N1 to P2 amplitude post-blast as indicated by 2-way RMANOVA (F (2, 12) = 12, $P = 0.0014$). There was no significant change in the P2N2 or N2P3 intervals. See Table 7 and Table 8 below for *Mean, SD* and *F*-test results.

Table 7 Difference between Local Minima and Maxima Potential for Left and Right Hemisphere fVER recordings Post-blast Exposure

Peaks (ID)	Hemisphere	Pre-blast Amplitude difference *Mean ± SD (μV)*	1-day Amplitude difference *Mean ± SD (μV)*	7-day Amplitude difference *Mean ± SD (μV)*
BLP1*	Left	-4.4 ± 3.0	-5.8 ± 2.3	-8.3 ± 3.0
	Right	-4.1 ± 8.2	-4.8 ± 4.5	-6.2 ± 3.2
P1N1	Left	57.1 ± 20.7	56.0 ± 12.9	47.0 ± 19.6
	Right	46.3 ± 22.4	42.6 ± 18.8	31.8 ± 13.1
N1P2	Left	83.0 ± 17.5	100.7 ± 21.0	73.8 ± 24.7
	Right	72.0 ± 29.1	76.8 ± 28.9	48.6 ± 13.6
P2N2	Left	14.0 ± 7.7	15.6 ± 9.9	10.0 ± 7.8
	Right	20.6 ± 21.5	12.4 ± 13.5	7.8 ± 5.2
N2P3	Left	25.5 ± 10.8	16.7 ± 15.0	17.0 ± 8.9
	Right	16.6 ± 7.9	13.7 ± 9.2	10.8 ± 6.0

*BLP1: Baseline (BL) is average of 200 ms baseline potential before PS-flash at 0 ms. BLP1 data are the actual values from the fVER, but the plotted values in Figure 28 B) are the absolute value of the difference between baseline and P1; this is the reason for the change from negative to positive values.

Table 8 Two-Way Repeated Measures Analysis of Variance for Testing Difference Between Peak Amplitudes of Left and Right Hemispheric fVER Recordings

Peaks (ID)	Interactions	*F*-test	
BLP1	Interaction	$F(2, 12) = 0.17$	$P = 0.85$
	Day	$F(2, 12) = 1.8$	$P = 0.20$
	Hemisphere	$F(1, 6) = 0.20$	$P = 0.67$
P1N1	Interaction	$F(2, 12) = 0.32$	$P = 0.73$
	Day*	$F(2, 12) = 11$	$P = 0.0018$
	Hemisphere	$F(1, 6) = 1.1$	$P = 0.33$
N1P2	Interaction	$F(2, 12) = 0.95$	$P = 0.42$
	Day*	$F(2, 12) = 12$	$P = 0.0014$
	Hemisphere	$F(1, 6) = 1.8$	$P = 0.23$
P2N2	Interaction	$F(2, 12) = 1.1$	$P = 0.37$
	Day	$F(2, 12) = 2.7$	$P = 0.11$
	Hemisphere	$F(1, 6) = 0.0028$	$P = 0.96$
N2P3	Interaction	$F(2, 12) = 0.36$	$P = 0.71$
	Day	$F(2, 12) = 2.5$	$P = 0.13$
	Hemisphere	$F(1, 6) = 1.0$	$P = 0.35$

Interaction refers to the variance of each hemisphere recording data point relative to recording day. Day refers to the variance of the amplitude-difference between recording sessions. Hemisphere refers to the variance between left and right hemisphere recordings. *Indicates a significant change in amplitude.

fVER Cross-correlation

Maximum cross-correlation (CXC) was performed in order to determine the similarity between an individual test subject's left and right hemisphere fVER while accounting for any time lag between the signals. The maximum CXC values increased in eight test subjects however, decrease in six test subjects. A one-way repeated measures ANOVA with Greenhouse-Geisser correction was conducted to compare the effects of explosive blast exposure on fVER maximum CXC in 1 day post-blast, 7 days post-blast and pre-blast conditions. There was not a significant effect of explosive blast exposure on the fVER maximum CXC [$F(1.1, 4.2) = 1.6$, $P = 0.27$]. Sphericity was not assumed so the Greenhouse-Geisser correction was applied, resulting in a Greenhouse-Geisser epsilon of 0.53. Maximum CXC results are illustrated in Figure 30.

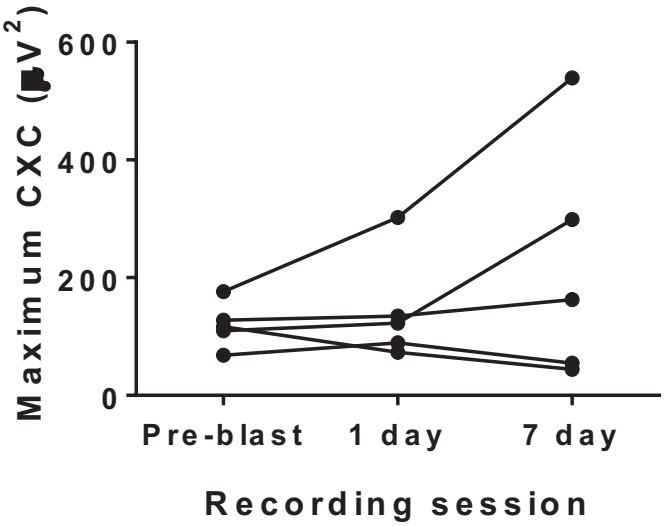

Figure 30 Maximum cross-correlation for fVER recording sessions. Plot of test subject's (n = 5) maximum CXC versus fVER recording session, where each data point is a test subject's left-right hemisphere maximum CXC for a given fVER session. There is a non-significant post-blast increase in the maximum CXC of left and right hemisphere VER recordings. A larger maximum cross-correlation value indicates a greater similarity between hemispheric recording channels for given time-lag position.

Structural Results

Test subjects brains were examined at time of euthanasia for gross injury identified as bleeding and cortical marking. In test subjects implanted with ECoG epidural screw electrodes and exposed to blast there were 6 test subject with no gross abnormalities and 15 with varying degrees of cortical tissue injury, see Figure 31. The non-implanted test subject brains showed no gross abnormalities.

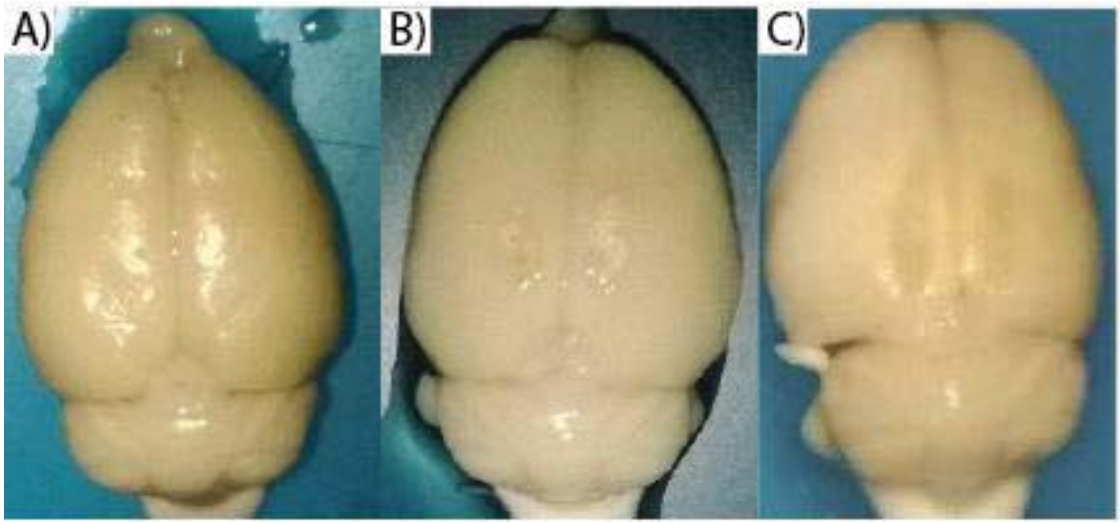

Figure 31 Brains of test subjects implanted with epidural screw electrodes and exposed to explosive blast. A) Clean brain with no electrode markings (138 kPa blast). B) Bilateral electrode injury (124.1 kPa blast). C) Bilateral electrode gouge injury (110.3 kPa blast). The PMMA containing the electrodes was found secure to the test subjects head at time of euthanasia.

Overall quality of the cresyl echt violet (CV) staining was good and provided enough detail to analyze basic histopathology changes in blast and control brains, see Figure 32. Preparatory work performed to determine electrode placement and depth indicated the CV staining was able to identify injury due to electrodes, see arrows in Figure 32 B. In our test subjects without implanted screw electrodes, we couldn't see any indications of intracranial hemorrhage, axonal injury (with the so called 'axonal bulb'

formation), acute or chronic inflammatory reaction or cell death. The anatomical structures we examined appeared intact, free of any evidence of injury.

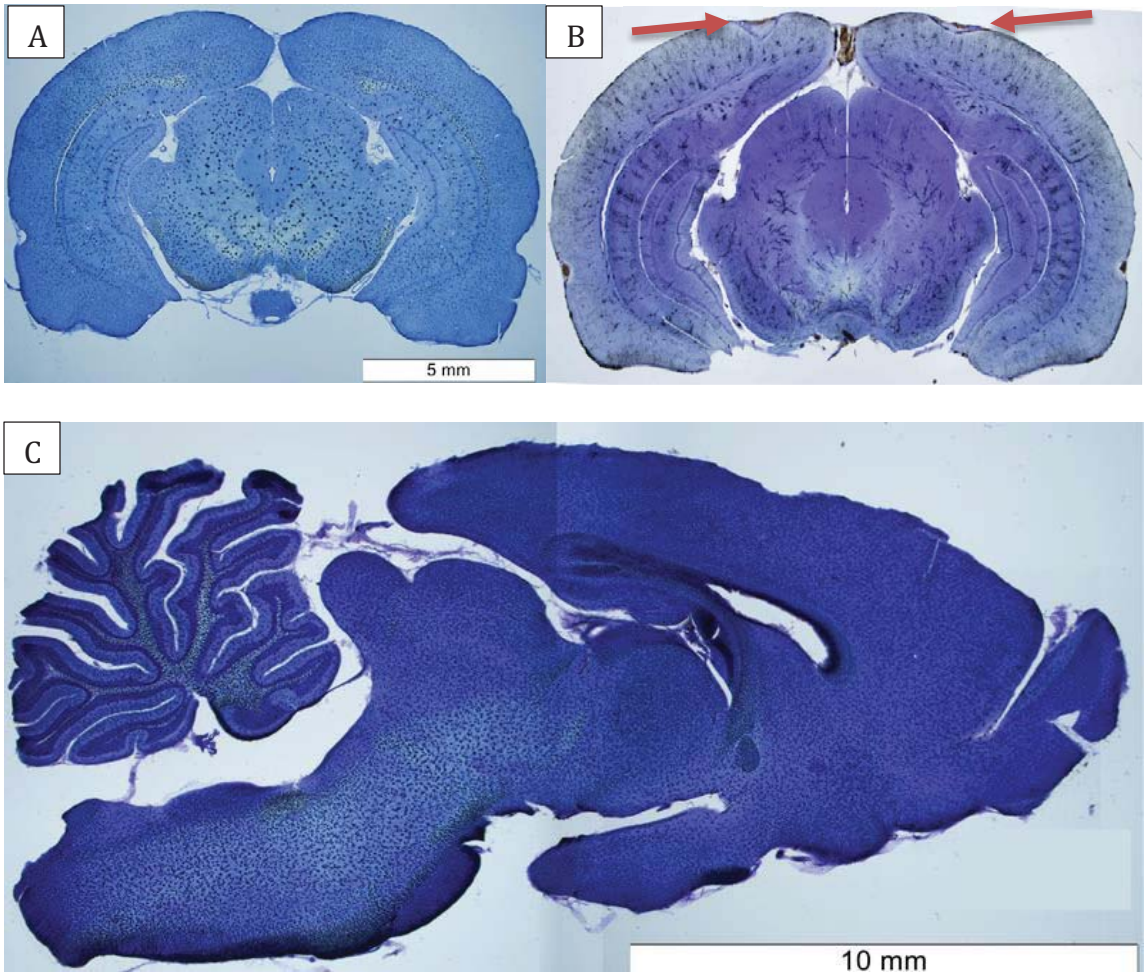

Figure 32 Pathology analysis with cresyl echt violet stain. No gross blast pathology was noted in brains without implanted electrodes with the cresyl violet staining. All pictures are of electrode implanted subjects exposed to a single mild blast, 108-138 kPa. A) Coronal section showing no blast pathology or screw electrode injury when screw electrodes are only placed to a depth of the dura. B) Test-subject from our methods optimization study in which screw electrode depth was not optimized and cortical injury is indicated by the red arrows. Screw electrodes should be placed to a depth where the tip of the screw is flush with the inner surface of the skull to prevent cortical tissue disruption, as identified by the red arrows in the photo. C) Sagittal section with no gross pathology.

Dendritic spine morphometric analysis

To determine the effect of explosive blast on cortical dendritic spines, we examined the cortical layer II/III pyramidal neuron dendritic spine density in test subjects 1 day or 7 days post-blast exposure, see Figure 34. Golgi-Cox stained sections were prepared and examined using bright-field microscopy at 63x magnification to visualize and count the dendritic spines. Dendritic spine counts are from the auditory, visual and somatosensory cortices of control (n = 5), 1 day (n = 5) and 7 days (n = 9) groups; see Figure 18 and Figure 19 for counting procedure. Two double-blind counts by different investigators were performed. An unpaired t-test indicated a significant decrease in the dendritic spine density comparing blast exposed (M = 28.1, SD = 7.5) and non-exposed control (M = 31.6, SD = 6.8) conditions; $t(208) = 3.6$, $p < 0.001$, see Figure 33 (A). One-way ANOVA was performed in order to determine the effect of explosive blast on dendritic spine density between the pre-, 1 day post- and 7 days post-blast conditions. There was a significant decrease in dendritic spine density in the 1 day and 7 days post-blast groups compared to the pre-blast condition, [$F(2.0, 319.0) = 30.1$, $P < 0.001$], see Figure 33 (C) and Table 9.

Apical and dendritic spines densities were evaluated using a multiple comparisons one-way ANOVA with an uncorrected Fisher's LSD test. Apical and basal dendritic spine densities (n = 39) were compared in controls which indicated a significantly greater basal spine density (M = 35.2, SD = 6.0) than apical (M = 30.9, 6.3), $t(152) = 2.6$, p = 0.009. Blast exposure decreased apical spines significantly (M = 27.1, SD = 5.9), [$t(152)$ = 2.3, p = 0.02], and basal spines significantly (M = 30.2, SD = 9.6), [$t(152) = 3.1$, p = 0.002]; however, blast exposed apical and basal spine densities were no longer significantly different, see Figure 33 (D). No attempt was made to correct for spines

hidden beneath or directly above the dendritic segment; therefore, the dendritic spine density counts are likely to underestimate the actual dendritic spine density values.

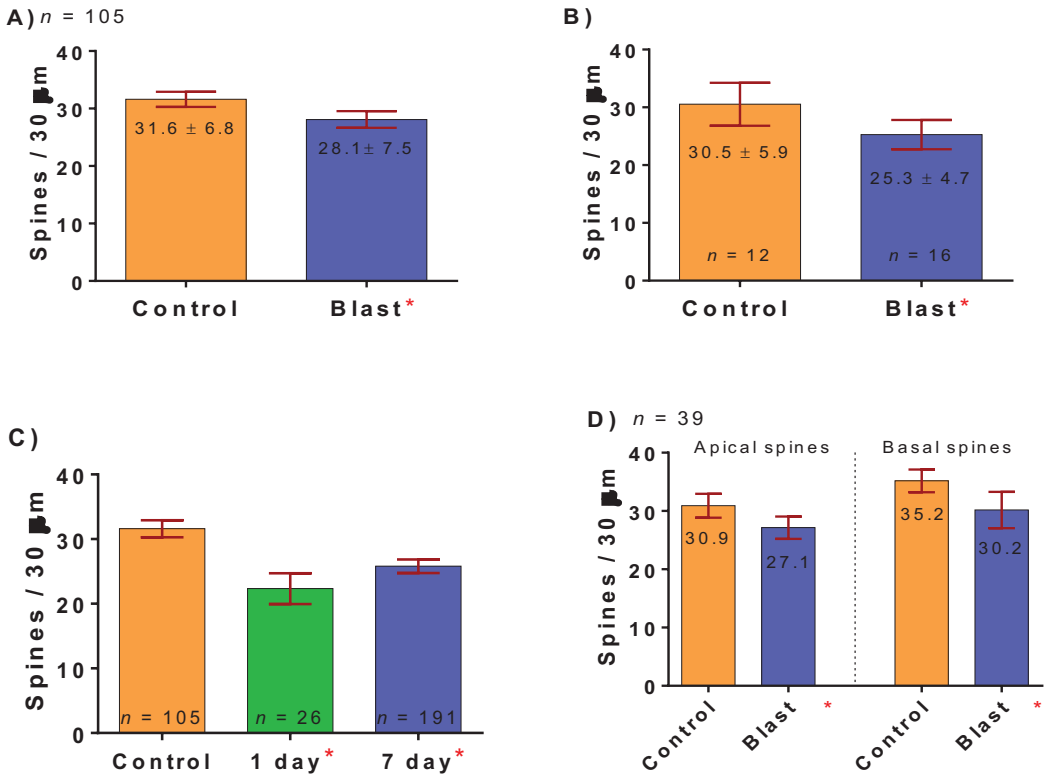

Figure 33 Cortical layer II/III dendritic spine density changes due to single explosive blast. Plots depict the number of dendritic spines per 30 µm versus control or blast-exposed test subject. Red error bars represent the 95% confidence interval about the mean. Counts were obtained from 15 test subjects. A) 105 separate counts from control and blast exposed groups. B) Double blind count results from independent investigator to confirm results noted in Figure A. C) Shows the decrease in dendritic spines at 1 day and 7 days post-blast. Number of counts are decreased for the 1 day group due to less test subjects. D) Plot shows the post-blast changes (blue) in apical and basal spine densities relative to their respective controls (orange). Count mean values are listed below the error bars.

Table 9 Dendritic Spine Density Changes at 1-day and 7-days Post-blast Exposure

	Test subjects (#)	Neuron (#)	Mean (spines/ 30 µm)	*SD* (± *spines)*	*SEM*	diff. 95% CI	*p*
Control	5	105	31.6	6.79	0.663	2.6	
1 day	5	26	22.3	5.89	1.16	4.7	< 0.001
7 day	9	191	25.8	7.36	0.533	2.1	< 0.001

$p < 0.05$ is considered significant.

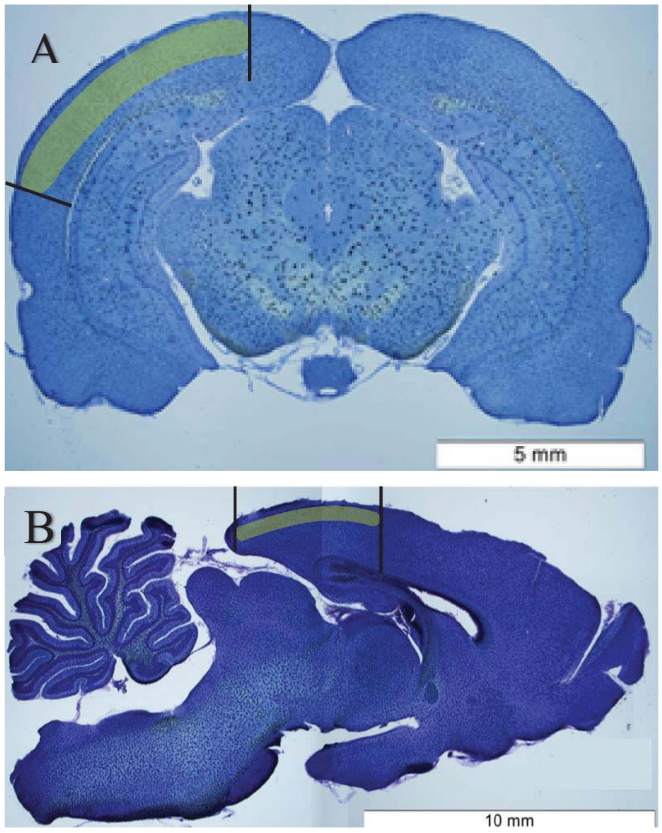

Figure 34 Neuronal location for dendritic spine counts. (A) Coronal section through the rat brain. (B) Sagittal section of rat brain. Both slices have Golgi-Cox primary stain and cresyl echt violet counterstaining. The yellow bars on each image indicate an approximate area where the cells were located for dendritic spine counting.

CHAPTER 5: Discussion

The studies presented in this dissertation focused on determining the brain injury threshold following a single explosive blast. Specifically, the work was focused on identifying the effects of a single high-explosive blast exposure on cortical electrical potentials and neuronal dendritic spine density, in unprotected Sprague-Dawley rats. This work was undertaken to advance the understanding of the neuropathobiology of mild bTBI so as to improve blast-related TBI management of US service members.

In order to identify explosive blast induced mild TBI, initial experimental design included modeling a relevant, reproducible and consistent explosive blast while minimizing secondary, tertiary and quaternary injury mechanisms. Composition-4 (C-4) explosive was used in this experiment due to it being a common military and civilian explosive, molding ability and relatively slight fume toxicity (93). The suspended spherical C-4 charge in the blast wave generator (BWG) produced calculable and consistent pressure-time relations between sessions. Initially we started at 138 kPa and decreased blast intensity to 108 kPa for the final blast session. The lower blast intensities were chosen for three reasons: first, because the test subjects were unprotected i.e., they did not have any thoracic or head protection. Next, our prior lab experiments have indicated variable neuronal degeneration in the deep brain region of the superior colliculus due to a protected 210 kPa blast exposure. On the opposite end of the injury spectrum, our unprotected lung injury threshold is 126 kPa; therefore, the threshold of mild blast injury should be at or around the lower pressure. Finally, a lower explosive blast intensity was more likely to be associated with the threshold of injury.

Once we established a reproducible explosive blast we attempted to minimize injury mechanisms. By design, the BWG is intended to minimize secondary injury by placing the explosive in a debris-free environment eliminating any ejecta which otherwise would be directed towards the test subjects. Tertiary injury, due to acceleration, was minimized by Velcro® straps securing the test subjects hips, shoulders and head to the blast grid. We were not able to visualize the animal position during the blast, but were limited to visual inspection of the test subject's position before and after the blast exposure. The securing straps are not optimal for securing of the head due to some animals slipping from the restraint during the blast. A more effective securing method needs to be devised. Test subjects maintained their positions in 85% of the blast iterations and no coup/contrecoup or bruising in general was identified on histological evaluation; therefore, we consider the tertiary injury being minimized by the experimental design. Quaternary injury due burns was minimized using an elastic-cotton sleeve around the test subject, placing the test subjects outside of the explosive-generated fireball and using fans to vent fumes after the explosion. No singeing of hair or protective sleeve was identified, so we believe this project also minimizes the quaternary injury.

The relative contribution of primary and tertiary injury mechanisms to mild bTBI are difficult to separate. It must be stated that this project is not intended to determine the difference between primary and tertiary injury; however, experimental design intended to minimize the secondary, tertiary and quaternary mechanisms. By minimizing those injury mechanisms we are able to isolate the primary mechanism of an explosive blast. Therefore, we are stating that functional and structural injury noted during this experiment were due to an isolated-primary mechanism.

ELECTROCORTICOGRAPHY

Placement of cortical screw electrodes was a challenge due to the varied literature information about recording location and surgical procedure as well as lack of information for use of electrodes during blast experiments (17; 35; 46; 83). The visual cortex was chosen for electrode placement due to prior unpublished laboratory data indicating occurrence of neuronal cell death in areas of the subcortical visual pathways due to explosive blast. Electrodes were placed at the V1 monocular region of the primary visual cortex of each hemisphere in order to better record isolated hemispheric signaling from respective eyes. An initial proof-of-methods trial was performed in order to determine the following: whether skull screw-electrodes could hold in place during explosive blast, proper depth of the screws, recording locations of screw-electrodes as well as stain optimization. Initial blast testing indicated the implanted screw electrodes would remain secure but unfortunately the traditional method of seating the electrodes into the epidural space or through the epidural space in contact with the cortex, resulted in cortical damage during blast. Optimal depth of screw-electrode was determined to be flush with the inferior aspect of the calvarium in contact with the epidural space in order to prevent screw injury to the cortex during blast. Unfortunately, screws placed at the thin areas of the skull are prone to injure the cortex during blast which may be due to compression of the skull into the cortex or movement of the brain within the skull; this will be discussed further in the pathology section below. Future researchers may find it more effective placing recording electrodes near the relatively thicker boney area of the lambdoid suture. This would decrease the recording distance between electrodes but may prevent loss of test subjects due to blast induced electrode injury noted at the anterior electrode position.

We noted no significant changes in the ECoGs due to blast and the theta (4-8 Hz) bandwidth was the dominant recording frequency. The theta bandwidth is usually present in a state of meditation or inactivity which indicates the recording is appropriate for the limited activity of the test subjects observed during testing.

The mirrored box testing chamber allowed the test subjects to move free within the box but most test subjects showed limited roaming behavior and remained stationary. Allowing the test subjects to move during recording provides relevant translation data to a clinical environment where military personnel are tested. During the initial experimental design process we considered anesthetizing test subjects in order to remove movement artefact, however we decided to use unanesthetized test subjects to more represent the clinical setting military personnel would experience when being evaluated for a mild TBI; unanesthetized with freedom of movement.

Time of day at which recordings occurred varied. This was intended to mimic the variability of times at which recordings would occur within the military population. The ECoG recordings did not show any significant changes due to blast using a clinical recording protocol administered in a manner intending to mimic military recording conditions. A recording frequency of 200 Hz allowed collection of data every 5 ms. Future researchers may wish to increase recording frequency to >1000 Hz allowing analysis of millisecond variability in ECoG recordings.

VISUAL EVOKED RESPONSE

A control test subject was studied in order to determine how signal averaging affected fVER latency and amplitude. An increasing number of fVERs were collected and compared for changes in latency and amplitude of the local minima and maxima. As

shown in Figure 24, latency is consistent across all fVERs. In contrast, the amplitude required the averaging of >140 fVERs in order to identify consistent peak amplitudes. Visual evoke response amplitude is convoluted by factors such as complexity of neuronal connectivity, attention and physical activity. The visual pathway is composed of multiple signal networks at the retinal-geniculate and superior collicular-cortical pathways as well as redundancy at the lateral geniculate-medial lemniscus-superior collicular pathways which convolutes the fVER amplitude and cause greater variable than fVER latency (5; 100). Physical activity and attention affect the recorded signal by distorting the peaks through convolution of the electrical potentials (75). Ideally, the test subject should be in the same physical and mental state during the evoking of each response in order to generate a recording session that can eventually be compared to post-blast exposure recordings (92).

In order to determine the effect of blast exposure on neuronal function, we examined the fVER for changes in latency and amplitude pre-and post-blast exposure. Individual post-blast recording session fVERs were averaged, then compared to the pre-blast recording session. Flash-VER amplitude of the P1-N1 and N1-P2 intervals were decreased at seven days post-blast exposure. A decrease in ERP is an indication of decreased network connectivity (99) and has been found in patients with mTBI (58; 84). The decrease in P1-N1 amplitude is a disruption in the sensory pathway while the N1-P2 decrease is considered a cognitive disruption. This agrees with our previous laboratory findings which showed blast induced neurodegeneration in the superior colliculus (SC). The SC has projections to the primary visual cortex layer II/III which may be susceptible to blast injury. Another significant finding is an increase in latency of the right

hemisphere fVER P2 and N2 peaks at 1 day post-blast, see Figure 27. This appears to be a transient increase due to the nonsignificant 7-days recording latency being similar to the pre-blast latency. In addition, the limit of resolution of the recording equipment is ±2 ms which makes the subtle changes less believable. However, control recordings do not show variability between recording sessions or interhemisphere latency variability, see Figure 39. The transient and subtle changes in latency support the hypothesis that this level of blast is at the threshold of injury. To further evaluate latency changes a cross-correlation analysis performed to determine if there was a signal lag between brain hemispheres.

The maximum cross-correlation had nonsignificant changes at the three recording sessions, see Figure 30. The change in signal lag was akin to flipping a coin, ie., it increase 50% of the time or decreases 50% of the time; therefore, we do not believe there was a significant change in signal lag between hemispheres. The fVER latency two-way RMANOVA data indicated there was no hemispheric effect on significance which leads us to believe there is no signal lag in our test subjects. Literature review of electrophysiologic findings indicate that evoked response potentials in TBI have shown prolonged latency, decreased amplitude or both (34). Our findings agree with a decrease in fVER amplitude but we only identified a transient effect on signal latency. In order to determine if our decrease in fVER amplitude and transient latency changes had a structural component we conducted histopathology studies.

PATHOLOGY

After ascertaining that the explosive blast intensity used in these studies did not cause clinically detectable functional impairment, neuropathological studies were carried

out to determine if the same explosive blast exposure lead to gross and microscopic neuroanatomical pathological changes. Brains were inspected for gross pathology, such as hemorrhage. For microscopic analysis, Cresyl violet (CV) stain was primarily used as it is commonly employed to reveal Nissl in neurons. Other brain structures, such as blood vessels, meninges, and the ventricular system were also examined.

There was no evidence of blast-related brain injury on the CV stained brain specimens, see Figure 32. This is consistent with previous work done that indicated that mild blast doesn't create structural damage detectable by basic staining procedures, e.g., CV or H&E. There was no evidence of blast related intracranial hemorrhage, severe axonal injury (with the so called 'axonal bulb' formation), acute or chronic inflammatory reaction or cell death. The neuroanatomical structures examined appeared intact and free of any evidence of blast induced histopathological changes.

Lung injury is one of the most common consequences of blast exposure. The lung injury was variable, as noted in Figure 40 and Figure 41; however, when lung injury occurred it was most often found in the upper left lobe. This may be due the rats' side lying position during blast. When the rat is lying on its right side there is less pressure on the opposite, non-dependent, side (left side) relative to the dependent (right side). This may be due to a decreased tissue density in the left due to there being more air present. This type of positional lung injury has been noted in our previous blast experiments. The cause of the lung injury is believed to be due to spawling occurring at density disparities in the chest cavity (71). Spawling occurs when the blast wave is transmitted across materials of different densities resulting in turbulence that can disrupt tissue integrity (71). Areas in the body with an air chamber show the greatest effect of spawling injury.

Variability of injury may also be attributed to phase of the respiration cycle at which the blast exposure occurs. It is theorized that an inflated lung may be more prone to injury due less tissue compliance. Due to the fact the blast wave moves faster through tissue than air, spawling may more likely occur during maximum tidal volume, in upper lung margin of the non-dependent lung, causing the lung injury.

DENDRITIC SPINE DENSITY CHANGES

In this dissertation study, it was shown that explosive blast results in decreased dendritic spine density in all regions of cortical layers II/III. This decrease is most evident at 1 day after exposure. By 7 days post exposure, the dendritic spine density shows marked recover. Cortical dendritic spine trimming, occurring in mild bTBI, is significant because it identifies subtle structural changes to the neuron outside the traditional neuronal apoptotic and necrotic pathways. Decreases in dendritic spine density have been identified in studies using controlled cortical impact (CCI), lateral fluid percussion injury (FPI) and epidural bead implantation models of TBI (11; 19; 41; 97). In addition to these models of TBI, we found explosive blast results in decreased dendritic spine density in visual cortex layers II/III. This decrease in dendritic spine density may be due to tissue shearing or dendritic spine retraction.

Brain tissue shearing due to detonation-front impingement is expected to produce inflammatory markers as well as microglial activation, which we did not identify in this study. Another possible cause of decreased dendritic spine density could be transient disruption of the synaptic membrane/channels allowing extracellular ions, such as calcium, to enter the dendritic spines. Calcium is of particular importance for dendritic

spine plasticity due to its activation of calcium-stimulated phosphatases such as calcineurin (CaN).

Calcineurin is a calcium/calmodulin-stimulated serine/threonine phosphatase that can be found in neuronal tissue. An increase in CaN activity and its downstream substrate cofilin (56; 57) result in actin de-polymerization and effect spine retraction. This dendritic spine loss has been shown in lateral FPI and midline FPI (10). Kurz et al, showed the relative amount of CaN did not change in the injured rats but the enzymatic activity was increased (57) indicating transcription-translation of the enzyme was not changed but activation of the enzyme was increased. Increased calcium in the dendritic spine can activate CaN causing dephosphorylation of cofilin. Cofilin depolymerizes the actin cytoskeleton causing the spine to collapse. Systemic conditions may play a significant role in dendritic spine trimming.

Generally, in an explosive blast, the entire body is exposed to the blast wave. Systemic activation of repair mechanisms require greater energy reserves than would be expected relative to a focal injury. This may be one reason for varied results of focal methods of TBI (FPI, CCI) compared to a systemic methods of bTBI (BWG, BOP). In addition to the systemic exposure, on the battlefield, military personnel are often stressed, dehydrated, sleep-deprived and calorie restricted. This may result in a biological system which is less able to repair itself during the acute phase of injury. The cofilin enzyme is more likely to depolymerized ADP-actin than ATP-actin. In a biological system that is systemically injured, stressed and calorie restricted, the ADP-actin may be more prevalent resulting in enhanced dendritic spine trimming in blast injured military

personnel. This adds a level of complexity to the bTBI problem because it may prime stressed-personnel for a bTBI.

Time-line of TBI Pathobiology

In order to better save service personnel with head injuries, there has been a push to get those injured to a well-resourced operating theatre at the two to three hour point post-bTBI. Once past the four hour mark, data has indicated that the head injured begin to succumb to secondary brain injury (76). Primary TBI occurs when a strain on brain tissue exceeds the threshold of tissue deformation. Due to the viscoelastic material properties of the brain parenchyma combined with the surrounding skulls rigid properties, a single deformation intensity has not been identified. This is not surprising due to the complex material and environmental variables involved. What may be more important is understanding that bTBI is a continuum which begins with transient neuronal/glial membrane disruptions resulting in subtle changes to charge distribution, increased membrane channel ion flux or both. Experiments conducted using Sprague-Dawley rats receiving CCI have revealed a temporal change in concentration of cerebral metabolites at 24 h, between 24-48 h and finally at 48 h post-TBI (77). Further studies on rats and mice conducted by Hall et al., indicate that there are progressive increases in cortical, hippocampal and thalamic degeneration over the first 48 h following CCI (47). Correlating structural pathology with VER changes may provide clinicians with a greater understanding of the pathobiology of bTBI as well as assist in faster diagnosis of bTBI.

CONCLUSIONS

This dissertation work has successfully identified the explosive blast threshold of bTBI in rats. That threshold is 108-154kPa. At this threshold, early transient decreases in dendritic spine density are observed. These are manifest by 1 day after blast but have largely recovered by 7 days. These neuropathological changes are not associated with either changes in ECoG or fVER. An early trend of decreased amplitude and prolonged latency in fVER was noted but it was not significantly greater than the limit of resolution of the recording equipment. As such, in a clinical setting, it would not be diagnostic of functional impairment. These two important findings, definitive dendritic spine density reduction and no neurological functional impairment, are consistent with a threshold bTBI. To be precise, at threshold the TBI is clear structural brain injury that has not yet achieved the critical burden to lead to neurological deficit.

Knowing this threshold of bTBI will facilitate development of both diagnostic and prevention strategies. Knowing the threshold will enable equipment and material designers to have a clear objective target for which their innovations need to meet. Diagnostic tools must focus on identifying subtle changes in ECoG and fVER. The limit of resolution of currently available platforms needs to be improved. Finally, clinicians should recognize that the lack of overt neurological deficits does not mean the victim has not suffered injury. Although transient, these patients are especially vulnerable to systemic conditions which could exacerbate their condition. Thus, blast gauges need to be able to identify if and when a service member is exposed to the threshold explosive blast injury or higher in order to do proper triage and thus treat victims in the most rational and compassionate way.

FUTURE RESEARCH

Future research will need to determine what the result of higher and lower intensities of explosive blast will lead to, both functionally and neuropathologically. For example, at what blast intensity will permanent pathological changes occur or when will functional impairment occur and which functions are most sensitive. Such studies are essential as they will better characterize this condition.

In addition, research can go in multiple directions. As a military diagnostic method, electrophysiology needs to be measured by noninvasive transdermal electrodes. As in this study, the transdermal methods need to be tested for reproducibility and reliability. The data will need to be correlated with behavior. Next, increasing the blast pressure to identify histopathology, imaging (DTI) and electrophysiology thresholds. In addition, one will need to determine the effect of shielding the thoracic cavity and/or head on dendritic spine density and cortical electrical potentials. Finally, the effect of multiple blast exposure on dendritic spine density and cortical potentials will need to be investigated.

An alternative method of research is to correlate diffuse decreased dendritic spine density due to blast exposure using multipoint transcranial magnetic stimulation. This would obviate the need for recording from the same electrode location by averaging multiple points of stimulation in order to identify decreased signal amplitude. This technique would still require a baseline recording or a well-established registry of normative data.

LIMITATIONS

Electrophysiology recording equipment required a time constant of longer duration in order to record the later fVER components such as the P300 peak. The importance of these later components is that they have been used as an attentional signal for the brain computer interface (BCI) system; focused attention appears as an increase P300 peak (32). Use of recording equipment with a larger time constant (> 0.2) allows for capture of the cognitive components of the fVER.

During the second blast session there were multiple confounding variables: the rat securing grid began to loosen after each blast session, it was retightened but the effect during the blast may have introduced a confounding variable. There may have been a problem with the ket-xyl mix in which two animals died after injection. The ket-xyl has been shown to increase fVER amplitude, which is in contrast to our reported decreased amplitude, but may have decreased our observed blast injury effect.

Lung injury was quantified by visual inspection rather than by histological staining. Injury areas may have been cleared free of blood confounding the quantification by visual inspection.

MILITARY AND OTHER CLINICAL IMPLICATIONS

This data is important to the military due to increased use of improvised explosive devices and the fact war fighters will always be at risk of bTBI. We showed that dendritic spine density can be decreased due to explosive blast exposure which occurs below the threshold of gross neuronal pathology. These dendritic spin changes are outside the limit of resolution of current imaging studies. The use of electrophysiology functional testing indicated that the subtle changes may not be readily apparent under the current clinical

EEG/VER protocol and that a baseline recording is necessary in order to best identify subtle electrophysiology changes. A registry of normative electrophysiology data is necessary to better identify and classify changes in bTBI. The key aspects for identifying fVER changes with current techniques include: having recording equipment which can record from the same areas between multiple sessions and establishment of a registry of patient healthy-EEG and evoked response (ER) data in which to reference.

Such repeated recordings would occur during the initial medical evaluation at the military entrance processing station (MEPS) where prospective military personnel will undergo electrophysiology testing to include EEG and ER (auditory, somatosensory and visual). The VERs may be recorded during the vision screening exam while the AERs and EEG would be recorded during the hearing exam. All testing will be updated yearly during the soldier readiness processing (SRP), during schools physical exam (SWIC/Flight), at deployment physicals and finally at exit (ETS) screening. All data can be maintained electronically and accessed worldwide on the Armed Forces Health Longitudinal Technology Application (AHLTA); the military's electronic medical record system. Gathering and recording of the EEG/ERs in this manner would result in every war fighter having a minimum of two recording sessions, MEPS and pre-deployment, for a physician to refer in the event a suspected bTBI should occur in a combat zone.

Appendix 1: Electroencephalography Society clinical guidelines

Flash-visual evoked potentials (fVEP) are used to detect dysfunction of the visual pathways. Their use in clinical testing is generally limited to: (1) subjects unable to be tested with pattern reversal VEPs or possessing severe refractive errors and (2) subjects who are too young or too uncooperative to reliably fixate on a pattern stimulus. Test results should demonstrate flash responses which are reproducible and free of auditory or muscle movement artifact. Six major local maxima/minima generally occur within the first 250 ms of flash-stimulation(8).

Local maxima/minima are labeled sequentially I, II, III, IV, V, and VI. Any of the peaks may be replaced by several faster peaks. The latency of the individual peaks may vary considerably between test subjects and are dependent on the level of arousal. These characteristics often make it difficult to compare fVEPs between subjects(8).

Analysis of Clinical Evoked Potential Results

Stimulus response intervals are analyzed to identify reproducible local maxima/minima from baseline fluctuations(8). Peak latencies and peak-to-peak amplitudes are measured. The ratio of amplitude of left and right eye responses is calculated(8).

Criteria for Clinically Significant Abnormality

Flash-visual evoked potentials show high variability between test subjects; therefore, loss of response is considered a primary indicator of dysfunction. Marked asymmetries of amplitude or latency may be indicative of unilateral abnormality in the

eye with the lower amplitude or longer latency. Markedly increased response amplitudes may be indicative of brain dysfunction(8).

The measured latency or amplitude values should fall well beyond the laboratory normative data collected from normal subjects of similar age and level of arousal. Less dramatic alterations in waveform, latency, or symmetry between the eyes must be interpreted with extreme caution. If the fVEP is unobtainable, other tests are warranted. The absence of an occipital fVEP implies that no stimulation has reached occipital cortex(8).

Eliciting an intact fVEP indicates visual input has reached the occipital cortex; however, it cannot be determined whether this input arises from the macula or the peripheral retina, nor does it indicate cognitive processing of visual stimuli. In an infant or uncommunicative subject, the presence of an intact fVEP does not demonstrate the presence of conscious visual perception(8).

Appendix 2: ECoG FFT

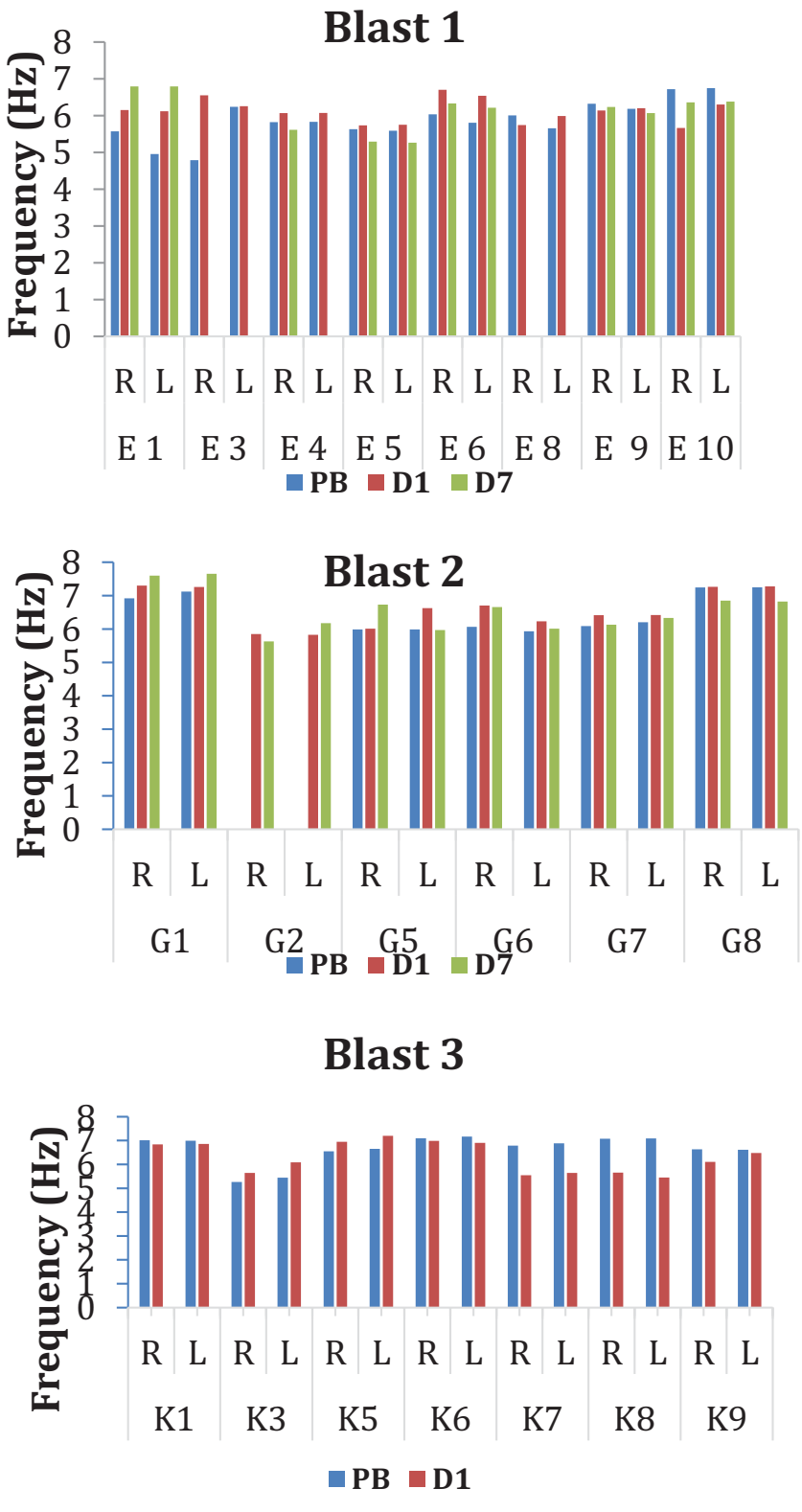

Figure 35 Fast Fourier Transformation of ECoG recordings pre-blast, post-blast 1d and post-blast 7d. No significant change in peak frequency was identified.

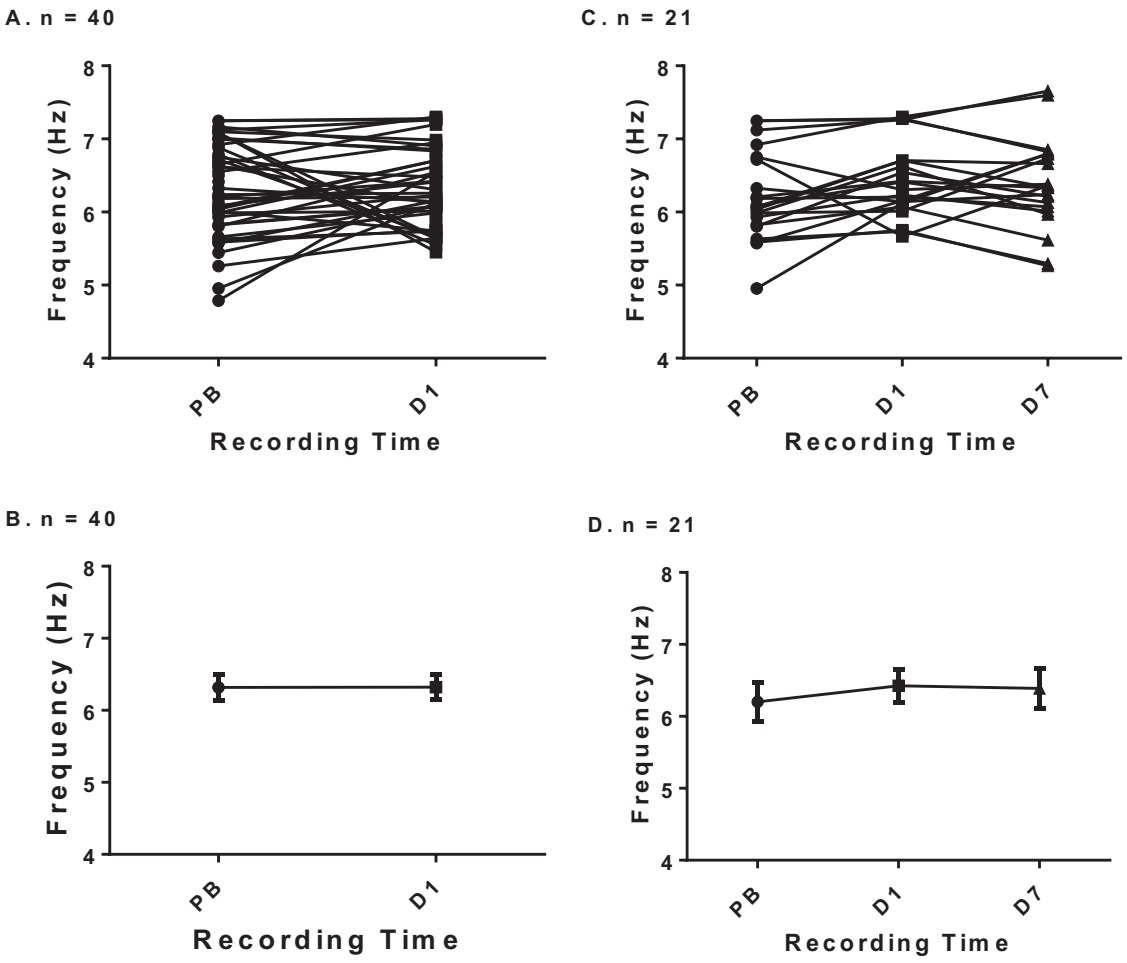

Figure 36 Peak frequency of averaged left and right hemisphere ECoG recordings. The FFT indicated the theta frequency (4-8 Hz) being the dominant frequency for all recordings. (A) Plot shows the averaged pre-blast and post-blast recordings for each test subjects, n = 40. Plot C shows only test subjects which had two post-blast ECoG recordings (n = 21) indicating 40% of test subjects had a decrease and 60% of test subjects had an increase in peak ECoG frequency when comparing pre-blast and seven-day post-blast recordings. Plots B and D show the average of all test subject recordings for a single post blast and two post blast recordings respectively. All plots are of the mean frequency while error bars represent the 95% confidence interval.

Appendix 3: Cross-correlation

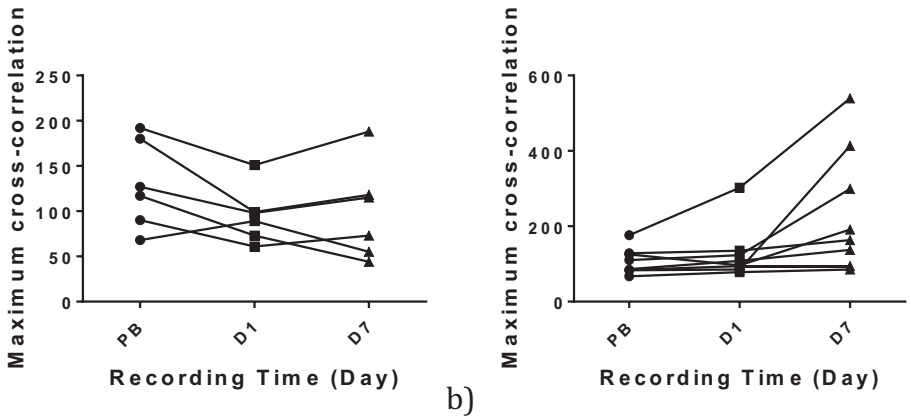

a) b)

Figure 37 Maximum cross-correlation for left and right hemisphere recording of rat VEP. a). Plot of decreasing cross-correlation coefficient. b). Plot of increasing cross-correlation coefficient. The cross-correlation was determined using an in-house generated MATLab® script. Cross-correlation for left and right hemisphere VEP recordings (n = 24) of the rats (n = 12) were determined for the pre-blast (PB), one-day post-blast (D1) and seven-days post-blast (D7) recording sessions. The larger the cross-correlation value indicates a greater similarity between recording channels.

Appendix 4: Control fVER Amplitude

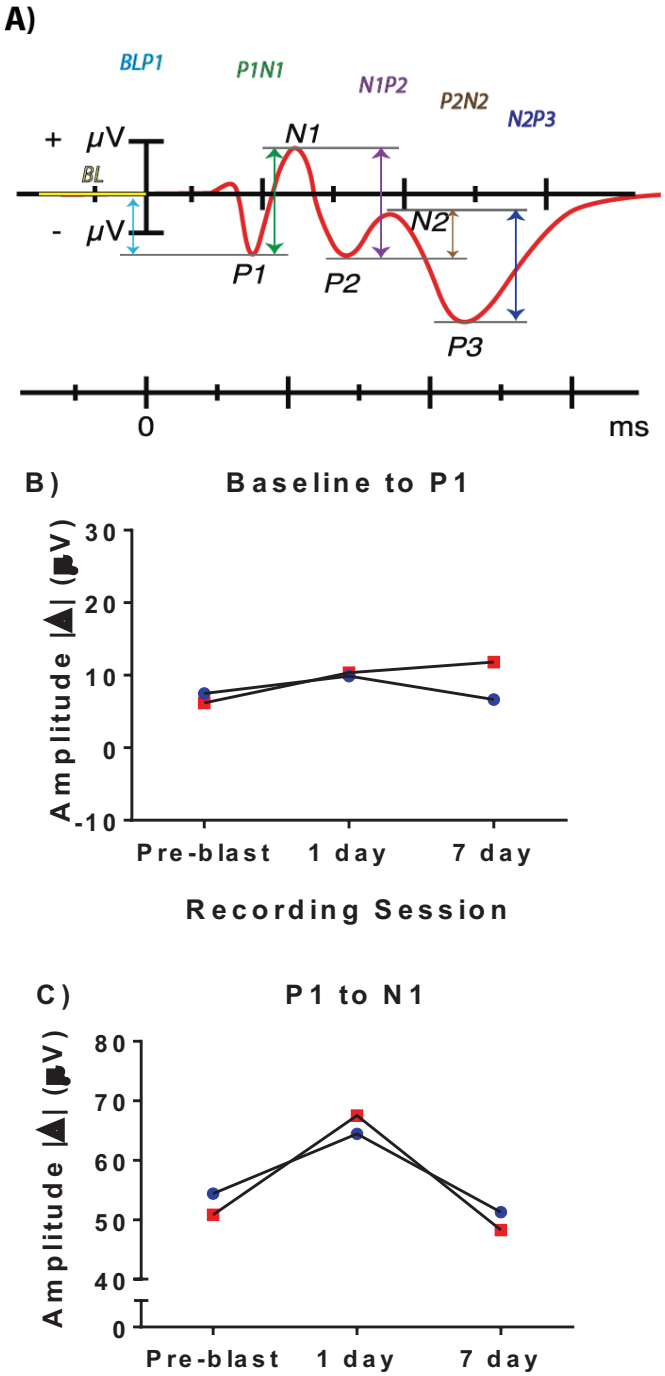

Figure 38 Control fVER amplitude change between local minima and maxima. Plots of absolute value of the difference between local minima and maxima versus recording session. Red (square) plots are right hemisphere recordings, blue (circle) plots are left hemisphere recordings. Control test subjects ($N = 3$) were surgically implanted with cortical screw electrodes in the same manner and array as test subjects. Controls were allowed to recover for five days then a pre-blast recording was performed. Pseudo-blast experiment was conducted in laboratory one-day after pre-blast recording. Control subjects were anesthetized with ketamine/xylazine then allowed to recover. Post-blast recordings occurred at 1d and 7d after pseudo-blast session. No significant amplitude changes were identified across all recording conditions.

D)

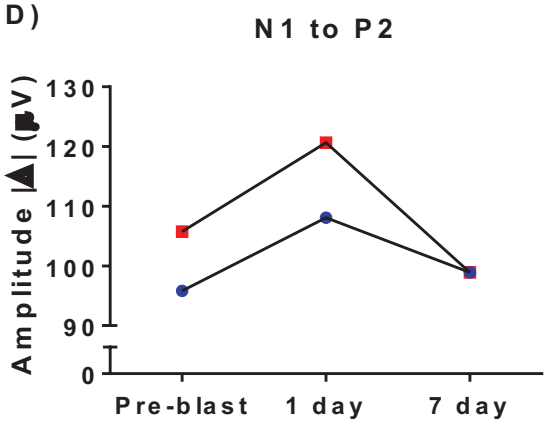
N1 to P2
Amplitude |▲| (μV)
130
120
110
100
90
0
Pre-blast
1 day
7 day

E)

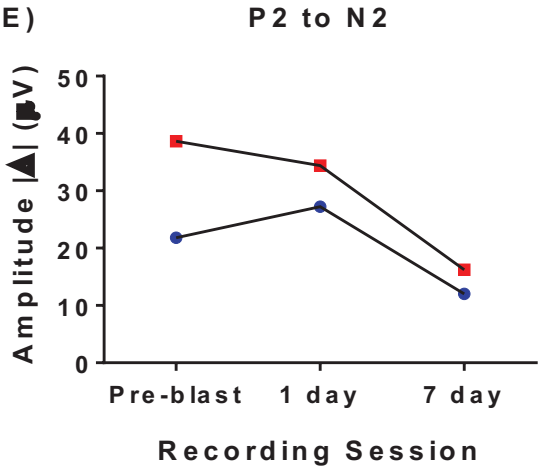
P2 to N2
Amplitude |▲| (μV)
50
40
30
20
10
0
Pre-blast
1 day
7 day
Recording Session

Table 10 Control Recordings: Difference between Local Minima and Maxima Potential for Left and Right Hemisphere fVER recordings (n = 3)

Peaks (ID)	Hemisphere	Pre-blast Amplitude difference *Mean ± SD (μV)*	1-day Amplitude difference *Mean ± SD (μV)*	7-day Amplitude difference *Mean ± SD (μV)*
BLP1*	Left	7.49 ± 4.91	9.89 ± 5.41	6.64 ± 1.92
	Right	6.18 ± 2.35	10.36 ± 6.60	11.81 ± 2.47
P1N1	Left	54.39 ± 18.84	64.45 ± 26.16	51.29 ± 4.60
	Right	50.83 ± 21.25	67.53 ± 16.27	48.25 ± 26.89
N1P2	Left	95.81 ± 32.43	108.07 ± 34.72	98.91 ± 4.85
	Right	105.76 ± 59.50	120.64 ± 35.82	98.90 ± 47.37
P2N2	Left	21.81 ± 14.00	27.23 ± 22.43	12.01 ± 17.99
	Right	38.63 ± 30.84	34.40 ± 19.34	16.24 ± 19.56

*BLP1: average of 200 ms baseline (BL) recording amplitude to first local minima (P1).

Table 11 Control Recordings: Two-Way Analysis of Variance for Testing Difference Between Peak Amplitudes of Left and Right Hemispheric fVER Recordings (n = 3)

Peaks (ID)	Interactions	F-test	
BLP1	Interaction	F (2, 16) = 0.63	P = 0.55
	Day	F (2, 16) = 1.10	P = 0.36
	Hemisphere	F (1, 16) = 0.43	P = 0.52
P1N1	Interaction	F (2, 16) = 0.063	P = 0.94
	Day	F (2, 16) = 1.20	P = 0.32
	Hemisphere	F (1, 16) = 0.015	P = 0.90
N1P2	Interaction	F (2, 16) = 0.035	P = 0.97
	Day	F (2, 16) = 0.33	P = 0.72
	Hemisphere	F (1, 16) = 0.17	P = 0.69
P2N2	Interaction	F (2, 21) = 0.22	P = 0.80
	Day	F (2, 21) = 1.80	P = 0.19
	Hemisphere	F (1, 21) = 1.30	P = 0.26

Interaction refers to the variance of each hemisphere recording data point relative to recording day. Day refers to the variance of the amplitude-difference between recording sessions. Hemisphere refers to the variance between left and right hemisphere recordings.
*Indicates a significant ($P < 0.05$) change in amplitude.

Appendix 5: Control fVER Latency

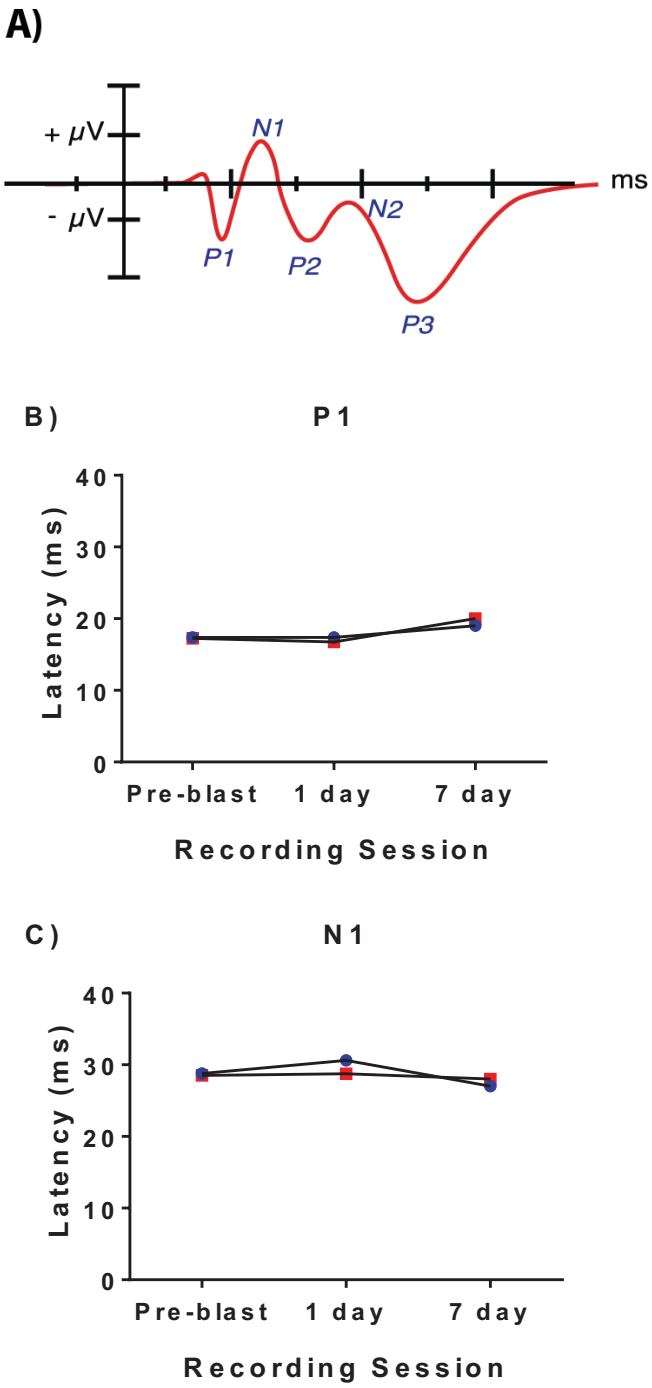

Figure 39 Control fVER peak latency for left and right hemisphere recordings pre-blast, 1 day post-blast and 7 days post-blast exposure. Plot data ($n = 3$) are peak latency (ms) versus recording session for five test subjects. Each data point is an average of five left or right hemisphere recording of 180 averaged fVEPs. Red (square) plot represent the right hemisphere recordings, blue (circle) plot represents the left hemisphere recording. A) Reference depiction of fVER and the peak location. B) and C) P1 and N1 peaks respectively, show no significant latency changes comparing all conditions.

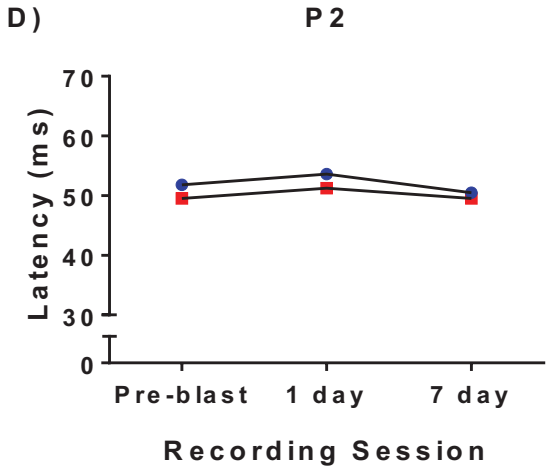

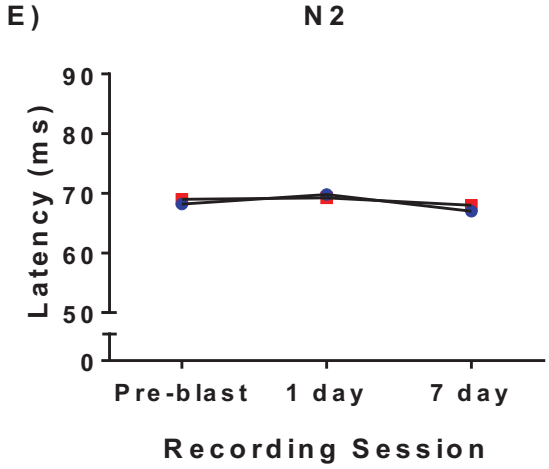

D) and E) Control fVER P2 and N2 peak latencies respectively. Both show no significant changes across all recording conditions.

Table 12 Control Recordings: Latency of Local Minima and Maxima for Left and Right Hemisphere fVER recordings

Peaks (ID)	Hemisphere	Pre-blast Latency *Mean ± SD (ms)*	1-day Latency *Mean ± SD (ms)*	7-day Latency *Mean ± SD (ms)*
P1	Left	17 ± 1	17 ± 2	19 ± 3
	Right	17 ± 2	17 ± 1	20 ± 3
N1	Left	29 ± 3	31 ± 4	27 ± 1
	Right	29 ± 4	29 ± 2	28 ± 1
P2	Left	52 ± 4	54 ± 6	51 ± 2
	Right	50 ± 1	51 ± 3	50 ± 1
N2	Left	68 ± 2	70 ± 3	67 ± 4
	Right	69 ± 1	69 ± 3	68 ± 4

Table 13 Control Recordings: Two-Way Analysis of Variance for Testing Latency of Local Minima and Maxima for Left and Right Hemispheric fVER Recordings

Peaks (ID)	Interactions	*F*-test	
P1	Interaction	$F(2, 16) = 0.3$	$P = 0.7$
	Day	$F(2, 16) = 3.1$	$P = 0.1$
	Hemisphere	$F(1, 16) = 0.008$	$P = 0.9$
N1	Interaction	$F(2, 16) = 0.3$	$P = 0.7$
	Day	$F(2, 16) = 0.7$	$P = 0.5$
	Hemisphere	$F(1, 16) = 0.1$	$P = 0.8$
P2	Interaction	$F(2, 16) = 0.1$	$P = 0.9$
	Day	$F(2, 16) = 0.8$	$P = 0.4$
	Hemisphere	$F(1, 16) = 1.0$	$P = 0.3$
N2	Interaction	$F(2, 16) = 0.2$	$P = 0.9$
	Day	$F(2, 16) = 0.9$	$P = 0.4$
	Hemisphere	$F(1, 16) = 0.1$	$P = 0.7$

Interaction refers to the variance of each hemisphere recording data point relative to recording day. Day refers to the variance of the latency between recording sessions. Hemisphere refers to the variance of latency between left and right hemisphere recordings. *Indicates a significant ($P < 0.05$) change in latency.

Appendix 6: Anesthesia

Attempts were made to obviate any effect of anesthesia by treating all test subjects and controls in a similar manner. We did not see any notable anesthesia induced effect on experimental results. As a reminder, three general anesthetics ketamine, xylazine and isoflurane and two local anesthetic bupivacaine HCl and ketorolac tromethamine were used at different times of the experiment.

Ketamine acts mainly on N-methyl D-asparate receptors (NMDAr) (55), xylazine on α_2 receptors and isoflurane on NMDAr, γ aminoburyric acid (GABA) and glycine receptors, all of which can be found in the brain and retina. Ketorolac is a nonselective cyclooxygenase (COX) inhibitor. Experiments by Charng et al., using Long-Evans rats, indicate that ketamine/xylazine increases P1-N1, N1-P2 amplitudes relative to controls. In the same experiment isoflurane was shown to increase latency of VER components (17). Ketamine, in combination with resultant loss of body temperature, has also been shown to increase VER latency (48). The decreased fVER amplitude noted in this experiment does not appear to be caused by a Transient latency changes could be due to ketamine or isoflurane but it is expected to affect both hemispheres rather than just one. Again, the increased latency was only noted at the 1 day time point and may be due to recording equipment limitations.

Dendritic spines rapidly change their shapes due to actin polymerization (51). The volatile general anesthetic isoflurane has been shown to block spine morphological plasticity by indirectly affecting the actin cytoskeleton rearrangment (51). In an experiment by Lin et al., using similar experimental parameters of isoflurane 1.2% for 2 h, rats exposed to lidocaine or isoflurane did not see a change in dendritic spine density

(64). This data indicates that isoflurane stabilizes the spines in what could be descibed as a neuroprotective effect. In contrast, theapeutic doses of ketamine has been found to have no effect on spine dynamic (51).

Ketorolac (IM) was used for post surgical analgesia. Ketorolac is a generalized COX enzyme inhibitor (59). The COX-2 isozyme can be found in cortical dendritic spines where it enzymatically generates prostaglandin-E_2 (PGE_2) resulting in increased post-synamptic membrane excitablility and increased long-term potentiation (18; 28). Inhibition of COX-2 enough to block PGE_2 increases dendritic spines and length of dendrites in Purkinje cells (28). Finally, comparison of fVER amplitude and spine control measures with experimental data indicates ketamine did not prolong latency and isoflurane did not stabilize the spines. Ketorolac did not decrease fVER amplitude because it was cleared from the test sujects body within 4-6 h after administration

Appendix 7: Abdominal and Thoracic Injury Considerations

The hypothesis of blast wave transmission from distal body regions to the brain is still controversial due to varied experimental results. Comparison of abdominal and brain pressure transients when either the abdomen or head is individually exposed to a blast wave indicates the blast pressure decreases rapidly from the point of exposure to the point of measurement downstream (82). Similarly, comparison of pressure transients in the heads of live swine to those in the heart and inferior vena cava during exposure to explosive blast indicate injury is not exclusively due to an intravascular pressure pulse (6). In contrast, experiments conducted by Suneson, et al., where pressure transients were measured in the abdomen and left frontoparietal brain parenchyma while a swine was shot in the left thigh with a rifle resulted in 270 kPa and 125 kPa pressure in the abdomen and brain respectively. High-energy missile impact, as described by Suneson, can transmit short lasting pressure waves of high frequency and amplitude through the body resulting in peripheral and central nervous tissue damage (90).

Variability in experimental results may be due to tissue density differences between solid organs, such as the liver and spleen, in comparison to air- or fluid-filled hollow organs such as the inner ear, lungs, bladder and intestines. The physical density of the lung depends on the lung tissue, blood, and air volume which continuously change during respiration (94). Lung tissue density gradient has been found to be significant at 10% vital capacity but decreases progressively as lung volume increases with the density gradient becoming increasingly smaller at 90% vital capacity (94).

Although not central to the objectives of this study, the lungs of all samples were visually inspected for ecchymosis on the dorsal and ventral aspects. Each area of ecchymosis was estimated as a percentage of lung area

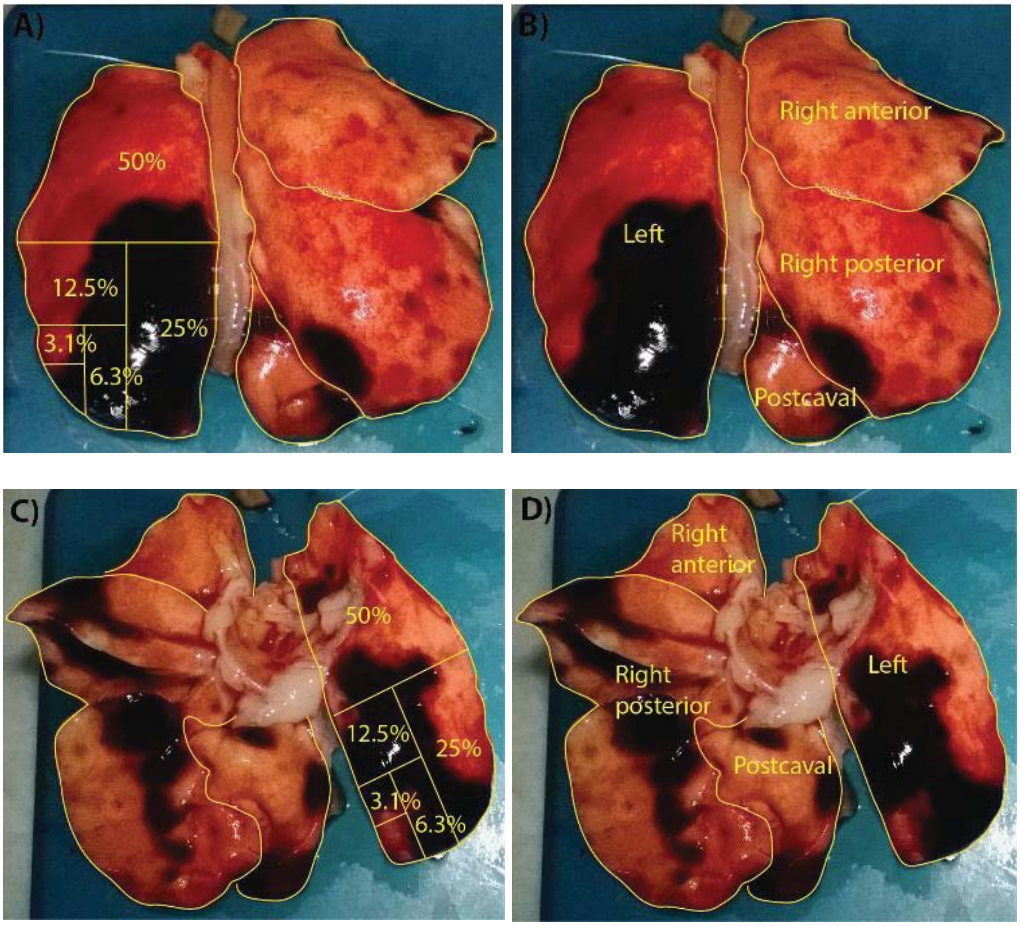

Figure 40 Lung quadrants and visual estimation of ecchymotic areas on dorsal and ventral lung surfaces. A) and B) show the dorsal aspect while C) and D) show the ventral aspect of the lungs. Ecchymotic changes were visually estimated as a percentage of total lung surface area.

Dorsal and ventral surfaces of the left lung, right lung and postcaval lobe were examined for ecchymotic areas as a percentage of each respective area. The percentages were summed. The left and right lung were considered equal in area while the postcaval lobe was considered ¼ the size of either lung. The summed ecchymotic areas were divided by total lung surface area and multiplied by 100 to determine estimated

percentage of lung ecchymotic areas. Evaluation of test subjects' lung injury was performed after euthanasia and perfusion. Lung injury estimations were performed by the same investigator for all test subjects. Examples of lung injury from blast are depicted in Figure 41. Inspection of blast-exposed test subjects (n = 32) lungs at euthanasia indicated a mean lung injury of 18.0 % ± 16.2%, see Figure 42. Blast 2 (n = 17) resulting in a mean lung injury of 24.5% ± 4.3 at seven days post-blast exposure. Blast 3 (n = 15) resulted in a mean lung injury of 10.5% ± 2.6 at one day post-blast exposure.

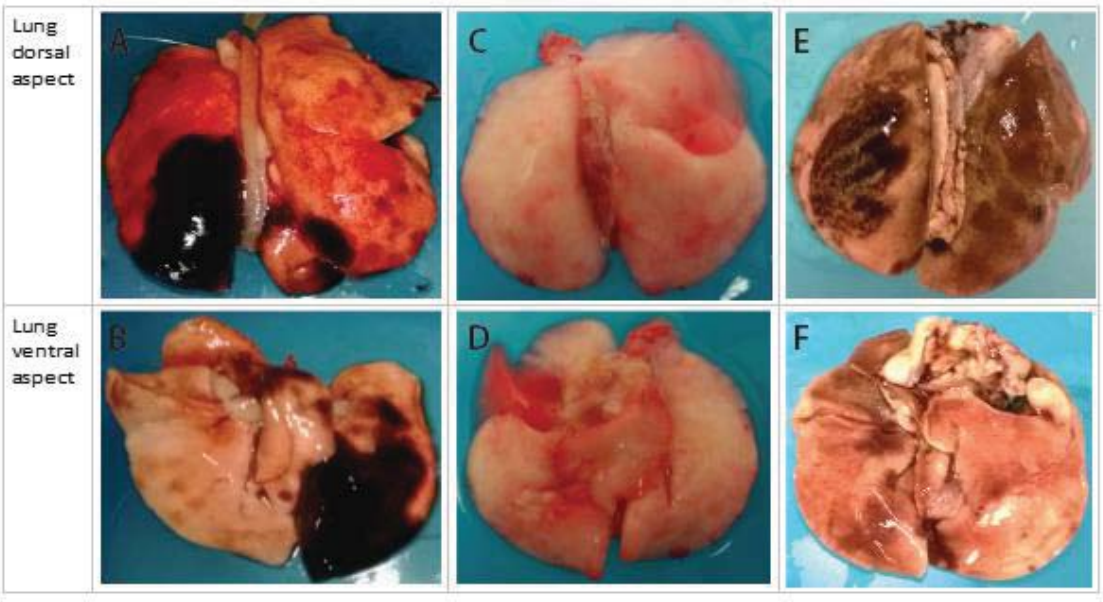

Figure 41 Blast induced lung injury. Test subjects were exposed to blast while lying on their side with their back and top of the head facing the explosive. Images A, C and E show the dorsal aspect of the lung while images B, D and F show the ventral aspect. (A, B), Lungs of a test subject euthanized and perfused at one day post-blast exposure. Lung injury is identified by the dark red/brown and black hemorrhagic areas. The left lung of image A was quantified as 50% injured, and the right is 5% injured. C and D, post-perfusion control animal lungs with no injury. E and F, show lungs placed directly into 4%PF, without perfusion, of a rat that died during blast. Note rib marks in image E.

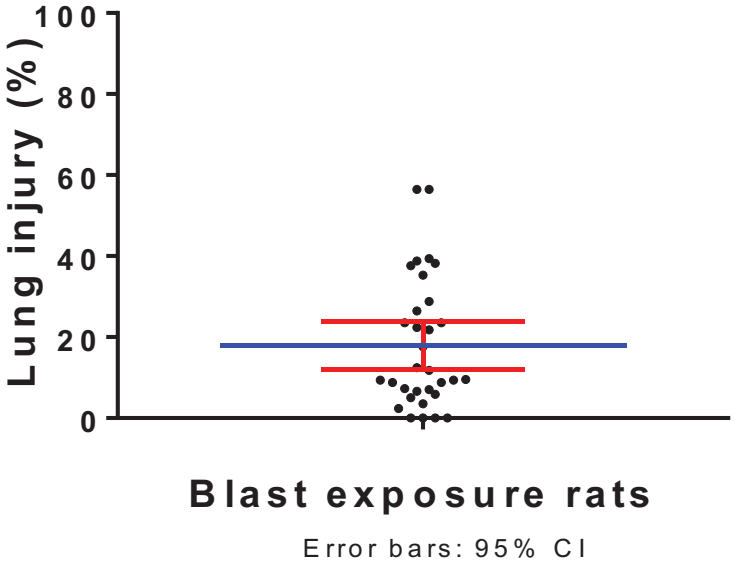

Figure 42 Percentage of lung injury in test subjects exposed to explosive blast. Each individual test subject is represented by a black dot, blue error bars represent the 95% confidence interval about the mean (red). Seven days post-blast survival group (n = 17) resulted in a mean lung injury of 24.5% ± 4.3. One day post-blast survival group (n = 15) resulted in a mean lung injury of 10.5% ± 2.6. Blast 1 and 2 combined (n = 32) 18.0% ± 16.0%. Lung injury was quantified by visual inspection of the ventral and dorsal aspect of the lungs post-perfusion with saline and 4% PF.

Lung injury is one of the most common consequences of blast exposure. The lung injury pathology was variable, as noted in Figure 54; however, when lung injury occurred it was most often found in the upper left lobe. This may be due the rats' side lying position during blast. When the rat is lying on its right side there is less pressure on the opposite, non-dependent, side (left side) relative to the dependent (right side). This may be due to a decreased tissue density in the left due to there being more air present. This type of positional lung injury has been noted in our previous blast experiments. The cause of the lung injury is believed to be due to spawling occurring at density disparities in the chest cavity. Spawling occurs when the blast wave is transmitted across materials of different densities resulting in turbulence that can disrupt tissue integrity. Areas in the

body with an air chamber show the greatest effect of spawling injury. Variability of injury may also be attributed to phase of the respiration cycle at which the blast exposure occurs. It is theorized that an inflated lung may be more prone to injury due less tissue compliance. Due to the fact the blast wave moves faster through tissue than air, we believe spawling occurs at the upper lung margin of the non-dependent lung causing the lung injury.

Appendix 8: Test Subject Attrition

Table 14 45 Test subjects excluded from functional and structural analysis

Cause of exclusion	Test subject (#)	Reason for exclusion
Anesthesia[1]	5	Died with no lung pathology
Blast lung[2]	10	Evidence of lung trauma
Electrode injury[3]	14	Confirmed by cresyl violet stain
Eye injury[4]	3	Ophthalmologic exam at euthanasia
Staining or slide[5]	7	Impregnation solution, slide adherence
Surgery death[6]	6	Respiratory arrest

[1]Anesthesia: ketamine/xylazine injection at blast site. Not exposed to blast.
[2]Noisy breathing and blood in lung upon necropsy after blast exposure. Anesthesia induced hypoxia is not ruled out as cause of death.
[3]Electrode markings on brain on visual inspection and/or by cresyl violet staining.
[4]Eye injury; Ophthalmologic exam performed at surgery and again at euthanasia. Injury considered non-visualization of blood vessels leading to area centralis.
[5]Staining; Golgi-Cox impregnation reagent did not stain 5 test subjects. Slide would not adhere brain slices.
[6]Surgery; Hydrogen peroxide clearing of skull surface caused rat to hyperventilate while on 1.2% isoflurane causing immediate cessation of respirations.

Appendix 9: Pre-test Surgical Procedures

In preparation for surgery, test subjects received induction anesthesia at 5% isoflurane and 1 LPM O2 for approximately three minutes. The head was then shaved, followed by securing the rats head in a stereotaxic frame (David Kopf, Tujunga, CA) with the use of ear bars. Anesthesia was maintained at 1.0-1.8 % isoflurane and O_2 0.8 LPM. Skin was cleaned with betadine and alcohol. Pre-incision subcutaneous local anesthetic, Marcaine® (bupivacaine hydrochloride; Hospira Inc., Lake Forest, IL), was injected midline of the head and allowed to diffuse for 10 minutes. Surgical incision was performed midline on the superior surface of the skull, rostral to caudal, from midline-posterior eyes to midline of the ears. Skull was cleaned of blood and tissue. Screw electrode coordinates were marked stereotaxically, see Figure 43.

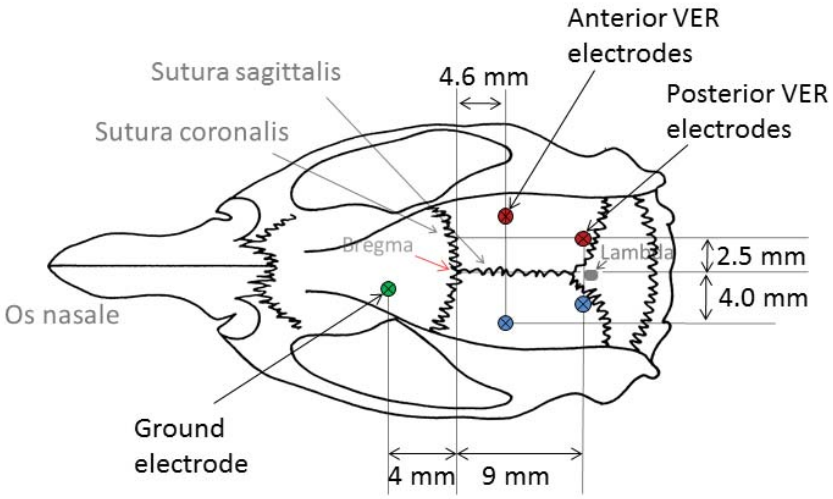

Figure 43 Epidural ECoG screw-electrode coordinates depicted on rat skull. The green circle represents the ground (reference) electrode, red circles are the right hemisphere electrodes while the blue circles are the left hemisphere electrodes. All electrode locations are referenced from bregma and lateral to the sagittal suture. Coordinates are taken from stereotaxic coordinate atlas (78): ground 4L1; anterior -4.6L4; Posterior -9.0L2.5. Figure abstracted from diagram provided by Michael Bodo, M.D., Ph.D.

All electrodes are referenced from bregma and coordinates are taken from stereotaxic coordinate atlas (78). Electrodes, pedestal, cables and SL6C commutator were made by PlasticsOne, Roanoke, VA. Epidural ECoG screw electrodes were tightened approximately 0.5 turns so that the bottom of the screw was flush with the inferior aspect of the skull and in contact with the dura. Screws can be easily dislodged from the holes due to the limited depth so an initial layer of poly(methyl methacrylate) (PMMA), of very thin consistency, was poured onto and around the screws to secure screws in place. Once secured, electrode ends were placed in six-pin pedestal and pedestal was secured atop initial PMMA with secondary layer of PMMA, see

A. Coordinates	B. Holes	C. Electrodes	D. Primary Cyanoacrylate	E. Secondary Cyanoacrylate

Figure 44 Stereotaxic placement of epidural screw electrodes. A) Stereotaxic marking of electrode location. B) Holes drilled in skull with 0.4 mm trephine bit. C) Screw electrodes placed; tip of screw flush with inferior aspect of skull. D) Primary layer of cyanoacrylate poured over screws to ensure no movement during pedestal placement or blast exposure. E) Secondary layer of cyanoacrylate placed to secure electrode wires and pedestal; would closed with staples.

After drying, intramuscular injections of penicillin-G (Sandoz Inc., Princeton, NJ) and ketorolac tromethamine (Hospira Inc., Lake Forest, IL) for infection prevention and post-surgery analgesia respectively were administered in the posterior thighs. Surgical incision was closed with staples rostral and caudal to the pedestal. Anesthesia was

discontinued and commutator cable attached in order to perform a post-surgery ECoG recording to establish integrity of electrodes.

Appendix 10: Electrocorticogram Test Equipment

Electrocorticograph amplifiers utilized included: Wide band A.C. pre-amplifier and integrator, Model 7P3C. D.C. driver amplifier, Model 7DAG; (Grass Instrument Co., Quincy MA) with a time constant (Tc) of 0.2 seconds, band-pass filter for 0.3 Hz (high pass) to 75 Hz (low pass) for amplification of the cortical potentials 10000 times. A 60 Hz notch filter was used to eliminate electrical background noise. Calibration voltage was set to ±100 μV and was included at the beginning and end of each electrophysiologic recording.

The mirrored box recording chamber (mirror box) was constructed using a standard plastic mouse cage (28 cm x 17 cm x 12 cm). Reflective Mylar (2 mil, 98% reflectivity) was wrapped around all sides except the top. A 3 cm diameter hole was pre-cut in the top of the translucent cage lid allowing passage and free movement of the commutator cable as the animal moved about the mirror box. The commutator was attached to a spring-loaded swivel stand model 2337-222 (LKB Bromma Co, Sweden) which enhanced freedom of travel of the commutator cable during animal movement. Photic stimulator flash lamp was attached to a laboratory ring stand and placed 24 cm above the base of the mirror box (bottom of lamp to floor of mirror box) with the bottom edge of the PS-flash lamp on the same vertical plane as the edge of the mirror box. The PS-lamp was angled towards the center of the box. The PS-flash lamp used a xenon flash tube with UV-filter, flash duration of 10 μs producing an illumination of 0.012 lumen/sec/cm^2 at an intensity setting of 8.

Appendix 11: Flash-VER Amplitude and Latency Including Injured Test Subjects

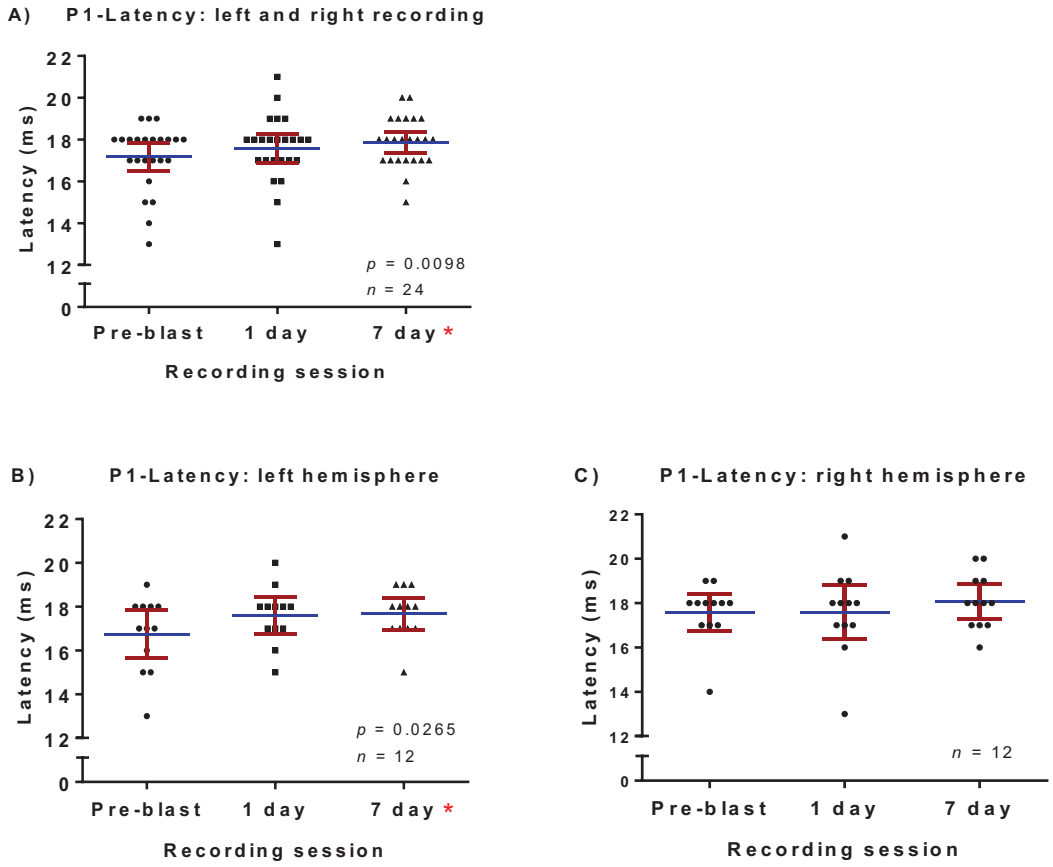

Figure 45 Flash VEP P1-peak latency for left and right hemisphere recordings pre-blast, 1-day and 7-days post-blast exposure. Plot data are P1-latency (ms) versus recording session for 12 test subjects. Each data point is a test subject's left or right hemisphere recording of 180 averaged fVEPs. Red error bars represent the 95% confidence interval, blue bar indicates the mean for each recording session, red asterisk indicates a significant increase in latency $p < 0.05$. A) Each test subject had a left and right cortical hemisphere recording which allowed comparison of 24 recordings for each recording session. Paired *t*-test indicated significant increase in latency at 7-days post-blast $t(23) = 2.815$, $p = 0.0098$. B) Left hemisphere recordings ($n = 12$) showed an increase in latency at 7-days post-blast with a paired *t*-test $t(11) = 2.561$, $p = 0.0265$. C) Right hemisphere recordings ($n = 12$) showed non-significant increased latency at 7-days post blast exposure.

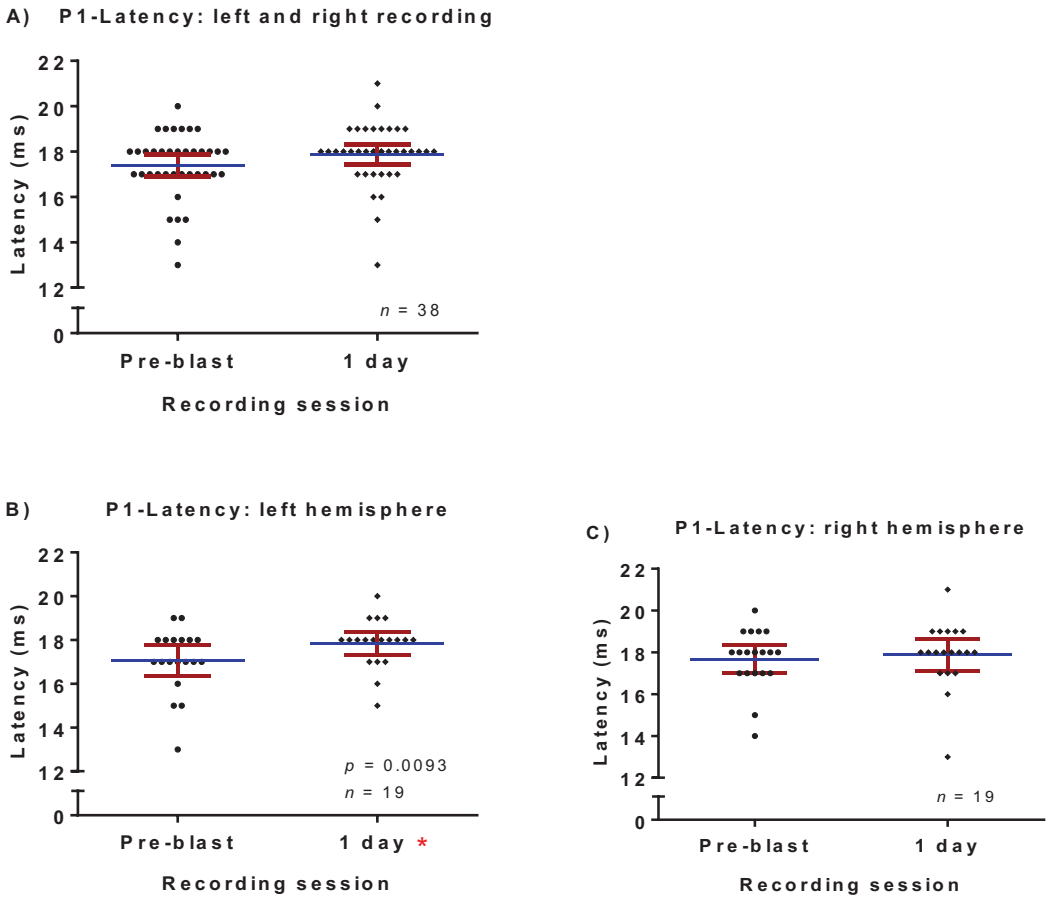

Figure 46 Flash VEP P1-peak latency for left and right hemisphere fVER recordings pre-blast and 1 day post-blast exposure. Plot data are P1-latency (ms) versus recording session for 19 test subjects. Each data point is a test subject's left or right hemisphere recording of 180 averaged fVEPs. Red error bars represent the 95% confidence interval, blue bar indicates the mean for each recording session, and red asterisk indicates a significant increase in latency $p < 0.05$. A) Left and right fVEP recordings ($n = 38$). B) Left hemisphere recordings ($n = 19$), paired t-test was performed indicating there was a significant difference in the latency comparing 1-day post-blast ($M = 17.84$, $SD = 1.119$) and pre-blast ($M = 17.05$, $SD = 1.471$) conditions; $t(18) = 2.911$, $p = 0.0093$. C) Right hemisphere recording ($n = 19$) indicates a non-significant increase in latency.

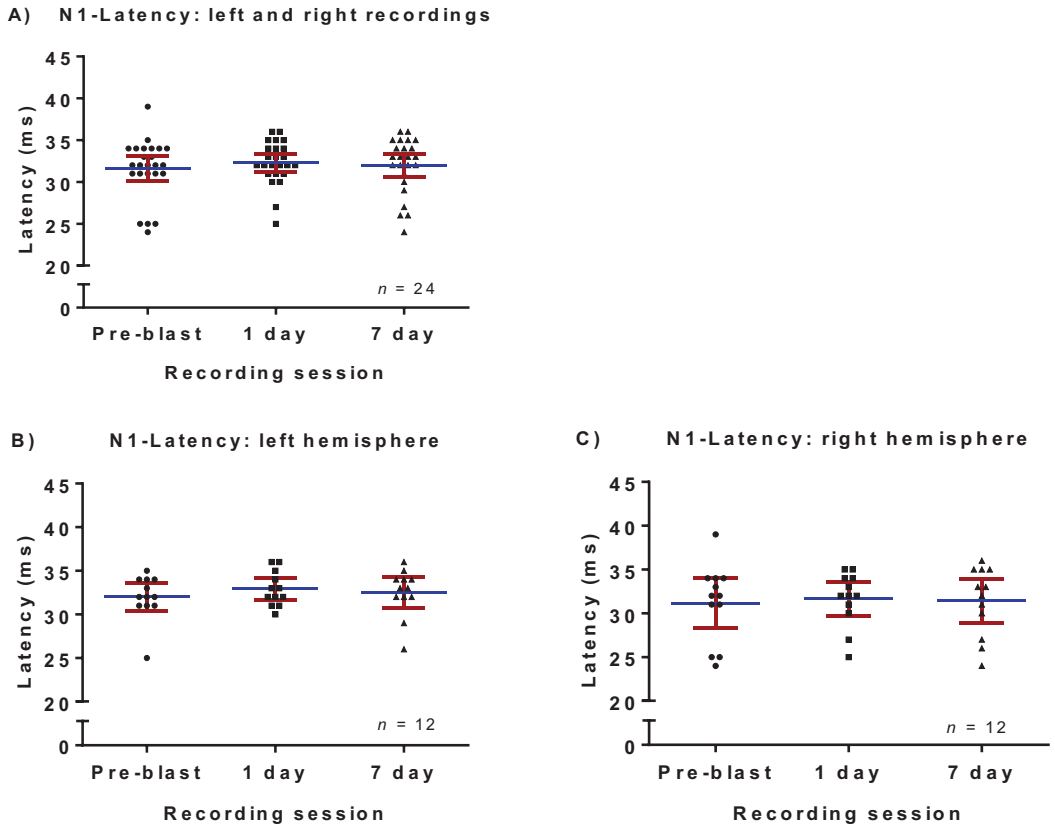

Figure 47 Flash-VEP N1-peak latency for left and right hemisphere pre-blast, 1-day post-blast and 7-days post-blast exposure. Plot data are N1-latency (ms) versus recording session for 12 test subjects. Data points are the individual left or right hemisphere recording N1-latency with each point being the average of 180 fVEPs. Red error bars represent the 95% confidence interval, blue bar indicates the mean for each recording session, and red asterisk indicates a significant increase in latency $p < 0.05$. There were no significant changes in N1-latency for test subject ($n = 12$) with two post-blast recordings sessions. A) Each point is an individual test subjects left or right hemisphere fVEP recording ($n = 24$) N1-latency. B) Left hemisphere recordings ($n = 12$). C) Right hemisphere recordings ($n = 12$).

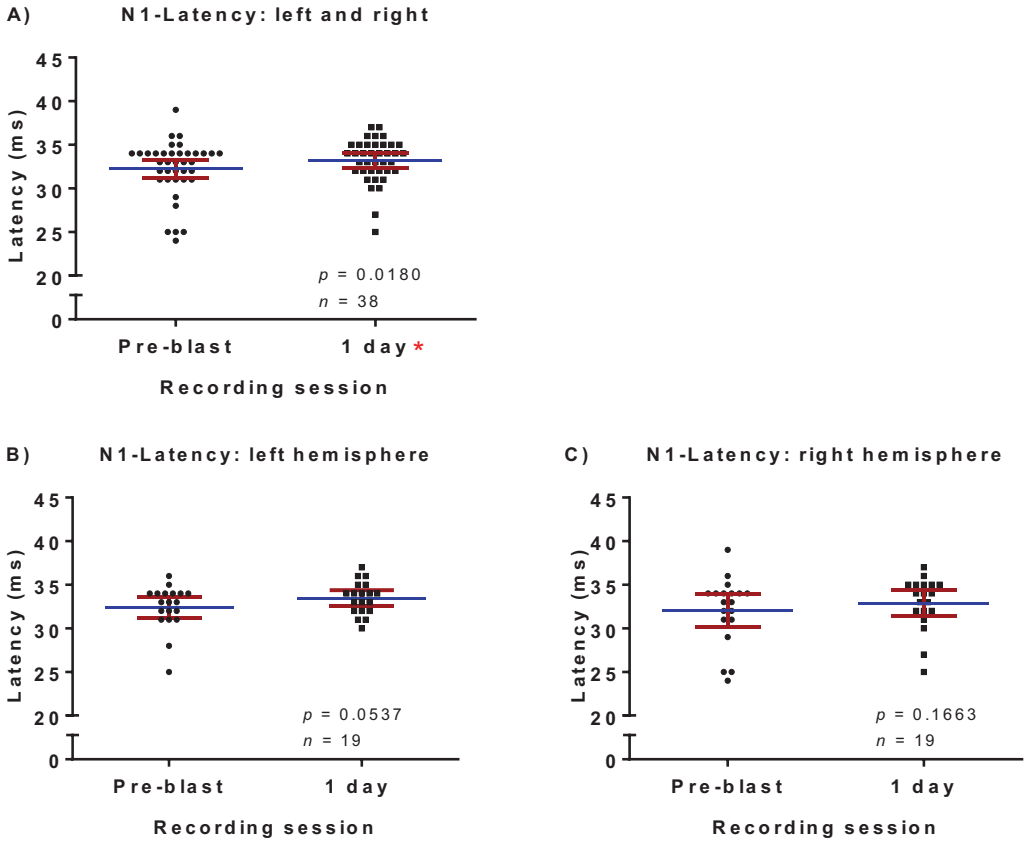

Figure 48 Flash-VEP N1-peak latency for left and right hemisphere pre-blast and1-day post-blast exposure. Plot data are N1-latency (ms) versus recording session for 19 test subjects. Data points are the individual left or right hemisphere recording of N1-latency with each point being the average of 180 fVEPs. Red error bars represent the 95% confidence interval, blue bar indicates the mean for each recording session, and red asterisk indicates a significant increase in latency $p < 0.05$. A) Left and right hemisphere recordings paired *t*-test indicated a significant increase in N1-latency at 1-day post-blast, $t(37) = 2.476$, $p = 0.0180$. B) Left hemisphere recordings ($n = 19$) showed a non-significant increase in latency post-blast. C) Right hemisphere recordings ($n = 19$) showed non-significant increase in latency post-blast.

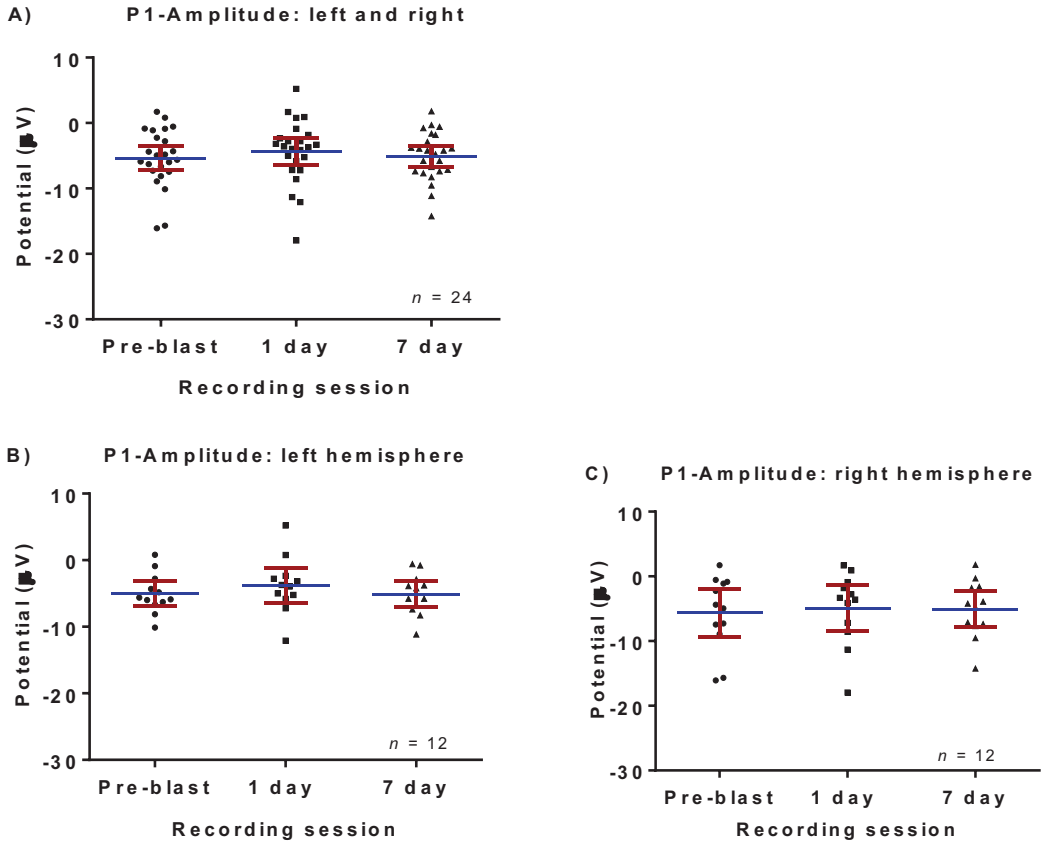

Figure 49 Flash-VEP P1-peak amplitude for left and right hemisphere recordings pre-blast, 1 day post-blast and 7 days post-blast exposure. Plot data are P1-potential (μV) versus recording session for 12 test subjects. Data points are the individual left or right hemisphere recording P1-amplitude with each point being the average of 180 fVEPs. Red error bars represent the 95% confidence interval, blue bar indicates the mean for each recording session. A) Each point is an individual test subjects left or right hemisphere fVEP recording (n = 24) P1-amplitude. There were no significant changes in P1-amplitude post-blast exposure. B) Left hemisphere recordings (n = 12). C) Right hemisphere recordings (n = 12).

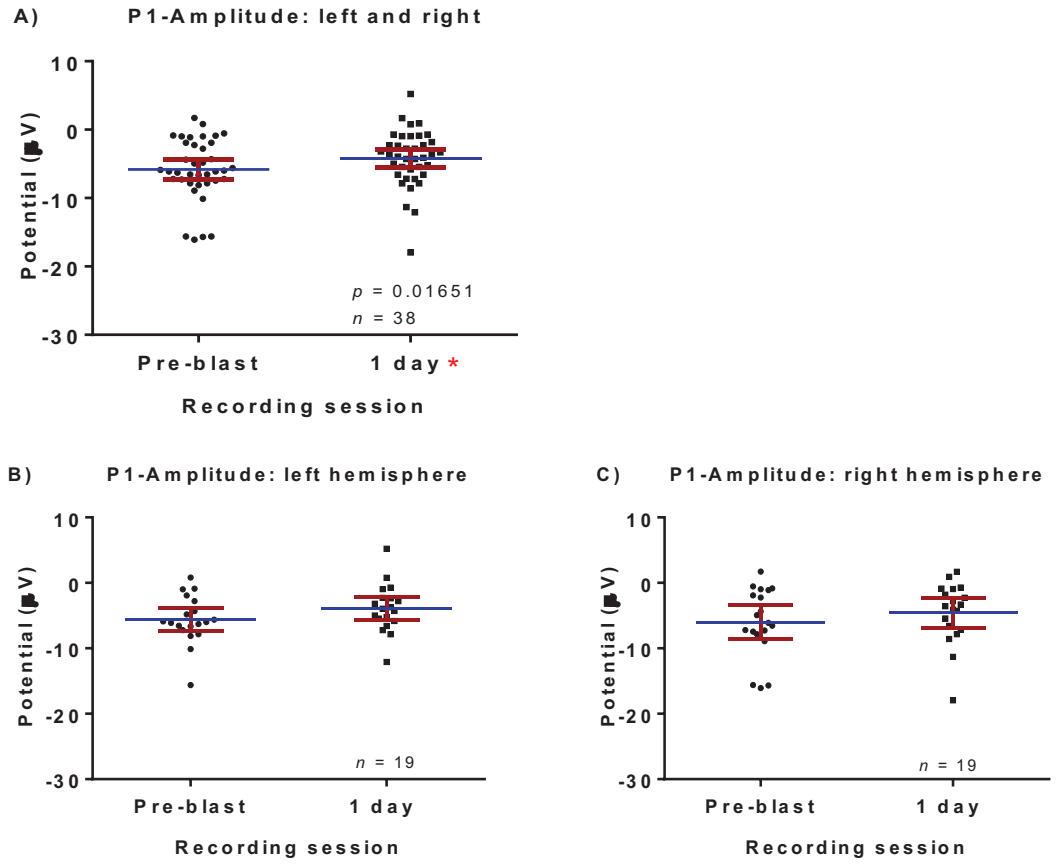

Figure 50 Flash-VEP P1-peak amplitude for left and right hemisphere recordings pre-blast and 1 day post-blast post-blast. Plot data are P1-potential (µV) versus recording session for 19 test subjects. Data points are the individual left or right hemisphere fVEP P1-amplitude with each point being the average of 180 fVEPs. Red error bars represent the 95% confidence interval, blue bar indicates the mean for each recording session, and red asterisk indicates a significant decrease in amplitude $p < 0.05$. A) Plot of left and right hemisphere fVEP P1-amplitude ($n = 38$), paired t-test indicates a significant decrease in signal amplitude at 1-day post-blast exposure ($M = -4.224$, $SD = 4.156$) compared to the pre-blast recording ($M = -5.812$, $SD = 4.511$), $t(37) = 2.512$, $p = 0.0165$. B) Left hemisphere recordings ($n = 19$). C) Right hemisphere recordings ($n = 19$).

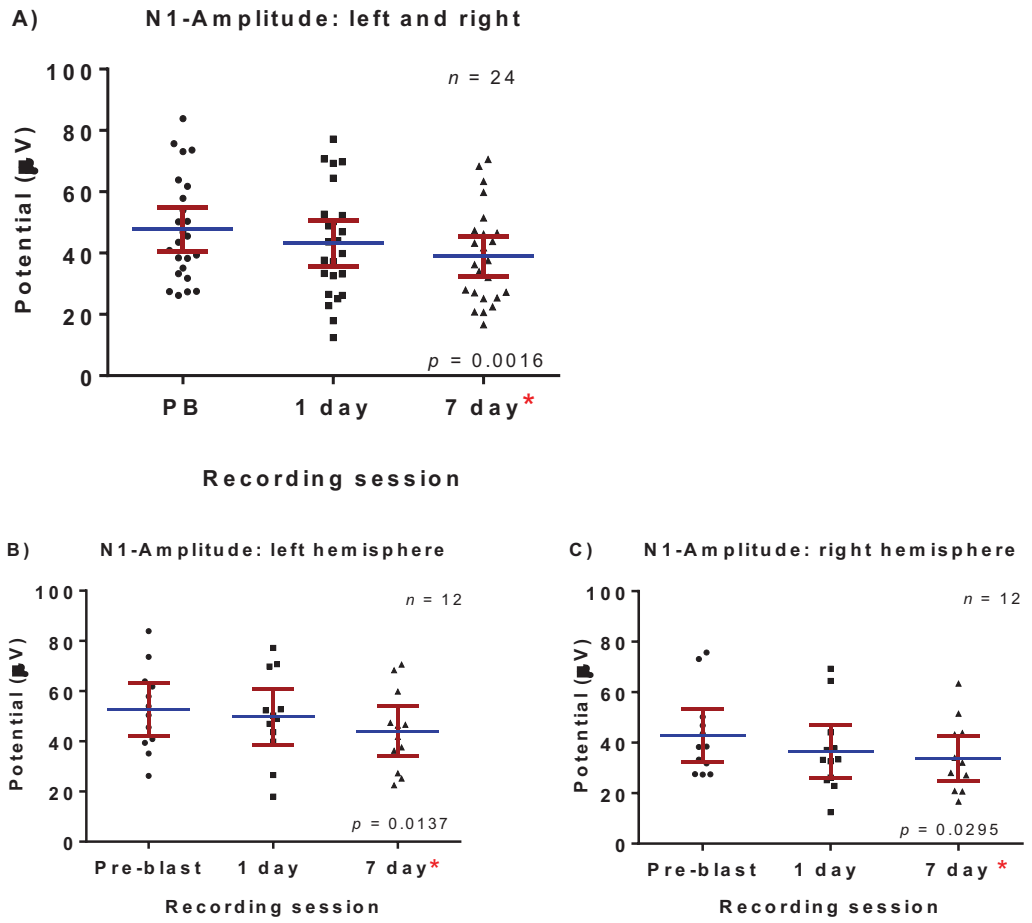

Figure 51 Flash-VEP N1-peak amplitude for left and right hemisphere recordings pre-blast, 1 day post-blast and 7-days post-blast exposure. Plot data are N1-potential (μV) versus recording session for 12 test subjects. Data points are the individual left or right hemisphere recording of N1-amplitude with each point being the average of 180-fVEPs. Red error bars represent the 95% confidence interval, blue bar indicates the mean for each recording session, and red asterisk indicates a significant decrease in amplitude using a paired *t*-test, $p < 0.05$. A) Plot of left and right hemisphere fVEP N1-amplitude ($n = 24$). A pairwise repeated measures ANOVA indicated a significant decrease in N1-amplitude at 7-days post-blast (F (1.863, 42.85) = 7.841, $P = 0.0016$). B) Left hemisphere recordings ($n = 12$) with significant decrease in amplitude at 7-days post-blast $t(11) = 2.930$, $p = 0.0137$. C) Right hemisphere N1-amplitude indicating a significant decrease in right hemisphere N1-amplitude at 1-day and 7-days post-blast in comparison to pre-blast recordings by paired *t*-test.

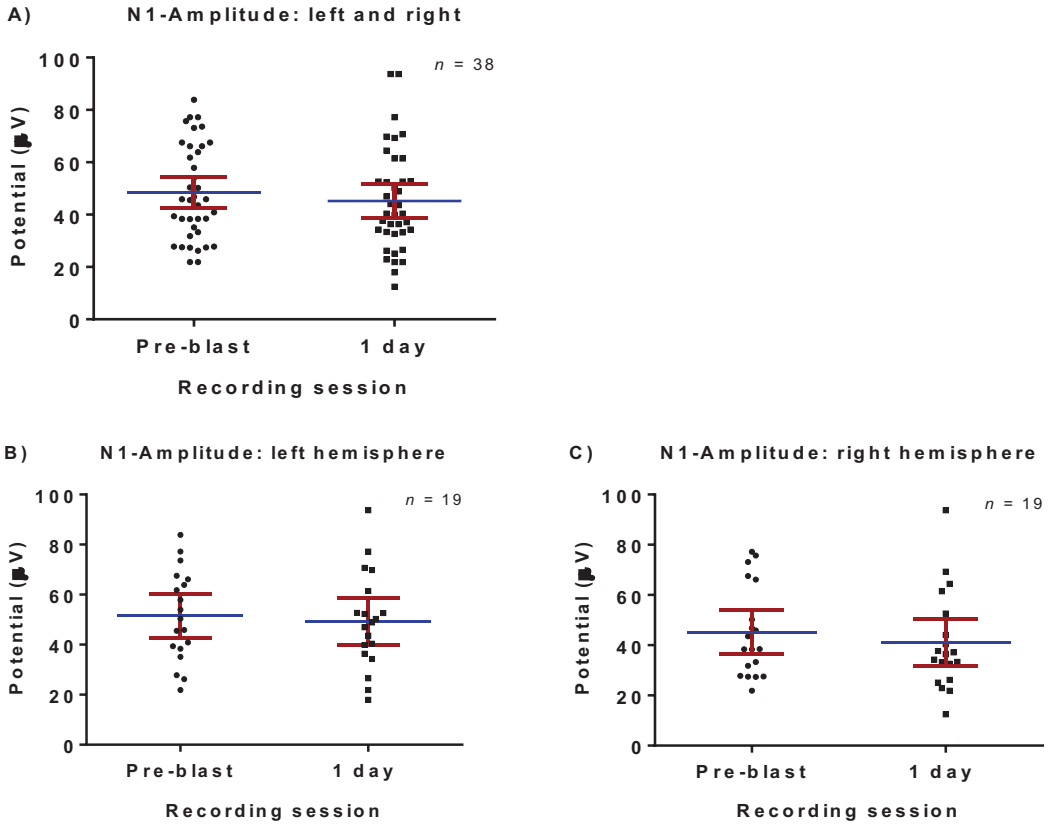

Figure 52 Flash-VEP N1-peak amplitude for left and right hemisphere recordings pre-blast and 1-day post-blast exposure. Plot data are N1-potential (μV) versus recording session. Data points are the individual left or right hemisphere recording of N1-amplitude with each point being the average of 180 fVEPs. Red error bars represent the 95% confidence interval, blue bar indicates the mean for each recording session, and red asterisk indicates a significant decrease in amplitude $p < 0.05$. Each recording session consisted of 19 test subjects with each subject averaging 180 flash-VEPs per recording session. A) Combined left and right recordings of all test subjects 1 day post-blast fVEPs. B) Left hemisphere fVEPs. C) Right hemisphere fVEPs.

REFERENCES

1. Aladjalova NA. 1957. Infra-slow rhythmic oscillations of the steady potential of the cerebral cortex. *Nature* 179:957-9
2. Arciniegas DB. 2011. Clinical electrophysiologic assessments and mild traumatic brain injury: state-of-the-science and implications for clinical practice. *International journal of psychophysiology : official journal of the International Organization of Psychophysiology* 82:41-52
3. Atienza M, Cantero JL, Quian Quiroga R. 2005. Precise timing accounts for posttraining sleep-dependent enhancements of the auditory mismatch negativity. *Neuroimage* 26:628-34
4. Baloyannis SJ, Mauroudis I, Manolides SL, Manolides LS. 2011. The acoustic cortex in frontotemporal dementia: a Golgi and electron microscope study. *Acta oto-laryngologica* 131:359-61
5. Baseler HA, Sutter EE, Klein SA, Carney T. 1994. The topography of visual evoked response properties across the visual field. *Electroencephalography and clinical neurophysiology* 90:65-81
6. Bauman RA, Ling G, Tong L, Januszkiewicz A, Agoston D, et al. 2009. An introductory characterization of a combat-casualty-care relevant swine model of closed head injury resulting from exposure to explosive blast. *Journal of neurotrauma* 26:841-60
7. Bittner T, Burgold S, Dorostkar MM, Fuhrmann M, Wegenast-Braun BM, et al. 2012. Amyloid plaque formation precedes dendritic spine loss. *Acta neuropathologica* 124:797-807
8. Blumhardt LD, Barrett G, Halliday AM, Kriss A. 1978. The effect of experimental 'scotomata' on the ipsilateral and contralateral responses to pattern-reversal in one half-field. *Electroencephalography and clinical neurophysiology* 45:376-92
9. Buzsaki G, Anastassiou CA, Koch C. 2012. The origin of extracellular fields and currents--EEG, ECoG, LFP and spikes. *Nature reviews. Neuroscience* 13:407-20
10. Campbell JN, Low B, Kurz JE, Patel SS, Young MT, Churn SB. 2012. Mechanisms of dendritic spine remodeling in a rat model of traumatic brain injury. *Journal of neurotrauma* 29:218-34
11. Campbell JN, Register D, Churn SB. 2012. Traumatic brain injury causes an FK506-sensitive loss and an overgrowth of dendritic spines in rat forebrain. *Journal of neurotrauma* 29:201-17
12. Candole d. 1967. Blast Injury.
13. Cantero JL, Atienza M. 2005. The role of neural synchronization in the emergence of cognition across the wake-sleep cycle. *Reviews in the neurosciences* 16:69-83
14. CDC. 2006. Explosions and Blast Injuries: A Primer for Clinicians. Atlanta, GA: Centers for Disease Control and Prevention
15. Celander H, Clemedson CJ, Ericsson UA, Hultman HI. 1955. A study on the relation between the duration of a shock wave and the severity of the blast injury produced by it. *Acta Physiol Scand* 33:14-8

16. Cernak I, Merkle AC, Koliatsos VE, Bilik JM, Luong QT, et al. 2011. The pathobiology of blast injuries and blast-induced neurotrauma as identified using a new experimental model of injury in mice. *Neurobiology of disease* 41:538-51
17. Charng J, Nguyen CT, He Z, Dang TM, Vingrys AJ, et al. 2013. Conscious wireless electroretinogram and visual evoked potentials in rats. *PLoS One* 8:e74172
18. Chen C, Magee JC, Bazan NG. 2002. Cyclooxygenase-2 regulates prostaglandin E2 signaling in hippocampal long-term synaptic plasticity. *Journal of neurophysiology* 87:2851-7
19. Chen LJ, Wang YJ, Chen JR, Tseng GF. 2015. NMDA receptor triggered molecular cascade underlies compression-induced rapid dendritic spine plasticity in cortical neurons. *Experimental neurology* 266:86-98
20. Cigánek L. 1958. *Stavba elektrických strojů; vysokoškolská učebnice*. Praha,: Státní nakl. technické literatury. 714 p. pp.
21. Clemedson CJ, Jonsson A. 1961. Transmission and reflection of high explosive shock waves in bone. *Acta Physiol Scand* 51:47-61
22. Coronado VG, McGuire LC, Sarmiento K, Bell J, Lionbarger MR, et al. 2012. Trends in Traumatic Brain Injury in the U.S. and the public health response: 1995-2009. *Journal of safety research* 43:299-307
23. Cullis IG. 2001. Blast waves and how they interact with structures. *J R Army Med Corps* 147:16-26
24. Daroff RB, Bradley WG. 2012. *Bradley's neurology in clinical practice / [edited by] Robert B. Daroff ... [et al.]*. Philadelphia, PA: Elsevier/Saunders
25. Davenport ND, Lim KO, Armstrong MT, Sponheim SR. 2012. Diffuse and spatially variable white matter disruptions are associated with blast-related mild traumatic brain injury. *Neuroimage* 59:2017-24
26. de Candole CA. 1967. Blast injury. *Canadian Medical Association journal* 96:207-14
27. de Lanerolle NC, Bandak F, Kang D, Li AY, Du F, et al. 2011. Characteristics of an explosive blast-induced brain injury in an experimental model. *Journal of neuropathology and experimental neurology* 70:1046-57
28. Dean SL, Wright CL, Hoffman JF, Wang M, Alger BE, McCarthy MM. 2012. Prostaglandin E2 stimulates estradiol synthesis in the cerebellum postnatally with associated effects on Purkinje neuron dendritic arbor and electrophysiological properties. *Endocrinology* 153:5415-27
29. Defense and Veterans Brain Injury Center (DVBIC). 2016. *DoD WorldwideTBI Numbers 2000-2016 Q1-Q2*. http://dvbic.dcoe.mil/dod-worldwide-numbers-tbi
30. Desmoulin GT, Dionne JP. 2009. Blast-induced neurotrauma: surrogate use, loading mechanisms, and cellular responses. *The Journal of trauma* 67:1113-22
31. Doi R, Morita K, Shigemori M, Tokutomi T, Maeda H. 2007. Characteristics of cognitive function in patients after traumatic brain injury assessed by visual and auditory event-related potentials. *American journal of physical medicine & rehabilitation / Association of Academic Physiatrists* 86:641-9
32. Donchin E, Spencer KM, Wijesinghe R. 2000. The mental prosthesis: assessing the speed of a P300-based brain-computer interface. *IEEE transactions on*

rehabilitation engineering : a publication of the IEEE Engineering in Medicine and Biology Society 8:174-9
33. Doukas AG, McAuliffe DJ, Lee S, Venugopalan V, Flotte TJ. 1995. Physical factors involved in stress-wave-induced cell injury: the effect of stress gradient. *Ultrasound Med Biol* 21:961-7
34. Duncan CC, Kosmidis MH, Mirsky AF. 2003. Event-related potential assessment of information processing after closed head injury. *Psychophysiology* 40:45-59
35. Eckert MJ, Guevremont D, Williams JM, Abraham WC. 2013. Rapid visual stimulation increases extrasynaptic glutamate receptor expression but not visual-evoked potentials in the adult rat primary visual cortex. *The European journal of neuroscience* 37:400-6
36. Estopinal CB, Wolf AB, Donahue SP. 2013. Retinoblastoma detected by preschool vision screening using visual-evoked potentials. *J Pediatr Ophthalmol Strabismus* 50:e41-3
37. Ferrante RJ, Kowall NW, Richardson EP, Jr. 1991. Proliferative and degenerative changes in striatal spiny neurons in Huntington's disease: a combined study using the section-Golgi method and calbindin D28k immunocytochemistry. *The Journal of neuroscience : the official journal of the Society for Neuroscience* 11:3877-87
38. Frattalone AR, Ling GS. 2013. Moderate and severe traumatic brain injury: pathophysiology and management. *Neurosurgery clinics of North America* 24:309-19
39. Freed S, Hellerstein LF. 1997. Visual electrodiagnostic findings in mild traumatic brain injury. *Brain injury : [BI]* 11:25-36
40. Fuhrmann M, Mitteregger G, Kretzschmar H, Herms J. 2007. Dendritic pathology in prion disease starts at the synaptic spine. *The Journal of neuroscience : the official journal of the Society for Neuroscience* 27:6224-33
41. Gao X, Chen J. 2011. Mild traumatic brain injury results in extensive neuronal degeneration in the cerebral cortex. *Journal of neuropathology and experimental neurology* 70:183-91
42. Gao X, Deng P, Xu ZC, Chen J. 2011. Moderate traumatic brain injury causes acute dendritic and synaptic degeneration in the hippocampal dentate gyrus. *PLoS One* 6:e24566
43. Goldstein LE, Fisher AM, Tagge CA, Zhang XL, Velisek L, et al. 2012. Chronic traumatic encephalopathy in blast-exposed military veterans and a blast neurotrauma mouse model. *Science translational medicine* 4:134ra60
44. Goodrich GL, Kirby J, Cockerham G, Ingalla SP, Lew HL. 2007. Visual function in patients of a polytrauma rehabilitation center: A descriptive study. *Journal of rehabilitation research and development* 44:929-36
45. Graveland GA, Williams RS, DiFiglia M. 1985. Evidence for degenerative and regenerative changes in neostriatal spiny neurons in Huntington's disease. *Science* 227:770-3
46. Guarino I, Loizzo S, Lopez L, Fadda A, Loizzo A. 2004. A chronic implant to record electroretinogram, visual evoked potentials and oscillatory potentials in awake, freely moving rats for pharmacological studies. *Neural plasticity* 11:241-50

47. Hall ED, Bryant YD, Cho W, Sullivan PG. 2008. Evolution of post-traumatic neurodegeneration after controlled cortical impact traumatic brain injury in mice and rats as assessed by the de Olmos silver and fluorojade staining methods. *Journal of neurotrauma* 25:235-47
48. Hetzler BE, Melk AM. 1989. Effects of ketamine, naloxone, and physostigmine on flash evoked potentials in rat superior colliculus. *Pharmacology, biochemistry, and behavior* 32:511-8
49. Hoffmann NA, Dorostkar MM, Blumenstock S, Goedert M, Herms J. 2013. Impaired plasticity of cortical dendritic spines in P301S tau transgenic mice. *Acta neuropathologica communications* 1:82
50. Iwamura Y, Fujii Y, Kamei C. 2003. The effects of certain H(1)-antagonists on visual evoked potential in rats. *Brain research bulletin* 61:393-8
51. Kaech S, Brinkhaus H, Matus A. 1999. Volatile anesthetics block actin-based motility in dendritic spines. *Proceedings of the National Academy of Sciences of the United States of America* 96:10433-7
52. Kan EM, Ling EA, Lu J. 2012. Microenvironment changes in mild traumatic brain injury. *Brain research bulletin* 87:359-72
53. Kasture S, Vinci S, Ibba F, Puddu A, Marongiu M, et al. 2009. Withania somnifera prevents morphine withdrawal-induced decrease in spine density in nucleus accumbens shell of rats: a confocal laser scanning microscopy study. *Neurotoxicity research* 16:343-55
54. Kolb B, Cioe J, Comeau W. 2008. Contrasting effects of motor and visual spatial learning tasks on dendritic arborization and spine density in rats. *Neurobiology of learning and memory* 90:295-300
55. Kress HG. 1997. [Mechanisms of action of ketamine]. *Der Anaesthesist* 46 Suppl 1:S8-19
56. Kurz JE, Hamm RJ, Singleton RH, Povlishock JT, Churn SB. 2005. A persistent change in subcellular distribution of calcineurin following fluid percussion injury in the rat. *Brain research* 1048:153-60
57. Kurz JE, Parsons JT, Rana A, Gibson CJ, Hamm RJ, Churn SB. 2005. A significant increase in both basal and maximal calcineurin activity following fluid percussion injury in the rat. *Journal of neurotrauma* 22:476-90
58. Larson MJ, Clayson PE, Farrer TJ. 2012. Performance monitoring and cognitive control in individuals with mild traumatic brain injury. *Journal of the International Neuropsychological Society : JINS* 18:323-33
59. Lenz H, Raeder J. 2008. Comparison of etoricoxib vs. ketorolac in postoperative pain relief. *Acta anaesthesiologica Scandinavica* 52:1278-84
60. Leonardi AD, Bir CA, Ritzel DV, VandeVord PJ. 2011. Intracranial pressure increases during exposure to a shock wave. *Journal of neurotrauma* 28:85-94
61. Lew HL, Jerger JF, Guillory SB, Henry JA. 2007. Auditory dysfunction in traumatic brain injury. *Journal of rehabilitation research and development* 44:921-8
62. Lew HL, Pogoda TK, Baker E, Stolzmann KL, Meterko M, et al. 2011. Prevalence of dual sensory impairment and its association with traumatic brain injury and blast exposure in OEF/OIF veterans. *The Journal of head trauma rehabilitation* 26:489-96

63. Lew HL, Poole JH, Guillory SB, Salerno RM, Leskin G, Sigford B. 2006. Persistent problems after traumatic brain injury: The need for long-term follow-up and coordinated care. *Journal of rehabilitation research and development* 43:vii-x
64. Lin D, Cao L, Wang Z, Li J, Washington JM, Zuo Z. 2012. Lidocaine attenuates cognitive impairment after isoflurane anesthesia in old rats. *Behavioural brain research* 228:319-27
65. Ling G, Bandak F, Armonda R, Grant G, Ecklund J. 2009. Explosive blast neurotrauma. *Journal of neurotrauma* 26:815-25
66. Lopes da Silva FH, Storm van Leeuwen W, Rémond A. 1986. *Clinical applications of computer analysis of EEG and other neurophysiological signals*. Amsterdam ; New York, NY, USA: Elsevier ;. xvi, 508 p. pp.
67. Lu J, Ng KC, Ling G, Wu J, Poon DJ, et al. 2011. Effect of Blast Exposure on the Brain Structure and Cognition in Macaca fascicularis. *Journal of neurotrauma*
68. McKee AC, Robinson ME. 2014. Military-related traumatic brain injury and neurodegeneration. *Alzheimer's & dementia : the journal of the Alzheimer's Association* 10:S242-53
69. Mellor SG, Cooper GJ. 1989. Analysis of 828 servicemen killed or injured by explosion in Northern Ireland 1970-84: the Hostile Action Casualty System. *The British journal of surgery* 76:1006-10
70. Monfils MH, Teskey GC. 2004. Induction of long-term depression is associated with decreased dendritic length and spine density in layers III and V of sensorimotor neocortex. *Synapse* 53:114-21
71. Nakagawa A, Manley GT, Gean AD, Ohtani K, Armonda R, et al. 2011. Mechanisms of primary blast-induced traumatic brain injury: insights from shock-wave research. *Journal of neurotrauma* 28:1101-19
72. Needham CE, Ritzel D, Rule GT, Wiri S, Young L. 2015. Blast Testing Issues and TBI: Experimental Models That Lead to Wrong Conclusions. *Frontiers in neurology* 6:72
73. Niedermeyer E, Lopes da Silva FH. 1982. *Electroencephalography, basic principles, clinical applications, and related fields*. Baltimore: Urban & Schwarzenberg. x, 752 p. pp.
74. Niedermeyer E, Lopes da Silva FH. 2005. *Electroencephalography : basic principles, clinical applications, and related fields*. Philadelphia: Lippincott Williams & Wilkins. xiii, 1309 p. pp.
75. Odom JV, Bach M, Brigell M, Holder GE, McCulloch DL, et al. 2016. ISCEV standard for clinical visual evoked potentials: (2016 update). *Documenta ophthalmologica. Advances in ophthalmology* 133:1-9
76. Parker PJ. 2007. Casualty evacuation timelines: an evidence-based review. *J R Army Med Corps* 153:274-7
77. Pascual JM, Solivera J, Prieto R, Barrios L, Lopez-Larrubia P, et al. 2007. Time course of early metabolic changes following diffuse traumatic brain injury in rats as detected by (1)H NMR spectroscopy. *Journal of neurotrauma* 24:944-59
78. Paxinos G, Watson C. 1986. *The rat brain in stereotaxic coordinates*. Sydney ; Orlando: Academic Press. xxvi, 237 p. of plates pp.
79. Rachidi M, Lopes C. 2008. Mental retardation and associated neurological dysfunctions in Down syndrome: a consequence of dysregulation in critical

chromosome 21 genes and associated molecular pathways. *European journal of paediatric neurology : EJPN : official journal of the European Paediatric Neurology Society* 12:168-82
80. Reid MW, Miller KJ, Lange RT, Cooper DB, Tate DF, et al. 2014. A multisite study of the relationships between blast exposures and symptom reporting in a post-deployment active duty military population with mild traumatic brain injury. *Journal of neurotrauma* 31:1899-906
81. Rosenfeld JV, Bell RS, Armonda R. 2015. Current concepts in penetrating and blast injury to the central nervous system. *World journal of surgery* 39:1352-62
82. Saljo A, Arrhen F, Bolouri H, Mayorga M, Hamberger A. 2008. Neuropathology and pressure in the pig brain resulting from low-impulse noise exposure. *Journal of neurotrauma* 25:1397-406
83. Sarkadi A, Inczeffy Z. 1996. Simultaneous quantitative evaluation of visual-evoked responses and background EEG activity in rat: normative data. *Journal of pharmacological and toxicological methods* 35:145-51
84. Shu IW, Onton JA, Prabhakar N, O'Connell RM, Simmons AN, Matthews SC. 2014. Combat veterans with PTSD after mild TBI exhibit greater ERPs from posterior-medial cortical areas while appraising facial features. *Journal of affective disorders* 155:234-40
85. Snell FI, Halter MJ. 2010. A signature wound of war: mild traumatic brain injury. *Journal of psychosocial nursing and mental health services* 48:22-8
86. Sotrel A, Williams RS, Kaufmann WE, Myers RH. 1993. Evidence for neuronal degeneration and dendritic plasticity in cortical pyramidal neurons of Huntington's disease: a quantitative Golgi study. *Neurology* 43:2088-96
87. Spiga S, Acquas E, Puddu MC, Mulas G, Lintas A, Diana M. 2011. Simultaneous Golgi-Cox and immunofluorescence using confocal microscopy. *Brain structure & function* 216:171-82
88. Spiga S, Puddu MC, Pisano M, Diana M. 2005. Morphine withdrawal-induced morphological changes in the nucleus accumbens. *The European journal of neuroscience* 22:2332-40
89. Sponheim SR, McGuire KA, Kang SS, Davenport ND, Aviyente S, et al. 2011. Evidence of disrupted functional connectivity in the brain after combat-related blast injury. *Neuroimage* 54, Supplement 1:S21-S9
90. Suneson A, Hansson HA, Seeman T. 1987. Peripheral high-energy missile hits cause pressure changes and damage to the nervous system: experimental studies on pigs. *The Journal of trauma* 27:782-9
91. Teasdale G, Jennett B. 1974. Assessment of coma and impaired consciousness. A practical scale. *Lancet* 2:81-4
92. Tobimatsu S, Celesia GG. 2006. Studies of human visual pathophysiology with visual evoked potentials. *Clinical neurophysiology : official journal of the International Federation of Clinical Neurophysiology* 117:1414-33
93. United States Army Training and Doctrine Command (TRADOC). 2007. FM 3-34.214 Explosives and Demolitions. ed. DotA Headquarters, pp. 2-6: United States Army Training and Doctrine Command (TRADOC)

94. Verschakelen JA, Van fraeyenhoven L, Laureys G, Demedts M, Baert AL. 1993. Differences in CT density between dependent and nondependent portions of the lung: influence of lung volume. *American Journal of Roentgenology* 161:713-7
95. Wang T, Ma S, Guan Y, Du J, Liu G, Zhao X. 2016. Double function of noninvasive intracranial pressure monitoring based on flash visual evoked potentials in unconscious patients with traumatic brain injury. *Journal of clinical neuroscience : official journal of the Neurosurgical Society of Australasia* 27:63-7
96. Weichel ED, Colyer MH, Bautista C, Bower KS, French LM. 2009. Traumatic brain injury associated with combat ocular trauma. *The Journal of head trauma rehabilitation* 24:41-50
97. Winston CN, Chellappa D, Wilkins T, Barton DJ, Washington PM, et al. 2013. Controlled Cortical Impact Results in an Extensive Loss of Dendritic Spines that Is Not Mediated by Injury-Induced Amyloid-Beta Accumulation. *Journal of neurotrauma* 30:1966-72
98. You Y, Klistorner A, Thie J, Graham SL. 2011. Improving reproducibility of VEP recording in rats: electrodes, stimulus source and peak analysis. *Documenta ophthalmologica. Advances in ophthalmology* 123:109-19
99. You Y, Thie J, Klistorner A, Gupta VK, Graham SL. 2012. Normalization of visual evoked potentials using underlying electroencephalogram levels improves amplitude reproducibility in rats. *Investigative ophthalmology & visual science* 53:1473-8
100. Youssofzadeh V, Prasad G, Fagan AJ, Reilly RB, Martens S, et al. 2015. Signal Propagation in the Human Visual Pathways: An Effective Connectivity Analysis. *The Journal of neuroscience : the official journal of the Society for Neuroscience* 35:13501-10